Corso di Laurea Magistrale in Ingegneria Energetica e Nucleare

Tesi di Laurea Magistrale

Computational Methods for the Integrated Deterministic and Probabilistic Safety Assessment of a Simplified Cooling Circuit for a Tokamak Superconducting Magnet

Relatori

Prof. Nicola Pedroni

Dr. Francesco Di Maio

Candidato

Rosario Bellaera

Correlatori

Prof. Laura Savoldi

Prof. Roberto Zanino

Dr. Roberto Bonifetto, PhD

Luglio 2018

Abstract

The objective of this thesis is to consider the safety analysis of the simplified cooling circuit of a single module of the ITER (International Thermonuclear Experimental Reactor) Central Solenoid (CS) in a cold test facility, in order to identify the most relevant abnormal transient conditions and (combination of) component failures that may drive the system into a Loss Of Flow Accident (LOFA). To this aim, the Integrated Deterministic and Probabilistic Safety Assessment (IDPSA) framework is embraced, which combines phenomenological models of system dynamics with stochastic process models. To the best of the author's knowledge, it is the first time that the IDPSA approach is adopted to study the dynamic response of a nuclear fusion system to accidental transients. Two different operating conditions for the ITER CS module are considered: in the first, a constant current flowing in the module is assumed for the sake of simplicity; in the second, the real ITER current scenario is analyzed to derive some preliminary insights on the safety of the ITER reactor in the presence of abnormal transients. In both case studies, a set of 100 different accidental scenarios is randomly generated according to the principles of Multiple Value Logic (MVL) and the corresponding system behavior is simulated using the validated, state-of-the-art 4C thermal-hydraulic code. Finally, the Spectral Clustering algorithm is applied to group the scenarios thereby obtained according to a measure of similarity between them and, thus, to characterize the principal patterns of system evolution. These clusters are assumed as the "prototypical behavior" of the system in abnormal condition and, therefore, used to spot out important safety insights, e.g., the most relevant components failures that lead the system into a LOFA.

List of Figures

List of Tables

Contents

1 Introduction

Starting from the XX century, there has been a growing demand of energy. To satisfy it, fossil fuels have been extracted and massively used during the last century. Thanks to these sources of energy, many countries have modified their economic policy and started the development of the industrialisation process. In these years, it has been become clear that the living standards were, and still are, directly related to the amount of energy available (Freidberg, 2007). Energy has become fundamental in every sector of human life, from food production to the industries facilities and transportation. The importance of energy is reflected by the need of having a reliable and economic energy source: the deep penetration of carbon as fuel meets this request. Nowadays, the energy mix is very different for different countries in the world; in general, richest nations have a variegate mix that ranges from renewable sources (such as solar, wind and hydroelectric) to fossil fuels and nuclear energy. The energy situation is different in developing countries, e.g., China and India: these nations are trying to reduce the economic gap with the richest economies through an aggressive industrialization based on cheaper manpower: the energy mix is almost the same, but the use of the fossil fuels is more intense (International Energy Agency (IEA), 2018).

In the actual society the economic growth and the energy consumption are strongly coupled and the massive use of fossil fuels to satisfy the energy demand is no more feasible in the light of the associated relevant environmental issues. There is growing evidence that greenhouse gases are have a negative impact on the environment. Most of these gases are emitted in the atmosphere as consequence of the use of fuel fossils: the worst is carbon that is also the most widely used in the developing countries due to its low cost and high availability. The best alternative fossil fuel is represented by natural gas: however, if it will be consumed at the actual rate, in the next few decades the available resources will be extinguished (International Energy Agency (IEA), 2017). In order to limit the greenhouse effect, we should thus limit the consumption of fossil fuels encourage the use of low-carbon energy sources and increase the efficiency during the entire chain of energy consumption. It is a well-known problem that is widely discussed in the literature, in politics and is strongly affecting the public opinion (IPCC, 2007).

The United Nation (UN) has proposed many roadmaps to reduce the emission of greenhouse gases in several conferences organized in the last years. The Kyoto protocol, signed in 1997, represented a breakthrough, which for the first time posed the problem as central for the entire world. The last agreement has been reached at the Paris climate conference (COP21) in December 2015, during which 195 countries adopted the first-ever universal, legally binding global climate deal. The aim of the agreement is to limit the increase of temperature up to 1.5 °C, applying mitigation actions.

The European Union (EU) has decided to plan short-, mid- and long-term strategies to meet the COP21 request (European Environment Agency, 2017). The 2020 package has been set by the EU leaders in 2007 and has three key features: (i) greenhouse gas emissions must be reduced by 20% with respect to the 1990 levels; (ii) the 20% of the EU energy must be produced by renewable sources, and (iii) the 20% improvement in energy efficiency should be achieved. The results must be obtained by the EU as a “single continent”, thus different constraints are posed to the member states in order to consider their different conditions and starting points: for example, more stringent limits are posed to those states that already have a high energetic efficiency and a high production of energy from renewable sources. The mid-term climate and energy framework sets three goals for the 2030: (i) a reduction of at least 40% in greenhouse gas emissions with respect to the 1990 levels; (ii) at least the 27% of energy a production from

renewables, and (iii) at least the 27% improvement in energy efficiency. The accords were adopted in 2014 and are in line with the long-term plan that suggests, to get a low-carbon economy, to reduce the gas emission to 80% below 1990 levels.

Nuclear energy has already an important role in limiting greenhouse gases emissions. In 2009, the 13.4% of the electricity production came from nuclear fission power plants, being the second largest low-carbon source (OECD, 2012); in 2017, it is the first source of low-carbon electricity in the OECD countries, with a 17.6% of the electricity production (International Energy Agency (IEA), 2018). In this light, nuclear energy could represent a major actor, which could help cutting greenhouses emissions and meeting the present and future (environmental) goals. Within the nuclear context, whereas fission power plants are already in use from the 50s, fusion reactors are still at a research level. In the present thesis, we focus on nuclear energy coming from fusion reactions.

The central focus of fusion research is the Deuterium-Tritium (D-T) reaction, being the easiest fusion reaction to initiate, which involves the fusion of a deuterium nucleus with a tritium one: as a result, an α-particle, a neutron and 17.6 MeV are obtained. The distribution of the energy produced among the resulting particles is inversely proportional to the mass of the elements generated: the energy associated to the neutron is equal to 14.1 MeV, whereas 3.5 MeV is the energy of the α-particle. The reaction rate of the fusion reaction depends on the temperature: in the case of the D-T reaction the maximum is reached at temperature of the order of tens keV. This implies that the deuterium and tritium nuclei must be "heated up" to temperature of the order of 10^8 K by means of an auxiliary external heater, through Radio Heating systems, to start the fusion reaction: this produces a large number of neutrons, but it requires a supply of tritium. This element is not present in nature, because it is radioactive and has a half-life of 12.26 years. The most favourable chemical element that can be employed to produce tritium is lithium. In nature, lithium is present in the following forms: 7.4% ${}_3Li^6$, that produces tritium and releases energy, when reacting with a slow neutron; and 92.6% ${}_3Li^7$, that produces tritium and energy, when reacting with a fast neutron (Freidberg, 2007).

Nuclear fusion presents several advantages over fission, which include reduced radioactivity in operation and in waste, large fuel supplies, and increased safety (European Commission. Directorate General for Research., 2004). Moreover, it is a literally endless source of energy. Deuterium can be extracted from water (which is a well-known technology), and lithium can be mined. The actual reserves of these two elements can satisfy the world energy demands for millions of years. The most promising configuration for electrical energy production from fusion is the tokamak that is under study in different countries. The concept of the tokamak is based on the magnetic confinement of the plasma. The fusion reaction takes place in a toroidal camber and the plasma is confined by means of high magnetic field. Nowadays, all the tokamaks have been built to study the physic of the fusion reaction and not to produce electric power. Several fusion experimental devices are operating or under construction in Europe. The aim of the Europe fusion research is to produce electric power from fusion until the 2050. The roadmap toward this goal relies on three devises: Joint European Torus (JET), International Thermonuclear Experimental Reactor (ITER) and a demonstration reactor called DEMO. JET is a pure scientific experiment even if it is currently the world's largest magnetic fusion device. It was the first tokamak to generate an amount of fusion power equal to the energy given in input to start the fusion reaction. It is the only experimental machine that can use tritium and now its experiments are devoted to the validation of the ITER choice and operation. DEMO is expected to be the first fusion plant able to supply electrical energy to the grid. The ultimate goal of the DEMO is to prove the competitiveness of the electricity made by fusion power plant (Alzbutas and Voronov, 2015).

ITER is now under construction at Cadarache (France), under an international collaboration between seven-member entities (i.e., China, the European Union, India, Japan, Korea, Russia and the United States) (Ikeda, 2010). ITER aims to make the transition from experimental studies of plasma physics to full-scale fusion power plants. It has been designed to demonstrate the fusion reaction can be used to extract more energy than that used to initiate it. In particular, the input power of ITER will be of 50 MW and the design output power is set to 500 MW. Nevertheless, no electricity will be generated with ITER.

Nuclear fusion reactors will use superconducting (SC) magnets to generate a powerful magnetic field needed to confine the plasma in the shape of a torus, where D-T fusion reactions occur at a temperature of the order of 10^8 K. On the other hand, all the SC coils need to be cooled at cryogenic temperatures in order to avoid the quench of the magnets (i.e., the loss of their superconducting state) during operation: for example, the ITER SC coils are cooled by supercritical helium (SHe) at a pressure of 0.5–0.6 MPa and temperature of about 4.5 K (Mitchell et al., 2008). In ITER, the magnet system consists in 18 Toroidal Field (TF) coils and 6 Central Solenoid (CS) modules, made in Nb_3Sn, and 6 Poloidal Field (PF) and 18 Correction Coil (CC) in NbTi (D'Amico et al., 2016; Mitchell et al., 2012, 2008). The superconductive properties of the coils depend by three parameters: the temperature of the strands, the current density that flows in the SC and the magnetic field in which the SC is immersed. Dedicated cryogenic cooling loops remove the heat load from the magnets, releasing it to saturated liquid helium (LHe) pools, acting as thermal buffers in the transfer of the load to the refrigerator (Hoa et al., 2012; Zanino et al., 2013b).

In this thesis, we focus on the ITER CS. The CS assembly is formed by six independent and modules and the General Atomics (GA) is under contract for the construction of seven modules, six plus one spare being the modules interchangeable (Smith et al., 2013; Spitzer et al., 2015). The facility for the construction of each CS Module (CSM) is located in Poway, CA: it has been designed to manufacture and test the CSMs. Before starting the production of the modules, a mock-up coil is realized, without superconductive magnet, to assess the capability of the facility to effectively complete the necessary tests. A first set of tests is conducted at room temperature, whereas a second set is carried out at 4 K: to this aim, a proper cryogenic cooling circuit has been designed, in which the SHe flows and cools down the CSM. The time needed cool down time the CSM is approximately 14 days (Schaubel et al., 2017).

The safety of nuclear fusion systems has to be proved and verified by a systematic analysis of the system behaviour under normal transient and accidental conditions (Perrault, 2016; Rivas et al., 2015; Taylor and Cortes, 2014; Wu et al., 2016), for two main reasons. First, the presence of radioactive sources (e.g., tritium and materials activated by the neutrons produced by the fusion reactions) imposes a careful study to avoid the contamination of the workers, the public and the environment (Taylor et al., 2017; Taylor, 2016). Second, in view of the cost of the SC magnet system its protection and integrity should be guaranteed (Mitchell et al., 2012, 2008).

One challenge to the related safety analyses is that the operation of tokamaks presents complex dynamic features, as it is based on the transformer principle. In particular, they employ SC magnets, a subset of which operates with *variable* current to generate one of the components of the magnetic field needed to confine the plasma in the chamber where nuclear fusion reactions occur (Zohm, 2015). In this respect, the classical *static* approaches traditionally used in safety assessments (e.g., Fault Trees-FTs and Event Trees-ETs) have limitations in treating dynamic variations that usually occur during the operational time of a process (Khakzad et al., 2012) due to: (i) stochastic disturbances (e.g., equipment failures), (ii) deterministic plant responses (i.e., transients), (iii) controls, and (iv) operator actions (Vorobyev and Kudinov, 2011). The *order* and *timing* of failure events occurring along an accident scenario, the

magnitude of failures and the *values* of the process variables at the *time* of event occurrence are critical in determining the evolution of the system response (Aldemir, 2013; Kirschenbaum et al., 2009; Turati et al., 2018, 2017; Zio, 2014; Zio et al., 2010; Zio and Di Maio, 2010; Zio and Maio, 2009). The static ET/FT approaches (where the order of events is *pre-determined* by the analyst based on his/her experience and the failure magnitude is always set to the *most conservative* value) are not capable of capturing these aspects and may fail to identify and analyze vulnerable sequences, which would, then, remain uncovered (Zio, 2014).

In this thesis work, in order to address the above mentioned issues, the Integrated Deterministic and Probabilistic Safety Assessment (IDPSA) framework (Di Maio et al., 2016) has been embraced, which combines (*deterministic*) *phenomenological* models of system *dynamics* with (*probabilistic*) *stochastic* process models. The IDPSA methodology is here used, for the first time to the best of the author's knowledge, to analyse the response - to abnormal transient conditions - of the cooling system of a SC magnet, namely a single ITER Central Solenoid Module (CSM) in the GA (cold) test facility (Spitzer et al., 2015). In particular, the interest is in identifying the failures that may lead the system into a Loss-Of-Flow Accident (LOFA). Two different operative conditions have been considered corresponding to the two different current scenarios analysed. In the first case, a constant current is given in input to the CSM, whereas in the second scenario the current that flows in module is equal to the ITER-like cycle. The 4C code (Savoldi Richard et al., 2010), developed at the Politecnico di Torino, is employed for the (deterministic) simulation of the system behaviour, taking advantage of its capability to simulate both the magnet system and the refrigeration circuit. Multiple Value Logic (MVL) is adopted for the description of the components failures (Garribba et al., 1985). The MVL allows describing that the components can fail at any time along the scenario, with different (discrete) magnitudes (Di Maio et al., 2015; Zio, 2013).

The MVL theory has been used for accurately modelling the behaviour of the system, where timing and sequences of component failure events can be critical in determining the system failure mode. In fact, MVL theory increases the limited description capability of binary variables in real cases, and components can thus be in different states of operation. Nevertheless, there is a combinatorial explosion of scenarios generated that must be analysed and post-processed to get relevant information on the response of the system to the different states of the components. To post-process the scenarios, clustering algorithms are typically adopted. Clustering entails grouping (in an unsupervised manner (Baraldi et al., 2013)) different scenarios in different clusters combining information from both the event sequences and the patterns of evolution of the process variables. Several clustering algorithms have been proposed and used in practice, like Fuzzy C-Means (FCM) (Bezdek, 1981) and Symbolic Aggregate approXimation (SAX) (Lin et al., 2003) to find prototypical behaviors of systems working in abnormal conditions (Di Maio et al., 2012, 2011), and Spectral Clustering (Von Luxburg, 2007), typically used for fault diagnostics (Baraldi et al., 2013). In this thesis work, the capability of Spectral Clustering to deal *also* with the (unsupervised) identification of prototypical behaviors of abnormal transients and the most relevant among them is also shown.The proposed methodology has been applied to the above mentioned ITER CS module working in two different operating conditions: in the first, a constant current flowing in the module is assumed for the sake of simplicity, with the main aim of proving the capabilities of the approach developed; in the second, the real ITER-like current scenario is analyzed to validate the methodology and derive some preliminary insights on the safety of the ITER reactor in the presence of abnormal transients. In both case studies, the following steps have been undertaken:

1. a set of N different scenarios is randomly generated by MVL;

2. for each scenario, the corresponding dynamic behavior/response of the system (i.e., the simplified cooling circuit of the ITER CSM) is simulated by the 4C code, the cooling helium pressure at the inlet and outlet, the hot-spot temperature of the strands and the voltage (substituted, in the ITER-like current scenario, by the ratio between the current flowing in the CSM and the critical current) have been monitored during each transient;
3. the scenarios thereby generated are *grouped* by means of the Spectral Clustering according to a measure of similarity between them, in order to characterize the principal patterns of system evolution (Al-Dahidi et al., 2015a; Alpert and Yao, 1995; Baraldi et al., 2013; Von Luxburg, 2007). The performance of the Spectral Clustering in this task is also compared with that of ESAX (Butler and Kazakov, 2015; Lin et al., 2003; Lkhagva et al., 2006). To analyse and compare the clustering algorithms performances, the Silhouette and Davies-Bouldin indexes (Davies and Bouldin, 1979; Rousseeuw, 1987) have been used to quantify the similarity of the data belonging to the same cluster and the dissimilarity to those in other cluster and the ratio of the within-cluster and between-cluster distance, respectively. The obtained clusters are assumed as the "prototypical behavior" of the system in abnormal condition and, therefore, used to spot out important safety insights, e.g., the most relevant components failures that lead the system into a LOFA.

The thesis is organized as follows. In Section 2, a general overview of ITER with details on the single ITER CSM in the cold test facility is presented together with the corresponding simulator. In Section 3, the literature review of previous safety work applied to the fusion systems is presented together with the concept of Deterministic and Probabilistic Safety assessment. In Section 4, the Integrated Deterministic and Probabilistic Safety Assessment (IDPSA) and its necessity is explained together with detailed explanation of the three steps followed. In Section 5, the methodologic procedure is applied to a reference simplified case, in which a constant current flow in the CSM, and the corresponding results are illustrated and critically analysed. In Section 6, the methodologic procedure is applied to a more realistic case study, considering the ITER-like current scenario, and the results are shown and commented. Finally, conclusions are drawn and summarized in Section 7.

2 Description of the system

ITER (Figure 2.1, left) is the most important facility, actually under construction, with the aim to demonstrate that it can be achieved a fusion gain, i.e. the ratio between the power extracted from the fusion process and the power given in input to start the reactions, $Q = 10$. One of the most important components are the magnets; they must form, control and drive the plasma generating extremely high magnetic fields. Superconductive magnets are needed to produce magnetic fields of the order of 1-10 T.

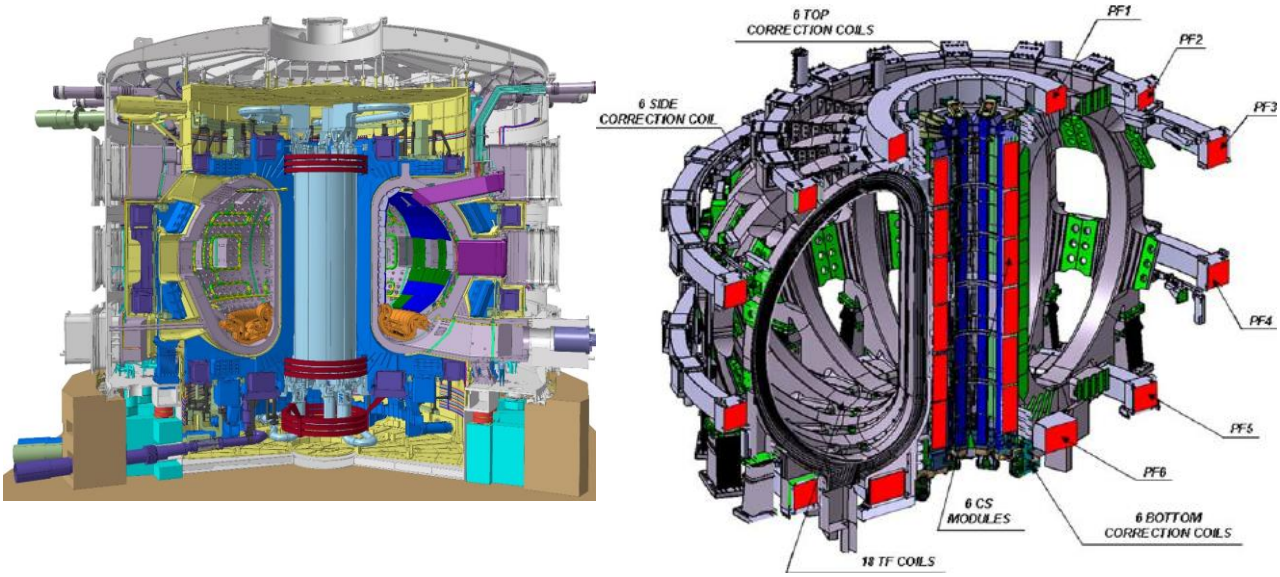

Figure 2.1 A cutaway of ITER (left [source https://www.iter.org/]); The ITER magnet system (right [Ref. (Knaster et al., 2011)]

In ITER, there are four different types of magnets (Figure 2.1 right): 18 Toroidal Field coils (TF), the Central Solenoid (CS), 6 Poloidal Field (PF) coils and 18 Correction Coils (CC) (Knaster et al., 2011; Mitchell et al., 2012).

The TF coils and CS are made by Nb_3Sn, the PF and the CC coils are in NbTi. The supercritical helium cools down the coils at an inlet temperature of 4.5 K. This temperature provides good heat capacity of the helium flow and it guarantees that both the operating point of the Nb_3Sn and the NbTi fall in the zone in which it is assured the desired magnetic field. The difference is in the performance request to the different coils: the TF coils and the CS must produce the higher value of magnetic field carrying the higher values of current. For the PF and CC coils, instead, a cheaper material can be used due to different operative requirements. Multiple monitoring and protections systems are built into the design to limit the effect of magnet faults on the machine availability due to difficulty of repair; some examples are inherent feature, testing system when plasma pulsing is interrupted and detection/monitoring systems. From the safety point of view, the magnets withstand high forces and contain high stored energy that may lead to the damage of neighbouring systems like the tritium confinement barriers.

The conductors are Cable-In-Conduit Conductors (CICCs) with a circular multistage cable consisting of approximately 1000 strands cabled around a small central cooling tube with a spiral wall. In the case of the TF coils, the cable is contained in a circular jacket, instead for the other coils it is in a jacket with an outer square section. The TF coils, in which a maximum

current of 68kA flows, generating 11.8 T, determine the toroidal contour of the machine, having a characteristic D shape (Figure 2.2). The case is the main structural components of this magnet system and it encloses the winding pack.

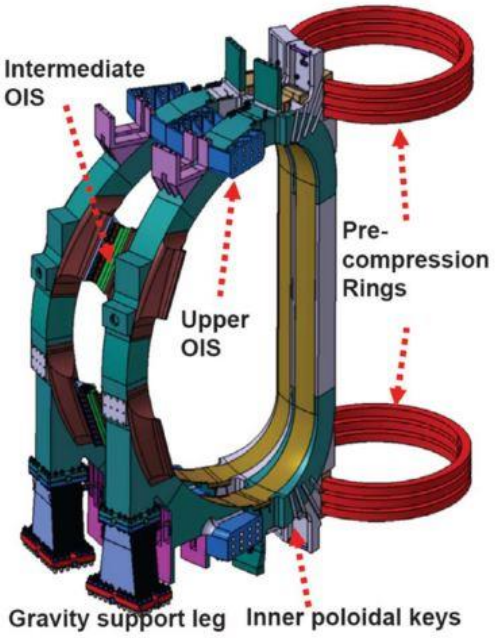

Figure 2.2 Two TF coils and the pre-compression rings [Ref. (Mitchell et al., 2008)]

The six PF coils, in which a current of 45-55 kA flows generating a peak field of 6.0 T, are attached to the TF coil cases with flexible plates or sliding supports to allow radial displacements. The position and sizes have been optimized to satisfy the plasma requirements. The CCs use a reduced size conductor, with a nominal current of 16 kA, with about 300 strands and without the central cooling channel. Three independent sets of CCs are located outside the TF coils and mounted on their cases. In each set, six coils are arranged around the toroidal circumference above (top CC), at (side CC) and below (bottom CC) the equator of the tokamak (Figure 2.3 right). Pairs of coils on opposite sides of the machine are connected in series. The function of these coils is to correct the toroidal asymmetry in the positioning errors in the TF, PF coils and CS (Mitchell et al., 2008).

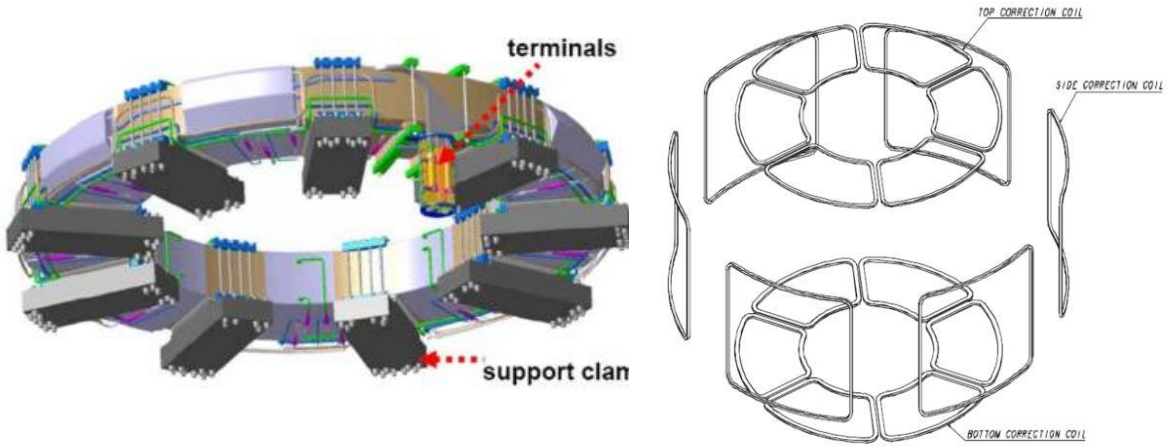

Figure 2.3 One out 6 PF, in particular PF6 (left); The 18 CC (right) [Ref. (Mitchell et al., 2008)]

The CS assembly consists of six independent modules vertically stacked, supported from the bottom of the TF coils through its pre-load structure. The number of modules has been selected to meet the requirement on the plasma shaping (Mitchell et al., 2008). The CS Modules (CSM) use a square section jacket which is self-supporting against the radial and vertical magnetic forces. Each module (called from bottom to top CS3L to CS3U) is identical and independently operated; the assembly has a diameter of 4.3 m and its height is more than 16 m (Figure 2.4, left).

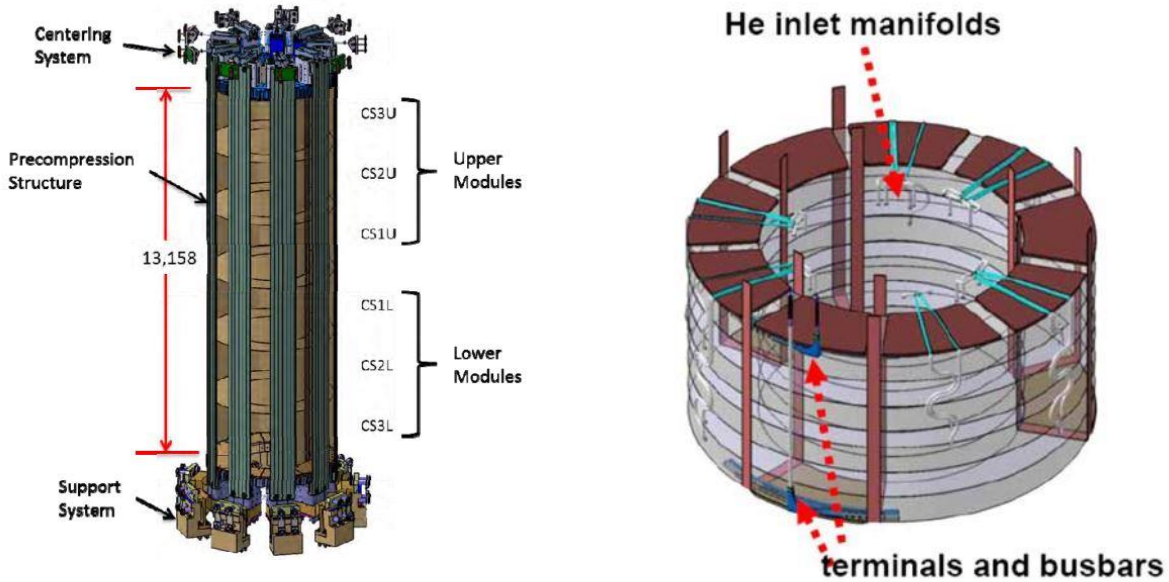

Figure 2.4 The CS assembly (left) [Ref. (Everitt et al., 2013)]; A CSM (right) [Ref. (Mitchell et al., 2008)]

The CS is a key component in ITER providing the inductive power to initiate and sustain the plasma current, shaping and limiting the plasma. It has been designed by a collaboration between the US ITER Project and the ITER Organization. The CS conductor has two design conditions: the initial magnetization and the end of burn (Everitt et al., 2013). In the former condition, a current of 40 kA flows in all the modules generating a peak field of 13.0 T. In the latter operational condition, the current is concentrated in the central CS generating a lower

magnetic field with a peak value of 12.5 T, but requiring a higher current 45-46 kA. The conductor design is a compromise between the two conditions. The modules, fully identical and interchangeable, are pancake wound with 40 pancakes and 14 turns per layer. The CSM is made from seven separate winding requiring six joints. The 40 layers are constructed from six hexa-pancakes (HPs) and one quad-pancake (QP) resulting in 7 pancake-wound conductors, namely 6 hexa-pancakes and 1 quad-pancake; the winding arrangement minimizes the number of joints at the outer diameter. Each pancake is cooled in parallel, resulting in 40 parallel cooling channels per module. All the pancakes of each module are electrically connected in series through suitable joints (Libeyre et al., 2016). The HPs and QP are linked using a six-petal splice joint, located at the module outer diameter and embedded within the winding pack. At both ends of the module winding, the conductor direction is changed from horizontal to vertical, and the outer shape of the jacket from square to circular such a way no parts of the module exceed the outer dimeter. The helium is supplied from the ring header to the module through isolation voltage breaks to 20 supply inlet bosses welded to the inter turns of the module. Two different conditions must be simultaneously satisfied: the high field regions cooled by the coldest helium through inner bore between each double pancake and it must be guaranteed a good distribution of helium in the six subcables (called petals) of each conductor. Local reinforcement must be placed in the inlet region to allow the opening in the conductor jacket without excessive stress intensification. The outlets are close to the crossover regions between pancakes. The requirements on stress and flow distribution at the outlet are less severe resulting in a simpler design than the inlet.

The General Atomics (GA) of San Diego has been awarded a contract by the US ITER to develop, design and build the CS modules. The GA has established a fabrication facility in Poway, CA (Smith et al., 2013). The system chosen in this work is the cooling circuit of one Central Solenoid Module (CSM) in the reference facility. The 4C thermal hydraulic code (Savoldi Richard et al., 2010) has been used here to model both the coil and its cooling loop.

2.1 Description of the facility

GA is currently under contract to fabricate the ITER Central Solenoid Modules. In particular, the contract includes the design and qualification of manufacturing processes and tooling necessary to fabricate seven superconducting CSM (6 + 1 spare) that constitute the ITER Central Solenoid (Spitzer et al., 2015). The CICC has been manufactured by the ITER Japanese Domestic Agency (JADA) and shipped to GA in two sizes: the longest one is used to form the hexa-pancake and the shorter for the realization of the quad-pancake. In the first stage, it is scheduled the construction of a mock-up coil using dummy (without superconducting) conductors before to initiate the realization of the seven modules. The JADA is also responsible of the production of the dummy coils that must be shipped to the facility, to build the mock-up coil: this is the final qualification step necessary to validate the processes and tools before to start the manufacturing procedures of the Module 1. The mock-up coil and the CSM are processed identically expect the former has only 16 layers instead of 40. Ten workstations have been designed and manufactured to produce the CSM in 22 months:

i. Conductor Receiving: the CICC is received at the GA facility, it is inspected and prepared for the winding;

ii. Hex/Quad Pancake Winding: is the winding station where the conductors are wound into the hex/quad pancakes, each one formed by fourteen turns;

iii. Joint Preparation Station: a length of the jacket is removed from the superconducting cable in preparation to make the joints;

iv. Joining Station: the superconductor is joined together;

v. Reaction Heat Treatment Station: the coil must be heat treated to react the cable into a superconducting material. This process occurs at 650 °C for 200 hours with an allowable temperature difference of 10 °C;

vi. Turn Insulation Station: after heat treatment, each turn must be separated (staying within the strain limits), insulated and then rebuild the coil as it was originally. These operations must be done carefully because, after the thermal treatment, the CSM is strain sensitive;

vii. Ground Insulation Station: the ground insulation is manually applied to the external surface of the CSM;

viii. Vacuum Pressure Impregnation (VPI) Station: the insulated coil is impregnated with a two-part resin. The impregnation starts with the installation of metal panels to the vertical surface of the coil. The outside panels became part of the coil and the inner parts are removed after the resin is cured;

ix. Piping station: the coil is inverted and insulated helium pipe assemblies are welded in place and it is performed a helium leak check of each joint after the welding.

x. Final Test Station: it is carried out a two-step process at different temperature. First is at room temperature and the second step is at 4K. The more extensive tests are realized to the first module to confirm the design than modules 2-7. In the Table 2.1 it is reported the list of the full tests planned for the mock-up and the seven CSMs.

Table 2.1 Comparison of the test for the Mock-up and CSMs. [Ref. (Spitzer et al., 2015)]

Test	**Mock-up**	**CSM 1**	**CSM 2-7**
Room temperature test			
Global leak test at 3 MPa	X	X	X
Paschen test (30 kV)	X	X	X
Cold tests			
Cool to 4K	X	X	X
Charge/Discarge cycle (full current)		X	X
Joint/terminal resistance measurement		X	X
Current sharing temperature measurement (10 double pancakes)		X	
AC loss measurements (10 double pancakes)		X	
Ten charge/discharge cycles		X	
Current sharing temperature measurement Test 2 (10 double pancakes)		X	
Global leak test at 3 MPa (4K)	X	X	X
Final Room Temperature tests			
Global leak test (3 MPa, 4K)	X	X	X
Paschen test at RT		X	X
30 kV Hi-Pot test		X	X

During the tests, the facility and the CSM will be operated in two different regimes, briefly described as: a cold mode standby operation (e.g. during night or weekend), when the CSM is not charged and kept at about 4 K; no dangerous transients are expected from a LOFA in these conditions, so this regime is not analysed here. The regime of interest is the cold mode

experimental operation (i.e. during tests), when the CSM is charged at full or partial current. In this case, an accidental temperature increases up to (or above) the so-called current sharing temperature T_{CS} may lead to a quench, i.e., to a loss of the superconducting state. The T_{CS} is defined as the temperature, above which the current starts to flow also in the copper matrix of the SuperConductive (SC) strands and in the pure Cu strands, developing a non-zero voltage and causing Joule heat generation in the cable. The heat deposition can induce thermal stresses that may seriously damage the conductor, causing a degradation of its performance or, in the worst case, the loss of integrity of the conductor. The presence of a normal (non-SC) zone and, to some extent, variations in the conductor temperature above T_{CS} can be detected by measuring the voltage at the extremities of each pancake.

In the facility, it can be distinguished two main components: the He refrigerator, to cool down the supercritical helium to the necessary temperature, and the test chamber, where the module will be put into a cryostat. In addition, several manifolds, pipelines, heat exchangers (HXs), control valves (CVs) of the cryoplant and a liquid He (LHe) thermal buffer will connect the refrigerator to the coil, and a dedicated power supply system will provide a current up to 50 kA. In Figure 2.5 it is shown a scheme of the cooling circuit of the test facility. It can be noticed the CSM and the different components installed to perform the planned tests.

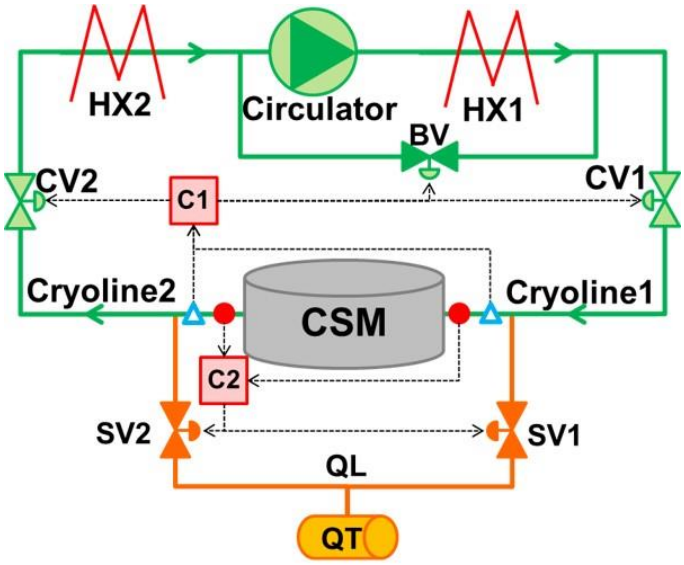

Figure 2.5 Scheme of the SHe cooling loop of the CSM. Solid red circles are pressure taps, open cyan triangles are flow meters (see the text for other abbreviations).

Focusing on the hydraulic path followed by the cooling helium, after the Circulator, a Centrifugal Pump (CP), the SHe is cooled down in a first heat exchanger (HX1) to remove the heat generated in the pumping process. It arrives at the inlet of CSM through the CV1 that is nominally open and the supply line (cryoline 1), then it flows in the 40-hydraulic path of the coil and removes the heat that is generated inside the module. At the CSM outlet it returns at the circulator passing through the return line (cryoline 2), the CV2, fully open at normal operation, and the second heat exchanger (HX2).

There are also present other three pipelines designed to counteract the foreseen malfunction of the system: the first is the by-pass line. It connects the outlet of the HX2 and the outlet of the HX1 through the By-pass Valve (BV). This has the function, opening and then equalizing the pressure at the circulator suction and discharge, to prevent any damage of the pump as fail-safe condition. The other two additional pipelines are the quench lines (QLs) that discharge the

helium in the quench tank (QT). The QT is isolated from the cryolines by the Safety Valves (SVs) that are normally closed. These are open in case the pressure at extremities of the CSM exceeds a certain safety threshold, i.e. 1.8 MPa, in order to avoid damages to the conductors. In add, two controllers, C1 and C2, are present: the C1 is connected to two flow meters, one at the inlet and one at the outlet of the CSM, and the C2 to pressure taps, located at the same position.

2.2 The 4C code

The Cryogenic Circuit Conductor and Coil (4C) (Savoldi Richard et al., 2010) code has been developed at the "Politecnico di Torino" as an evolution of the Mithrandir (Zanino et al., 1995) and multi-conductor Mithrandir (M&M) code (Savoldi and Zanino, 2000a).

The Mithrandir is a 1-D, two-fluid model in which the helium can flow in both the two regions of Cable-In-Conduit Conductor (CICC) as chosen for the superconducting magnets that constitutes the CSM. The helium in the cable bundle and the hole can have different velocities and different thermodynamic state. One fluid is coupled with the other, by means of mass, momentum and energy exchange, and with the jacket and conductor strands, with the convective energy transport. Jacket and strands can be heated by an external heater and/or by Joule effect, computed with a simple resistive model. The code solves the flow of low temperature supercritical helium taking advantages of the two following assumptions: being the transversal size of the conductor much smaller than its length, it assumes a one-dimensional treatment of the properties and the equations are derived from the 3-D case by appropriate averaging over the cross section.

The main limitation of the Mithrandir code is that it considers just one conductor. In the real systems there are more conducts coupled together. To overcome this problem the M&M code has been developed where an arbitrary number of one or two-channel CICCs are treated in a Mithrandir-like fashion. In (Savoldi and Zanino, 2000b), three validation cases are presented for the M&M code. It is recalled, for the importance to this work, the validation with respect to the heat exchange between petals in a Central Solenoid Module Coil-like (CSMC) conductor. In (Savoldi and Zanino, 2000a), the M&M code has shown good agreement with the experimental result in the evaluation of the current sharing temperature in the ITER CSMC.

Using the 4C code, thermal-hydraulic simulations of the entire ITER magnet system can be performed, with particular reference to the CICCs, the structures and the refrigeration circuit (Savoldi Richard et al., 2010). In (Zanino et al., 2010), it has been studied the quench analysis in the ITER Toroidal Field (TF) coil where the accuracy of the results it is guaranteed by the suitable convergence studies. In (Zanino et al., 2011) it can be found the first step of the 4C code validation against the standard 25 kA safety discharge of the ITER Toroidal Field Model Coil. In (Zanino et al., 2013b), the 4C code is applied to the HELIOS facility and a very good agreement is found between the computed and the experimental results and in (Zanino et al., 2013a) it is validated against the experimental data.

In the case study of this thesis work, the focus is posed on CSM under construction and the corresponding cooling circuit, simulated using the 4C code. In particular, the detailed CSM model solves the 1D transient mass, momentum and energy conservation equations. The temperature, pressure and velocity distribution are computed in each of the two regions (cable bundle and central, low impedance channel) of each pancake, as described in details in (Zanino et al., 1995). Then, the inter-turn and inter-pancake thermal coupling between adjacent turns and pancakes, respectively, is computed considering the insulation as a thermal resistance to evaluate the heat transfer between neighbouring conductors (Savoldi and Zanino, 2000a). In addition, the code solves the 1D mass, momentum and energy equation for compressible flow

in the cryolines and HXs. For the valves it assumes adiabatic and isenthalpic flow with standard equation for compressible fluid valves. In the pump, it is assumed an ideal isentropic transformation, with the real hydraulic characteristic. The helium bath, finally, is modelled as a fixed temperature source. Each of these components is expressed in terms of differential and algebraic equation, further details will be discussed in Section 2.3.

2.3 Description of the simulator

To model the behaviour of the superconductive magnet and the cooling circuit, the validated 4C thermal hydraulic code has been used. In the follow, there is a brief description on how the components are modelled in the code of the simulated cooling circuit, shown in Figure 2.6, as described in (Zanino et al., 2012).

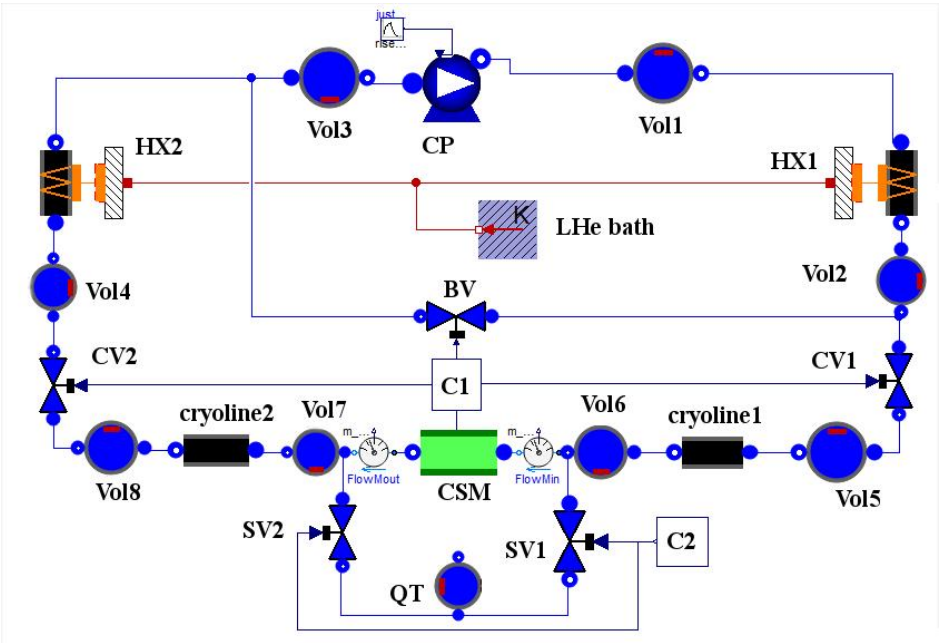

Figure 2.6 Scheme of the simulated cooling circuit

«The single-phase flow of helium [inside the cryoline] is described by a 1D finite-volume discretization of the mass, momentum and energy balance equations». The diameter of the two cryolines is set equal to 46 mm, the friction multiplier is $1 \cdot 10^{-5}$ and the length is 28 and 24 m for the cryoline1 and cryoline2, respectively.

«The helium bath is modelled by dynamic mass and energy balance equations, assuming perfect phase separation and thermodynamic equilibrium between the two phases». In this approach it has been supposed that the temperature of the bath is at the constant value of 4.5 K.

«The volume model contains the dynamic mass and energy balance equations for a homogeneous fluid». In Table 2.2, the initial conditions are shown for these volumes. The Vol3 and Vol1 represent the inlet and the outlet of the CP, respectively; their dimensions are bigger than the other volumes that are assumed arbitrary small, in order to account for additional dead volumes in the circuit.

Table 2.2 Initial conditions for the volumes.

Vol#	Volume [m^3]	Pressure [MPa]	Temperature [K]
1	10^{-1}	0.42	4.5
2	10^{-4}	0.42	4.5
3	10^{-1}	0.345	4.5
4	10^{-4}	0.345	4.5
5	10^{-4}	0.42	4.5
6	10^{-3}	0.42	4.5
7	10^{-3}	0.345	4.5
8	10^{-4}	0.345	4.5

The Quench Tank can be modelled as a volume and in Figure 2.6 it is indicated as QT. No information is available on the QT, pressure and temperature of this component in the facility chosen and guess values were used for this work. For the two different configurations analysed, two different initial conditions are imposed on the pressure and volume QT; the temperature is fixed at 300 K during all the simulations made. In the first part (exposed in detail in Section 5), the pressure is set equal to 0.42 MPa and the volume is 50 m^3. Nevertheless, it is found out that if the SVs are open, due to a failure, when the pressure at the ends of coil is lower than the set-point it can be realized a back-flow of helium from the QT to the circuit; in particular, this happens if the pressure at the inlet of the SV is lower than the outlet. To limit the case in which these situations can be occurred in the second part of the work (exposed in detail in Section 6), the pressure of the QT is reduced to 0.35 MPa and the volume is set equal to 10 m^3; the volume reduction is needed because in the ITER-like current scenario the pressure at the inlet and outlet of the CSM is higher and in case of opening of the SVs, the helium goes from the cooling loop to the QT and it is lost, i.e. it cannot come back to the cooling loop without an external action. But if the QT has a lower capacity, a lower quantity of helium is lost because a lower amount can be stored in the tank and it is lower the time need to equalize the pressure between the QT and the circuit.

In order to model the valves, «the flow-vs.-pressure-drop correlations are taken from the ISA S75 – IEC 60534 norms for control valves using compressible fluids. An isenthalpic transformation is assumed for the time being». The length of the valves is set equal to 0.2 m. The CVs and the BV have a flow area set equal to $3.46 \cdot 10^{-3}$ m^2. The flow area of the SVs is not set constant during the two-different tests-phases taking into consideration in this thesis work. In the first part, when the current that flows in the magnet is constant, the flow area is set equal to the value used for the other valves, instead in the second part it is reduced of one order of magnitude, i.e. $3.46 \cdot 10^{-4}$ m^2. This choice is related to the pressure values chosen for the Quench Tank. The valves are driven by two different controllers: the controller C1 measures the mass flow rate and takes decision. If the mass flow rate falls down under a certain value (in this approach, the 10% of the nominal mass flow rate), for a certain time, called validation time (here set equal to 1s) (Savoldi et al., 2018), it changes the state of the CVs and BV. The SVs are driven by the controller C2 that is a PID (with gain = $1 \cdot 10^{-7}$ Pa^{-1}, integration time = 0.2s, derivation time = 1s), with set-point 1.8MPa (Savoldi Richard et al., 2012). The controller paraments and set point are chosen equal to ones assumed in (Savoldi et al., 2018). The change of state of the valve happens in 1s and it has been used the convention for which if the state is set equal to 0 the valve is closed instead the valve is open if the state is equal to 1. The inherent flow characteristic implemented in the modelling of the valves is the fast opening and the calibration curve it is represented in Figure 2.7.

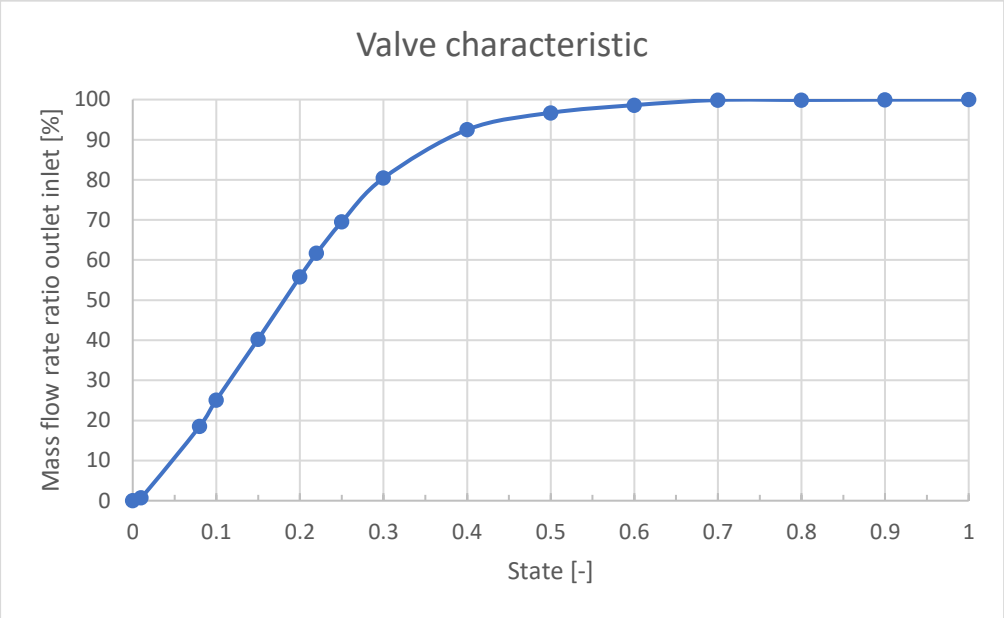

Figure 2.7 The inherent flow characteristic implemented in the modelling of the CVs, BV and SVs

This is a typical choice in case for on/off valves (Fisher, 2017). It can be noticed that to reduce to half the ratio between the mass flow rate at the outlet and the inlet, the state of the valve is equal to 0.18. The flow coefficient, the number of cubic meter per hour that will flow through a valve with one bar pressure drop, is set equal to 71m^3/h.

A real characteristic of the CP has been implemented as descripted in detail in (Zanino et al., 2013b). The length of the circulator is set equal to 0.2 m, the nominal mass flow rate is 0.32 kg/s and the flow area is $3.46 \cdot 10^{-3}$ m^2.

The two HX models are obtained «by the connection of the pipe model with a model of the convective heat transfer at the external pipe wall surface». It has been assumed that the HXs are composed by 11 parallel pipes with a diameter of 20 mm and a length of 31m. The friction multiplier is $1.5 \cdot 10^2$ and the wetted perimeter is 10^5 m. To the primary side of the HXs flows the SHe used to cool down the coil instead at the secondary side there is the LHe from the bath. It is supposed that the wall of the HXs are at the temperature constant of 4.5 K.

2.3.1 LOFA

The coils chosen as superconductive magnet in ITER gain the superconductive properties if they are immersed in a proper magnetic field, in its inside flow a specific current and are maintained a proper temperature. These three conditions must be verified at the same time. In the three-dimensional space of the magnetic field, current and temperature of the coil, it can be identified a limit curve that divides the space in two regions: one, inside the limit curve, in which the coil is operating as superconductor and the other, outside of the limit curve, where it losses these properties. In the 4C code, the current that flows in the magnet and the corresponding magnetic field generated are given as input instead the temperature of the supercritical helium and the coil are computed at every time step. These mean that during the normal operation the variation of the temperature is the only way to cross the limit curve and bring the conductor out of the superconductive region. It can be realized how much it is important to cool down properly the magnet in order to maintain the superconductive properties

of the CSM. In addition, if the temperature in the coil increases rapidly, it can happen that the temperature current sharing is reached and the quench starts. In the worst cases, if the quench is not detected, severe damages are foreseen and they can bring to the losses of the CSM due an increase of the dimension too fast. To reach the goal it is needed a proper mass flow rate of SHe to cool down the coil in all the operational phases. To monitor the mass flow rate, two ideal flow meters are present at the inlet and outlet of the Central Solenoid Module. The Loss Of Flow Accident is defined as the condition for which there is the loss of the pumping power, the coolant becomes stagnant and the consequence cooling capability is lost. This scenario must be avoided to guarantee the integrity of the CS during both the test procedure, like this facility and the object of this work, and the normal operation of ITER. A LOFA can be triggered by different initiating events that can lead to a total LOFA, in which almost 100% of the flow is lost, or a partial LOFA with a limited reduction of the flow. It has been assumed in this work, the total LOFA occurs in the case in which the mass flow rate at the inlet and the outlet of the CSM is lower than the nominal mass flow rate divided by a factor k sets equal to 10. The same approach can be found in (Savoldi et al., 2018). When the LOFA is detected, the control system implemented in the simulator is analogous to that adopted in ITER and described in (Savoldi Richard et al., 2017), to the cooling circuit of the Toroidal Field Coil.

The two ideal flow meters located at the ends of the coils send the information to the controller C1. The LOFA is detected when the mass flow rate at inlet and the outlet is lower or equal to the 10% of the nominal mass flow rate, i.e. lower or equal than 0.032 kg/s, for a certain time, called validation time (set equal to 1 s). Then the C1 closes the CVs and removes the current from the coil. The fast and controlled discharge of current from the CSM happens with a ramp of a fixed duration of 30 s independently from the value of the current at the time in which the LOFA has been detected. It must be recall that during the ramp the coil is heated by the AC losses that are proportional to the derivative of the current. At the dump time the BV is opened by the C1 too; equalizing the pressure at the CP suction and discharge, the circulator is in a fail-safe condition and further damages are avoided. From a hydraulic point of view, the cooling loop is divided in two independent part: the first in which is present the CP, the HXs and the BV and the other one in which there is the CSM and the CVs. In this second part there is no more pumping power and the helium is almost still. For sake of completeness, during the discharge, the helium is pushed outward from the coil due to the heat deposition; due to this phenomenon it can be seen an increase of the temperature and pressure in this part of the circuit. If the pressure increases too much the structural integrity of the coil can be lost. To avoid that the SVs can be opened by the controller C2, modelled as a PID, if it is exceeded the safety threshold of 1.8 MPa.

3 Safety assessment of nuclear fusion systems: a critical review of literature

The aim of this thesis work is to address the safety analysis of the cooling circuit of a superconducting magnet for nuclear fusion applications in a reference test facility. The importance of the safety analysis lies in its capacity to confirm the design basis for those items that are important to safety and to demonstrate that the overall plant design can meet the prescribed and acceptable limits. The safety assessment is needed for the licensing and renewing of the plant, its modification and upgrading projects. The safety analysis of nuclear fusion plants/facilities has been already addressed in the literature: both the deterministic and the probabilistic approaches have been undertaken. In Sections 3.1 and 3.2, the basic principles underlying the Deterministic Safety Assessment (DSA) and Probabilistic Safety Assessment (PSA), respectively, are briefly summarized, together with some examples of application to nuclear fusion systems.

3.1 Deterministic Safety Assessment (DSA)

The philosophy at the basis of the deterministic approach is that everything has a cause, and that a particular cause leads to a unique effect. The DSA is a wide-ranging technique intended to demonstrate the robustness of a system to tolerate infrequent faults. It requires a detailed and comprehensive knowledge of how the system responds to faults. The plant states are divided into "safe" (i.e., states of normal operation) and "faulty" (i.e., accidental conditions); the latter can be further subdivided into Design Basis Accidents (DBAs) and Beyond Design Basis Accidents (BDBAs) (historically, this has been done in particular in the nuclear industry) (Modarres and Kim, 2010). The DBAs are a selection of representative accidents, which are expected to occur during the lifetime of the plant or which cannot be excluded following human discretion (i.e., events that - according to the analysts - have a frequency larger than 10^{-6} $year^{-1}$). The design of the plant must be able to counteract the occurrence of such events without leading to unacceptable consequences for the environment. The approach for the selection of the DBAs is the following: all the mechanisms of (safety) barrier failure and all the processes that could cause the failure mechanisms to initiate have to be identified, in order to group all those processes characterized by a similar phenomenology. Once the different groups are available, for each group different possible scenarios should be recognized together with the corresponding initiating event. Finally, the original cause is determined (which can be an internal or external event). The DBAs are the smallest in number and the most representative different scenarios, in which the accidental situations can evolve. In the deterministic view, by hypothesis, the fault occurs with the highest magnitude and the plant state is assumed as the worst possible. In other words, conservative hypothesis are done, in order to prove the capability of the system to withstand the worst credible scenario. The analysis of these accidents is very important, since the design of the plant is done so that the occurrence of such an accident does not lead to unacceptable consequences for the environment.

The BDBAs are instead accidents characterized by multiple failures of the (safety) systems needed to handle the accidents and the occurrence of such events is understood as very unlikely (i.e., with a frequency lower that 10^{-6} $year^{-1}$). In contrast to DBAs, it cannot be excluded that radioactive substances in a harmful amount are released to the environment and no dose limits are defined for the people around the site. Since they are considered as very unlikely events, they are not taken into account in the DSA (Modarres and Kim, 2010).

In the DSA framework, to counteract the accidents, multiple levels of protection are foreseen, leading to the concept of physical barrier and the defence-in-depth. The former consists in the presence of barriers, active or passive, between the radioactive material and the environment and they must be independent from each other. The latter is a principle that applies to both the design and the operation of the facility. The accident may occur, but the systems are designed and installed to combat them and to ensure that their consequences are limited to a level that is acceptable for both the public and the environment. The defence-in-depth principles are applied in four different levels. The first is the prevention and surveillance, i.e. the items of the equipment are designed with adequate safety margins. The second level is protection: the incidents must be detected to prevent them from escalating through mitigation actions. In general, prevention has the priority over the mitigation. The third level is safeguard: special safety systems are designed to limit the consequences of severe accidents to an acceptable level. The fourth level consists in the off-site and emergency procedures to provide protection against the sever accident conditions, under which defences at the three levels described above are proven as inadequate (International Atomic Energy Agency, 2006).

As final remark, the rigour and conservatism is a matter of judgment, but increasing rigour and increasing conservatism is expected as the harm potential and uncertainty increase.

Hereafter, some examples of literature works are shown, where the deterministic approach has been applied to nuclear fusion systems.

In ITER, Current Leads (CLs) will be used to feed the superconductive magnet. The performance of the CLs must be proved both in normal and abnormal condition. In (Heller, 2009), the quench performance and the behaviour of the High Temperature Superconductor current leads (HTS-CL) during a LOFA are analysed. Applying the deterministic approach, it has been proved that the proposed design hardily fulfils the ITER requirements; the methodology is then applied to a new design that has better performance. For the calculations the 1-D CURLEAD code has been used; the results have been validated comparing the computational and experimental data for the specific LOFA run.

The consequence of a short circuit or an unmitigated quench are taken into account in (D'Amico et al., 2016). The objective is to analyse the structural integrity of the TF in off-normal condition by means of a 3D finite element model of the whole TF coil magnetic system. In faulty conditions, a strong asymmetric configuration of the load path, due to the non-symmetric current distribution, could cause severe damage to the structure. Two loading conditions are identified as the most critical for the integrity of the component: a short circuit in one TF coil and a quench in a TF without discharge in the other coils. The safety assessment has proven that the structural integrity of the component is not compromised by any of the loading conditions corresponding to the abnormal scenarios considered. The same 3D finite element model has been also applied in case of verification of the TF coils under construction (D'Amico et al., 2018). The TF coils are under manufacturing and nonconformity-reports and/or deviation requests can be provided by the manufacturers. Nevertheless, it is essential to ensure that the design updates would not jeopardize the mechanical integrity of the system that must be assured both in normal and abnormal condition.

A Loss Of Vacuum Accident (LOVA) is a unique event in fusion reactors. It is a postulated reference event for ITER: it consists in the failure of the penetration line leading to gas ingress in the Vacuum Vessel (VV) causing the termination of the plasma burning. The pressure of the VV increases until is almost equalized with the outside; after the pressure equilibration, due to the heat coming from the hot component surfaces, the air flows out of the VV causing a radiological problem. In (Honda et al., 2000) both the reference LOVA event for ITER and a hypothetical extreme event have been considered to investigate the ultimate safety margin. The

MELCOR code was used for the analyses. Several assumptions have been done on the accidental sequences with the final aim of computing the radiological release in abnormal conditions. It is found that during both the reference and the hypothetical scenarios analysed, the radiological releases are lower than the no-evacuation limit under the conservative weather assumed for ITER.

The other two types of thermal hydraulic accidents in fusion reactors are the Loss Of Coolant Accident (LOCA) and the Loss Of Flow Accident (LOFA). In particular, the former can be further divided into in-vessel (if the coolant interacts with the plasma facing components) and ex-vessel LOCA (when the fluid is discharged into the Heat Transfer System (HTS) vault). In this latter scenario, the plasma is terminated by the fusion power shutdown system, but if the system fails the in-vessel components are heated-up and they may be damaged. In case of excessive over-heating, the in-vessel components melt, resulting in an in-vessel LOCA, which worsensthe scenario. In (Honda et al., 1997), the ex-vessel LOCA in the first wall is analysed by considering impurity release and investigating a passive plasma shutdown scenario. The code used is the SAFALY that describes the plasma dynamics and the thermal behaviour of in-vessel components. The postulated conservative scenario confirms that the plasma can be shutdown passively before the melting of the in-vessel components. Nevertheless, the authors suggest further safety analyses to reduce the uncertainty in the model used.

In (Savoldi et al., 2018) is considered the protected LOFA in the ITER TF coil cooling circuit. The LOFA is initiated by a cold circulator trip modelled as an exponential decrease with a defined time constant that is parametrically varied from 1s up to 10 s. The rotational speed is reduced from the nominal value down to 0 in case of “total” LOFA or to 50% of “partial” LOFA. It has been considered four different cases: three for the total LOFA and one for the partial LOFA. In the first case, the LOFA can happen both at the Winding Pack (WP) and at the structures cooling loop (STR) and the quench is initiated only if the discharge time is long. In the second and third case the LOFA happens only in WP or STR circuit only; in both cases no criticalities are highlighted. Finally, it is considered a forth case in which a partial LOFA happens both in the WP and STR and it is suggested to pay attention to establish detection threshold and strategy to reduce the probability of an undetected accidents.

The deterministic approach is widely used in the first step of the design process to assess the performance of the developing component/system. In (Froio et al., 2017), an in-vessel LOCA is considered and applied to the EU DEMO fusion reactor. This initiating event is a DBA so that it is particularly important to properly design safety barriers that confine the radioactive material. The release of coolant in the VV is considered and the scenario is modelled using the GETTHEM code. Conservative assumptions are made and the scenario evolution is analysed and compared to the results of a validated code. Even in this case, the authors suggest performing parametric studies to understand which parameters are the most relevant to affect the system transient behaviour and identify the most effective counter measures that can be adopted.

3.2 Probabilistic Safety Assessment (PSA)

The use of a more comprehensive methodology than the DSA was suggested for the first time in (Farmer, 1967). According to Farmer, the distinction between credible and incredible accidents is not logical, because it is based only on the expert judgement. The failure probability and consequence are introduced for the first time leading to the concepts of risk. The risk is defined a triplet of scenario, probability of occurrence and consequence. The construction of

any plant implies the acceptance of a degree of risk and there is no engineered system that is risk-free. The object of a safety assessment is to compute the risk of the different scenarios that can arise, to define an upper bound for the risk and to propose suggestions to reduce the risk of the most challenging accidental evolutions, keeping in mind the concept of As Low As Reasonably Achievable (ALARA). The main idea behind the deterministic approach is to address the uncertainties in the system behaviour and modelling by making conservative assumptions. Important consequences of this approach can be found considering the Three Mile Island accident. In fact, the plant was designed following the DSA principles and a Large-Break (LB) LOCA was the DBA of reference. Nevertheless, the core melted because of a Small-Break LOCA. This scenario was not analysed by the analysts, because it had a lower magnitude with respect to the LBLOCA (but the consequence was indeed significant). On the other hand, the conservative assumptions, made during the design process, allowed the physical barriers to withstand to the accident: actually, only a small amount of radioactivity was released in the environment and no detectable health effects were found on plant workers or the public. This accident made clearer that considering only DBAs and conservative assumptions is not sufficient to ensure system safety; the probabilistic approach, thus, became more popular for its capabilities of treating uncertainties, reducing unnecessary conservatism and providing a more complete picture of the risk associated to a system (Modarres and Kim, 2010).

Following the definition of risk, a Probabilistic Safety Assessment (PSA) can be organized in four steps: the first is the identification of the accidental scenario; the second is the assessment of the scenario probability; the third consists in the evaluation of the scenario consequence and finally the risk evaluation (Zio, 2013). A large number of different techniques of literature can be found to address each step: The HAZard and OPerability analysis (HAZOP) and the Failure Mode and Effect Analysis (FMEA) are two alternative methods for the identification of the accidental scenario. The HAZOP is a systematic examination of a planned or existing process in order to identify and evaluate problems that may represent risks to personnel or equipment, or prevent efficient operation. As first, the system must be divided in study node at which the process parameters are investigated with the purpose to identify the functionally independent process units that are between the nodes. Then, for each node it necessary to determine its operation mode and the possible deviation from the nominal behaviour. The results are stored in an HAZOP table. A similar approach is followed applying the FMEA: the system is divided in functionally independent subsystems and it is defined the mission phases and the expected durations. For every mission phase, we define each of the independent units in term of required functions and outputs, expected equipment utilization and performance, internal and external restraints. Finally, a block diagram is constructed and the FMEA table can be compiled: for each component the failure mode, the failure effect, a criticality analysis and suggestions to improve the design of the already embedded barriers are listed. The result of this first step is the identification of the Initiating Events (IE), i.e., the events able to start the accident scenario (Rausand, 2013).

To evaluate the probability of an event (or a sequence of events) the Fault Tree Analysis (FTA) or the Event Tree Analysis (ETA) can be used. The FTA is a deductive logic tree that explains a failure event at level system, called top event, considering the basic events of components failure using appropriate logical operators (AND, OR, NOT, …). Typically, the top event is the negation of the normal operation of the system. The ETA represents a qualitative structure that describes how an accident can evolve. Given an initiating event, the accidental sequence evolves following a branch. Each bifurcation of the tree corresponds to the proper or abnormal functioning of a component/safety countermeasure. The ETA is extremely useful because it permits a qualitatively evaluation of accidental scenario and quantitatively one; in

fact, if it is associated at each bifurcation the probability with which the component works correctly, it can be computed the total probability of each branch (Čepin, 2011).

Proper codes or best practices can be used for the evaluation of the consequence of accidental scenario. For example, flow and transport codes are used with reference to the release of radiation in atmosphere; then, to compute the risk, the results of the codes are compered to limit and it is determined the risk associated to the specific scenario considered.

The uncertainties are treated considering a probability distribution on the results, whose percentiles represent confidence bounds on the results (Nutt and Wallis, 2004). Nevertheless, the results are affected by the uncertainty also in case of the probabilistic approach. The expert judgement is important in the choice of the accidental evolution and the hypothesis done to run the model used to simulate the scenario.

In the following, a review of papers containing the safety analyses of fusion system (according to a probabilistic approach) is presented.

The methodology exposed for the risk assessment has been applied in (Madrid et al., 1983) to the identification of the IE and the evaluation of the risk in case a malfunctioning of the Impurity Control Systems (ICSs) that is responsible for the magnetic confinement of the plasma. In case of accident, it can be safety-consequences, i.e. release of radioactivity in the environment or to the workers, and/or financial consequences. In this application, it has been chosen INTOR as fusion device choice to the risk assessment. The identification of the IEs is the first step required to build a Probabilistic Risk Assessment and at this aim it has been proposed a systematic methodology based on the Master Logic Diagram (MLD). Once the IEs are identified and grouped, the ETA has been used to evaluate the response of the system to each of the four groups identified, for the given case study. The resulting sequences are used to compute the risk.

A similar approach is find in (Xu et al., 2015) applied to the preliminary risk evaluation for the Tritium Extraction System (TES) of the Test Blanket System (TBS) of ITER. To obtain the different failure mode in which the system can diverge from the nominal working condition, the Failure Modes, Effects and Criticality Analysis (FMECA) is applied to the TES, having established the system boundary and the different working condition. The results are used to feed the FTA to get qualitative and quantitative results. The minimal cuts sets (MCS), i.e. the minimum number of the event that satisfy the top event, are identified to extract the information from the results of the fault tree; in particular it can be evaluate the system reliability, the top event failure probability and the consequence risk level. In this way, mitigation action can be suggested to reduce the risk level and assure a more reliable system. The results show that the risk level of the system considered satisfies the requirement of ITER.

A peculiar characteristic of the PSA approach is to take into account also the BDBA. In (Merrill, 2000) is treated the unmitigated quench of a Toroidal Field (TF) magnet even if is considered as high improbable event, i.e. the associated frequency is lower than 10^{-6} event per year. The magnet is predicted to melt in the cases examined but this fail would not result in a public safety concern.

Comprehensive safety analysis code system must be proposed to investigate quantitatively the safety of a nuclear fusion reactor; in (Honda et al., 1994b) is addressed the overpower event caused by the thermal instability of the plasma in ITER that causes the density and temperature changes from nominal steady-state condition. The increase of temperature produces an increase of the fusion power and the damage to the plasma-facing components. It has been assumed to consider a fluctuation ranging from 1% to 15% in the fuel density and external heating. From a safety point of view, the results have shown that the outboard and inboard structures are safe

and maintain their integrity during the overpower events if the cooling systems function normally. In (Honda et al., 1994a) the comprehensive analysis has been applied to study the thermal analyses during plasma disruptions. In ITER, the reference scenario is considered as a thermal quench followed by a current quench. Three different types of disruptions are considered: the first is a normal disruption that can occurs during normal operation, the second is a beta-limit disruption near the Troyon limit and the third is a vertical displacement event. A parametric analysis has been carried out supposing the thermal quench time of 0.1 to 3 ms and the current quench time of 5 to 50 ms. The results of the analysis have shown a dependency on the damage of the plasma facing component on the quench time, the types of disruption considered, the plasma size and on the material of the components. Suggestions are given for a better design of the components and estimations are proposed on the maximum number of cycles before which the components must be changed. In add, the authors propose to update the analysis once the new design of the system is available. In (Honda et al., 1996), the methodology is applied to the ex-vessel LOCA investigating the possibility of passive plasma shutdown due to the impurities. Three different scenarios have been analysed: a Large-Break LOCA and a Small-Break LOCA at the cold leg of the divertor cooling system of ITER and a Large-Break LOCA at the cold leg of the first-wall cooling system. In the first case, the plasma is shut down by the impurities, in the second it is expected that the plasma would be safely shut down before the reactor structures were seriously damaged but a proper design of the divertor must be assured. In the third case, the copper cooling tube have melted before the possibility to passively shutdown the plasma.

In ITER to perform the technical risk assessment, it has been devised the RAMI approach (van Houtte et al., 2010), i.e. Reliability, Availability, Maintainability and "Inspectability". The process starts during the design phase of a system evaluating the actual design, if the requirements are not met corrective actions are still possible at this stage. The procedure has four different steps: Functional Analysis (FA), Failure Mode, Effects, and Criticality Analysis (FMECA), risk mitigation actions and RAMI requirement. The aim of the FA is to create a functional break-down considering the system from its main functions to the basic functions using the Reliability Block Diagrams (RGBs). The FMECA is used to list the function failures, their causes and effects according to importance for the machine operation availability. The third step is necessary to evaluate the benefits of the risk mitigation actions and the RAMI requirements are the output of the process. The RAMI approach has been applied in (Wang et al., 2015) to the test blanket module in ITER. The FA was applied to evaluate the functional goal of the module and the FMECA was used once the results of the FA were available. The criticality level of each functions failure mode was derived quantifying the severity of the event and the occurrence of the causes. The RBD was prepared to estimate the reliability and the availability of the functions in the operating conditions. The RAMI requirements are orientated to increase the availability of the system reducing the time to repair or replace the components, suggesting to increase the number of spare parts. The RAMI approach has been successfully applied in (Kitazawa et al., 2014b) to the ITER Central Safety Systems and in (Kitazawa et al., 2014a) to the Central Interlock System; in both the works the RAMI requirements are orientated to increase the availability of the system under analysis and to reduce the risk suggesting many tips to these purposes. The results obtained can be used to assist the future ITER construction and operation. The goodness of the RAMI approach to perform the risk assessment of a component under design in the fusion system, it is confirmed in (Alzbutas and Voronov, 2015) being methodology applied to the Wendelstein 7-X (W7-X), a stellarator device, to ensure the reliable and efficient operation of the machine. Even in this case the FMEA is used as input to FTA to get the minimal cut sets. In add, it is carried out an importance and sensitivity analysis to better understand the impact of each component and parameter on the system reliability/unavailability and risk. The data used for the analysis are the one classically used for

the NPP safety equipment. In this work, it has been used the ALARA principle, in fact for the proposed suggestion to reduce the risk, the cost effectiveness has been computed confirming the validity of the mitigation action also from an economical point of view.

In literature, examples can also be found of the traditional PSA approach applied to the fusion devices. (Carpignano et al., 2016) is the first case here reported where the object is to highlight the Postulated Initiating Events (PIEs) and provide some safety insights during the preliminary design. It is under consideration for the design of the EU DEMO the addition of an Intermediate Heat Storage (IHS) to smooth the energy production of the machine from a pulsed-operation to a steady feeding of the steam generator. Two PIEs were found to be critical for the insertion of the IHS: the LOCA in the tubes of the HX between primary and intermediate circuit and the loss of heat sink for the first wall or the breeding zone. The Function Failures Modes and Effects Analysis (FFMEA) has been chosen to perform the analysis; in fact, it is a common approach for hazards identification at this stage of design. The advantage of the FFMEA is that helps to highlights the components failures that are selected as PIEs. It is also done a comparison with the design without the IHS. The addition of the component introduces new consequences and weakness. No major barriers were found to realize this concept but the authors suggest to carefully investigate the results of the analysis in the next phases of the design.

Another example of the PSA approach can be found in (Dongiovanni et al., 2017) where it is considered the ex-vessel LOCA in DEMO. Four cases have been analysed: the first is the loss of cooling water from the vacuum vessel cooling loop into galleries, the second one is the loss of helium from the TF coil cooling loop into galleries. Two BDBA are furthermore considered to have a worst-case scenario reference: the simultaneous loss of both the vacuum vessel and Toroidal Field coils coolant, and a complete loss of the TF coils inventory. In add, a sensitivity analysis has been carried out to reduce the arbitrariness of some assumptions. In all cases considered, the LOCAs seems to be a no-recovery accident with a fast evolution without the possibility of human intervention. To avoid that the pressure exceeds the safety limit the volume of the device must be properly sized with also respect to the Common Mode Failure (i.e. seismic and fire, quench valve failure).

ITER must be licensed as a basic nuclear installation that must respect the French regulation. The principal document amongst the Demande d'Autorisation de Création (DAC) is the Preliminary Safety Analysis Report whose main contents are summarized in (Taylor et al., 2009). Two are the main source of risk for the public and the workers: the release of the tritium fuel and the activated material. The concept of defence in depth has been widely used to minimize the frequency and the consequence of the accidents and the ALARA requirements are supplemented to minimize the occupational radiation exposure during the normal and abnormal operation.

4 IDPSA

The Integrated Deterministic and Probabilistic Safety Analysis (IDPSA) (Zio, 2014) is a collective name for the variety of different tools which use tightly coupled probabilistic and deterministic approaches to address in a consistent manner both the aleatory and the epistemic uncertainties. The use of the DSA (Section 3.1) is a useful tool to verify that acceptance criteria are met and the PSA (Section 3.2) determines the probability of damage for each barrier. The PSA has been developed to resolve the limit posed by the DSA in particular reducing the reliance on the conservative approach. Nevertheless, even the probabilistic approach contains uncertainties that arise from three main sources: the lack of comprehensive data, the reliability of data and the modelling assumptions. The analysis is expert-based and the analyst must do assumptions: in the accidental evolution (i.e. timing and the order of rupture of the components and the response of the systems) and in the model to simulate the scenario. These problems lead to inconsistencies form PSA to PSA performed by different analysts. The IDPSA, jointly using complementary methods of deterministic and probabilistic safety analysis, can provide additional help to the safety practitioners because it is a methodology with which it can be resolved the time dependent interactions between the components, the physical phenomena, the control logic and operator actions. It can be identified a-priori unknown vulnerable scenarios (or "sleeping threats") due to the reduction on the reliance on the expert judgment and the simplifying assumptions. In the conventional PSA modelling, it is assumed that the components can work correctly or are totally broken, the timing is decided by the analyst as well as the accidental sequence. In the safety analysis of dynamic and complex systems, the magnitude and the time of failure of the components have a strong dependence with the scenario evolution (Zio and Maio, 2009). Even the accidental sequence has an impact on the capacity of the system to manage or not the accidental evolution and in the way in which the system diverges from the nominal condition. Dynamic methodologies are defined as those that explicitly account for the time element in probabilistic system evolution and they are needed to have a better understanding of the system behaviour in case of hardware/process/software/human interaction.

The IDPSA methodology can be summarized in three steps: the scenarios generation, the scenario modelling and the post-processing of the information.

The dynamic accidental scenario generation consists in generating random failure times of the system components/items and recording the system evolution in time. Monte Carlo (MC) simulation can be used to sample the components failure times that in principle can fail at any time and with any magnitude. Nevertheless, the generation of scenarios is intractable within a continuous time and infinite states in a MC framework; it is supposed that the components can fail at discrete time with discrete magnitude. The Von Neumann approach can be used to record the system evolution in time. The Monte Carlo scenario generation entails the creation of random walks which guide the system from one configuration to others, at different times, for exploring all possible failure scenarios. Starting from a given nominal condition of the systems, when it occurs a transition to a new state of the plant, it must be determined which is the new components configuration reached by the system because of the transition and what is the resulting state condition. To satisfy those requests two ways are possible: the direct and the indirect MC approach. In the indirect approach the components times of transition between states are exponentially distributed. Starting from a nominal state, the transition time is sampled applying the inverse transform method; now, it must be determined which component has undergone the transition and to which arrival state. The inverse transform method is applied to the discreate distribution describing the probability that all the components undergo to any transition. When the component and the time of transition are known, it must be determined the

final state after the transition; it is sampled applying the inverse transform method to the set of discrete probabilities of the mutually exclusive and exhaustive arrival state. The simulation proceeds to sample the next transition time and the systems undergoes through the various transitions from one configuration to another up to the mission time is reached.

In the direct Monte Carlo approach, it is sampled the times of all possible transitions of all individual components of the system. Then, the transition times are arranged along a timeline in accordance to their times of occurrence and the first time is chosen as the new state of the system. After the first transition, the timeline is updated to the include the new possible transition that the transient component can perform from its new state. The procedure is repeated until the next first occurring transition time falls beyond the mission time. The direct approach is more suitable for IDPSA in fact it can be applied in case of systems whose components failure behaviours are represented by different stochastic distribution laws.

The scenario modelling can be divided in two parts: the phenomenological models and the probabilistic models. To describe the phenomena, mathematical models must be applied and turned operatively into computer codes for the simulations. The system under analysis cannot be characterized exactly and the knowledge of the undergoing phenomena is incomplete. The source of the uncertainty arises both as model parameters and on the hypothesis underlying the model structure; as result, the uncertainty is propagated to the model output. Two are major objectives of the phenomenological scenario modelling: the uncertainty analysis and propagation, i.e. to understand how the uncertainties of the input parameters propagates to the output, and the sensitivity analysis, carried out in order to identify the relative importance of the various model parameters and hypotheses. To satisfy the first objective, useful methodologies are the Code Scaling, Applicability and Uncertainty (CSAU) or the Automated Statistical Treatment of Uncertainty Method (ASTRUM). The sensitivity analysis can be carried out following two different approach: local and global. In the first case, given the nominal values of the input it is observed what happens at the results of the analysis with small variation of the input parameter in the neighbourhood of the nominal value. The global approach account for the whole input variability range and the interaction between the input. Saliency, Hellinger and Kullbac-Liebler are examples of methods that can be uses to perform a global sensitivity analysis. In general, better results are obtained using a global approach but the corresponding computational expense is higher. The details of these approaches are out of the scope of this work and therefore are ignored.

The dynamic accidental scenario modelling, using a probabilistic approach, attempts to integrate deterministic and stochastic processes to explicitly model the plant-crew interactions and to give variability of these interactions. The dynamic methodologies for the IDPSA can be continuous or discrete. The Continuous Event Tree (CET) is a continuous methodology that considers continuous time distribution for the event occurrence. Given in input the transition rates along the sequence of events, the probability that the system leaves a given configuration and the initial condition, the CET describes the system behaviour in terms of probability of finding the system in a given configuration at a given time. The Monte Carlo simulation is used as solution method. The same approach of the CET is applied in the Continuous Cell-to-Cell Mapping Technique (CCCMT) and in the Cell-to-Cell Mapping Technique (CCMT). In the former the change in the configuration of the system can happen at continuous time whereas the transition states are discrete, while in the latter also the time is discretized and it is therefore considered as a discrete technique. Another discrete methodology for the dynamic probabilistic modelling of the accidental scenario is the Dynamic Event Tree (DET) that consists in the identification of the time-points along the simulation (called branching points) at which stochastic events occur, i.e. a system, a component or an operator action is called for. Each branch represents a possible outcome of the stochastic event and simulating the scenario

evolution from all branching points allows exploring all possible behaviours of the system parameters and process variables. The DET employs system simulators in order to model the actual accident evolution; starting from an initiating event, the main idea behind the DET methodology is to let a system code determine the pathway of an accidental scenario within a probabilistic environment. The branching rules can be specified by user-input CDFs or by active components setpoints. The number of scenarios that arise in the analysis is much larger than that of the classical ET/FT, the analysis is more complete and a higher quantity of information are available but the computational burden of the simulation is increase as well as the difficulty of the a-posteriori information retrieval. An example of the DET is the Monte Carlo Dynamic Event Tree (MCDET): the MC simulation is used to sample the transition time and to take into account both the aleatory and the epistemic uncertainty.

The third step of the IDPSA approach consists in the post-processing of the information generated. The results of the first two steps are a huge amount of data, with respect to the DSA and PSA, that must be analysed to retrieve the most important features of the systems. The postprocessing can be divided in two parts: the failure domain identification and the failure scenarios characterization. The aim of the IDPSA approach is to distinguish, as output of the safety assessment, a region (safe domain) in which the plant evolution is safe and no problems arise from the safety pointy of view and a region (failure domain) in which the system is in a not-safe working condition. The safety analysts have at their disposal an increasingly sophisticated collection of computational tools; these high-fidelity codes are not compatible to address the quantification of uncertainties in models of physical system due to the computational expense required. To solve the problem, it is introduced the concept of the Reduced Order Modelling (ROM): the essential physics and dynamics captured by the high-fidelity model is retained at a much lower computational cost. The ROM must be predictive across the parameter space of interest; the idea is to run a low number of simulation with the expensive computational model in the space of interest and then to train a code that reproduce the behaviour of the original model with a lower computational cost. The Support Vector Machine (SVM) and the Artificial Neural Network (ANN) are example of ROM. The failure boundary divides the safe domain form the failure domain and it is determined using the ROM in order to have a higher exploration of the domain of the possible outcomes with a considerable saving of computational time. In this thesis work, it has been used the validated 4C code, it is a high-fidelity and computational expensive code. Two simplified thermal-hydraulic models, based on a ANN, have been developed at the Politecnico di Torino for the simulation of the ITER TF and CS coils (Froio et al., 2016; Savoldi Richard et al., 2014). To train the ANN, it has been used the results of the full 4C simulations.

During the failure scenarios characterization, the Prime Implicants (PIs) and the near misses must be identified throughout the data mining of the dynamic scenario modelling results. The prime implicants are the minimal accidental scenarios that lead the system into failure, i.e. the minimal cut sets. To identify it, it must be solved a set covering problem. Nevertheless, in a multi value logic, i.e. the component can fail at any (continuous or discrete) time and magnitude, the identification procedure cannot be carried out analytically. A way to find a solution to the set covering problem is the use of evolutionary optimization algorithm; it is a probabilistic search algorithm inspired by the rules of natural selection. Starting from a trial candidate solution, generation after generation, the algorithm advances towards the fittest (near optimal) solution. Some examples are the Genetic Algorithm (GA) and the Differential Evolution (DE) or its evolution the Hierarchical Differential Evolution (HDE).

The near misses are unplanned condition that incidentally keep the system into safe but endangered and insecure operational conditions: they have the potential to cause damage to the human or to the environment but the safety thresholds are not exceeded. The identification of

the near misses is based on the concept of risk *r(t)*: it is computed as the product of the probability *p(t)* and the consequence *c(t)*:

$$r(t) = p(t) \cdot c(t) \tag{4.1}$$

where the probability *p(t)* increases reducing of the distance between the selected features and the threshold, and the consequence *c(t)* increases with the velocity with which it is reduced the distance between the selected features and the threshold. To explicitly consider the dynamic evolution of the system, *r(t)*, *c(t)* and *p(t)* are time dependent quantities. The near misses identification is an unsupervised-clustering problem in which both the number of groups and the best set of features to compute *p(t)*, *c(t)* and *r(t)* are unknown. The risk-based clustering of these transients is typically carried out by a means of a wrapper approach. From a set of features, a subset is selected to feed the clustering algorithm and the performance of the results are evaluated. Among the all clusters obtained, the most danger, from the safety point of view, is the one that has the higher risk and the longer time of abnormal behaviour.

One of the new capabilities introduced by the IDPSA is the possibility to have an on-line classification of the undergoing scenario. In fact, after having classified the system evolution in safe, near misses and PIs, when a new sequence, not a-priori simulated, is available it can be predicted the accidental progression comparing the unknown scenario with the simulated cases. The Hamming distance, that at each time compute the distance from the scenario under observation and the already simulated ones, is method to perform the on-line clustering. The developing scenario is assigned to the cluster with the smallest Hamming distance. The use of the on-line classification can increase the safety of the system, in fact in principle an accidental scenario that lead the system in a failure condition can be identified before the safety threshold is crossed. The mitigation action can be taken in advance and it is increased the time that the human operators or the safety systems have to counteract the abnormal transient.

In this work, it has been applied the following approach, based on the three steps proposed by the IDPSA: the accidental scenario is generated using the Multi-Valued Logic (Section 4.1), the well-validated 4C thermal hydraulic code (descripted in details in Section 2.2) is used to perform the scenario deterministic simulations of the different scenarios and to post-process the information the Spectral Clustering (Section 4.2.1) is employed, for the first time, to identify the most relevant abnormal scenarios in conjunction with the ESAX (Section 4.2.2), a reference algorithm from literature. The results of two methods have been compared (Section 4.2.3) to qualify the best technique

4.1 Scenario generation

The first step of the IDPSA approach is the scenario generation. The accidental sequence is the results of abnormal behaviours of the components and/or the physical processes. In this work, with respect to the components in detailed exposed in Section 2.3, it has been supposed that the failures can happen just to the CP, the CVs, the BV and the SVs. The controllers C1 and C2 work correctly during all the operational phases. This hypothesis implies that if the LOFA occurs, it is correctly detected from the control system and the current is surely removed from the coil. The same reliability is guaranteed in case in which the pressure at the inlet and outlet of the coil reaches the 1.8MPa and the signal to open SVs, to avoid an over pressurization at the ends of the CSM, is correctly send from the controller to the valves. No leakages are considered for the QT, the performances of the HXs are assumed as nominal neglecting possible

decreases on the heat exchange properties and it is also supposed that the temperature of the helium bath is always constant without any fluctuation.

It has been chosen to consider an exponential reduction of the rotational speed, directly affecting the mass flow rate, of the CP independently from the causes of the failure itself. The valves, instead, can occupy any state between the open and closed position. The failure of any component can happen at any time. In principle, it can be considered all the different ways in which any components can fail but to avoid the explosion of the cases to analyse, some bounds to the analysis must be set. To reduce the variable to treat in the scenario generation, a useful strategy consists in discretizing both the magnitude of the failure of the components and the time in which they fail. The components cannot change their states from the nominal to any abnormal condition, but the final states after the transition are set by the analyst.

For brevity sake, just the following component failures can occur:

1. the Centrifugal Pump (CP) reduces exponentially the rotational speed, directly affecting the mass flow rate that can be reduced to i) 75%; ii) 50%; iii) 25%; iv) 0% of the nominal mass flow rate, i.e. in the last case down to a total loss of pumping capacity.
2. the two Control Valves (CVs) can fail in three different modes: i) stuck (open) at the nominal position; ii) stuck closed at 50% of the nominal position; iii) stuck totally closed.
3. the By-pass Valve (BV) can fail in three different modes: i) stuck (closed) in nominal position; ii) stuck open at 50% of the flow area; iii) stuck totally open.
4. the two Safety Valves (SVs) can fail in three different modes: i) stuck (closed) in nominal position; ii) stuck open at 50% of the flow area; iii) stuck totally open.

It is assumed that the failure can happen at random times in the time horizon $[0,T_R]$ second; T_R is the maximum time at which the failure can happen and it set T_R = 600 s in the constant current scenario (Section 5) and T_R = 1800 s in the ITER-like current scenario (Section 6). The time of occurrence of the failures have been sampled by a uniform distribution with a Monte-Carlo approach. It is unphysical to treat the time of the failures as a continuous variable and a convenient approach is to discretize even the time. In this work, it has been chosen to divide the time horizon $[0, T_R]$ in six equally long, exclusive and exhaustive intervals. Every interval length is equal to 100s in the first part (exposed in Section 5), instead is equal to 300s in second case study (described in Section 6).

A Multiple Value Logic (MVL) scheme has been adopted to generate N=100 accidental scenarios. In the MVL, every accidental sequence is a vector of length equal to three times the number of components that can fail, i.e. in this case six different components can fail and the accidental sequence is a vector of eighteen cells. The construction of the accidental scenario is carried out as shown in Figure 4.1. The direct Monte Carlo approach is applied considering that the components can do at most one transition during the interval $[0, T_R]$. The failure magnitude and time are sampled from a uniform distribution as continuous value assuming every state is equally probable. Using the MVL approach, it is considered the stochastic (discrete) time interval (t) of occurrence of component failures, their (discrete) magnitude (m) and the order (ord) of events along the sequence. The random realizations of the discretized time and magnitudes values are included into a sequence vector that represents a generated scenario to be simulated, [m_{cp}, t_{cp}, ord_{cp}, m_{cv1}, t_{cv1}, ord_{cv1}, m_{cv2}, t_{cv2}, ord_{cv2}, m_{bv}, t_{bv}, ord_{bv}, m_{sv1}, t_{sv1}, ord_{sv1}, ms_{v2}, ts_{v2}, ord_{sv2}] (Di Maio et al., 2017). The following values are considered to convert the magnitude and time of the failure from continuous to discrete:

- time (t) discretization: we use the label t = 1, 2, 3, 4, 5 and 6, for failures occurring in the first, second, third, fourth, fifth, sixth interval, respectively; t = 0 means that the component

does *not* fail within the T_R of the scenario and the value "NaN" is used to identify the respective (non-)failure order (*ord*) in the sequence vector of the accidental scenario. Notice that, even if the failure order (*ord*) may seem redundant in the MVL representation, it is actually used to discriminate between scenarios where different components fail in the *same* time *interval t*. Also, it is worth highlighting that the *actual* time of component failure (used in the deterministic simulation of the accident scenario) is the one randomly sampled within the direct MC.

- Magnitude (*m*) discretization:
  - the CP magnitude is indicated with the label m_{cp} = 1, 2, 3 or 4 for failure states corresponding to an exponential decrease of the rotational speed down to 75%, 50%, 25% and 0% of the nominal value, respectively; if m_{cp} = 0, the component does not fail;
  - for each CV, the magnitude is indicated by the label m_{cv} =1, 2 or 3 if the component stays stuck (open) at the nominal position, stuck closed at 50% of the nominal position and stuck closed, respectively; if m_{cv} = 0, the component works correctly;
  - the BV magnitude is indicated by the label m_{bv} = 1, 2 or 3 if the component stays stuck in (closed) nominal position, stuck open at 50% of nominal flow area and stuck totally open, respectively; if m_{bv} = 0, the component does not fail;
  - for each SV, the magnitude is indicated by the label m_{sv} =1, 2 or 3 if the component stays stuck (closed) in nominal position, stuck open at 50% of nominal flow area and stuck totally open, respectively; if m_{sv} = 0, the component works in that scenario.

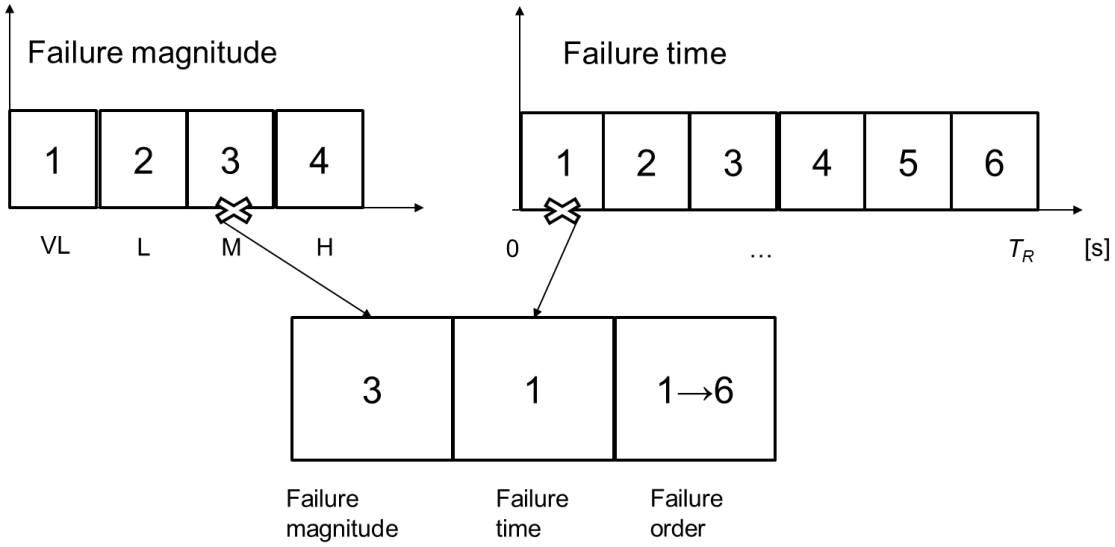

Figure 4.1 An example of the construction of the accidental sequence according the MVL

4.2 Post-processing

Introducing the MVL, there is a combinatorial explosion of scenarios generated that must be analysed and post-processed to get relevant information on the response of the system to the different states of the components. To post-process the scenario, clustering algorithms are typically adopted. Clustering entails grouping (in an unsupervised manner (Baraldi et al., 2013))

different scenarios in different clusters combining information from both the event sequences and the patterns of evolution of the process variables.

To mine the characteristics of most relevant abnormal transients among the MVL scenarios generated a Spectral Clustering approach (described in Section 4.2.1) is used and compared with ESAX (described in Sections 4.2.2 and 4.2.3).

Z=3 variables are monitored during each transient as "critical indicators" of the state of the system: the cooling helium pressure at the inlet p_{cin} of the CS magnet, the voltage dv measured at the coil extremities and the hot-spot temperature T_{hs} of the strands of the CSM. They are stored in Z different matrixes $\bar{\bar{X}}^k$ (with k=1, …, Z) each one of size [N, L], where L is length of the transients. Actually, if the $p_{cin} > 25$MPa, the conductors can be damaged; also, if the $dv >$ 0.1V for more than 1s, it means that the conductor temperature has exceeded the current sharing temperature T_{CS}, i.e., that the superconducting state of the magnet is lost. The voltage has been substituted, in the ITER-like scenario, with I/I_c the ratio between the actual current that flows in the coil and the critical current. The critical current is the maximum allowable current that can flow in the coil, specified the temperature and the magnetic field, without losing the supercritical properties.

4.2.1 Spectral Clustering

The Spectral Clustering approach (Strang and Nguyen, 1996) aims at classifying N different objects into C clusters by calculating a similarity measure μ between them. The similarity measure is strictly case dependent: in these applications, it is based on the functional characteristic of the Z=3 (i.e., p_{cin}, T_{hs} and dv or I_c) dimensional transients of length L. In line with (Zio et al., 2010), $\bar{\bar{X}}^k$ (k=1, …, Z) [N, L] are normalized in the range [0.2, 0.8] to obtain $\bar{\bar{Y}}^k$ [N, L].

For each *i-th* and *j-th* generic transient (with j and i=1,…, N) it is computed the pointwise distance δ_{ij} (Zio et al., 2010):

$$\delta_{ij} = \sum_{k=1}^{Z} \sum_{l=1}^{L} \left| y_{il}^k - y_{jl}^k \right| \tag{4.2}$$

The pointwise distance δ_{ij} is mapped into an "approximately zero" fuzzy set (FS), to get a gradual transition of the similarity measure (Joentgen et al., 1999)). Here, the bell-shaped FS (Dubois et al., 1988) is used:

$$\mu_{ij} = e^{-\left(-\frac{\ln(\alpha)}{\beta^2}\delta_{ij}^2\right)} \tag{4.3}$$

where μ_{ij} close to 0 means the evolution of the two transients are very different, whereas μ_{ij} close to 1 means they are similar. The parameters α and β are arbitrary and are set by the analyst: the larger the ratio $-\frac{\ln(\alpha)}{\beta^2}$ the stronger the definition of the similarity (Zio et al., 2010).

By so doing, a similarity matrix $\overline{\overline{W}}$ of size [*N*, *N*] is defined, whose generic element μ_{ij} represents the similarity measure between the *i-th* and *j-th* trajectory. Then, the diagonal matrix $\overline{\overline{D}}$ is computed, whose single elements $d_1, d_2, \dots, d_N$ are:

$$d_i = \sum_{j=1}^{N} \mu_{ij} \ , i = 1, \dots, N \tag{4.4}$$

Defining $\overline{\overline{L}} = \overline{\overline{D}} - \overline{\overline{W}}$ and being $\overline{\overline{I}}$ the identity matrix of size [*N*, *N*], the normalized Laplacian matrix $\overline{\overline{L}}_{sym}$ can be defined as equal to:

$$\overline{\overline{L}}_{sym} = \overline{\overline{D}}^{-\frac{1}{2}} \overline{\overline{L}} \overline{\overline{D}}^{-\frac{1}{2}} = \overline{\overline{I}} - \overline{\overline{D}}^{-\frac{1}{2}} \overline{\overline{W}} \overline{\overline{D}}^{-\frac{1}{2}} \tag{4.5}$$

To find the optimal number of clusters *C* in which the *N* transients are to be clustered, the eigenvalues $\lambda_1, \lambda_2, \dots, \lambda_N$ and the corresponding eigenvector $\overline{u}_1, \overline{u}_2, \dots, \overline{u}_N$ of the matrix $\overline{\overline{L}}_{sym}$ are computed. According to the eigengap heuristic theory (Mohar, 1997) *C* is set equal to the number of eigenvalues $\lambda_1, \lambda_2, \dots, \lambda_C$ much smaller then λ_{C+1} (Von Luxburg, 2007). This guarantees the *i-th* trajectory similarity with other trajectories to be well captured in the *C*-dimensional vector $\overline{u}_i$ corresponding to the *i-th* row of the matrix $\overline{\overline{U}}$. Finally, the matrix $\overline{\overline{T}}$ (*N*, *C*), where the first *C* eigenvectors $\overline{u}_1, \overline{u}_2, \dots, \overline{u}_C$ are stored, is fed to the Fuzzy-C-Means (FCM) clustering algorithm to assign each *i-th* transient in the corresponding cluster (Alata et al., 2008; Bezdek, 1981; Leguizamon et al., 1996) where the normalization Eq. 4.6 is proven to enhance clusters identification (Von Luxburg, 2007).

$$t_{ic} = \frac{u_{ic}}{\left(\sum_{c=1}^{C} u_{ic}^2\right)^{\frac{1}{2}}} \tag{4.6}$$

To guarantee that the trajectories are assigned to each cluster without misclassification error, the *i-th* trajectory is assigned to the cluster *c* if the corresponding membership $m_{ic} > 0.7$, where m_{ic} is the membership (that varies between 0 and 1) that the FCM assigns to each *i-th* transient of all cluster, $c = 1, .., C$.

4.2.2 ESAX

The Extended Symbolic Aggregate approXimation (ESAX) (Lin et al., 2003; Lkhagva et al., 2006) is an algorithm that allows users to transform a gaussian Z-dimensional time series of data $\overline{\overline{X}}$ into a series of symbols $\overline{\overline{P}}$. This can be done reducing the length *L* of $\overline{\overline{X}}$ into *n* intervals, and the range of values of $\overline{\overline{X}}$ into α intervals. It has been applied the following procedure:

Step 1: Choose *n* and α, according to the expert judgment;

Step 2: Build *Z* matrices $\overline{\overline{B}}^k$ (*k*=1, …, Z) [*N*, *L*] from $\overline{\overline{X}}$, whose the generic element b_{il}^k is:

$$b_{il}^{k} = \frac{x_{il}^{k} - E^{k}}{\sigma^{k}}, i = 1, \dots, N \; and \; l = 1, \dots, L \tag{4.7}$$

where

x_{il}^{k} is the generic element of the matrix $\bar{\bar{X}}$

$$E^{k} = \frac{1}{N\,L} \sum_{i=1}^{N} \sum_{l=1}^{L} x_{il}^{k} \tag{4.8}$$

$$\sigma^{k} = \sqrt{\frac{\sum_{i=1}^{N} \sum_{l=1}^{L} \left(x_{il}^{k} - E^{k}\right)^{2}}{N\,L}} \tag{4.9}$$

Step 3: Partition the time interval [0, T_M] into n equal sized intervals (see Figure 4.2);

Step 4: Partition the range of values of $\bar{\bar{B}}$ into α equi-probable intervals and assign a symbol to each region (see Figure 4.2);

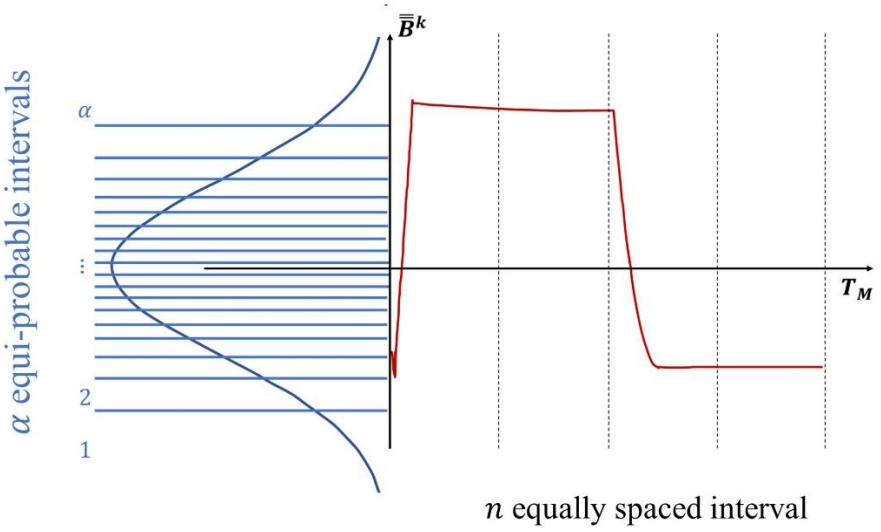

$$\bar{D}_i^k = [19\ 2\ 12\ 19\ 19\ 19\ 19\ 3\ 10\ 3\ 3\ 3]$$

Figure 4.2 Mapping of a generic i-th transient of the $\bar{\bar{B}}$ (solid line) in the corresponding sequence of symbols $\bar{D}_i^k$

Step 5: Build Z matrices $\bar{\bar{D}}^k$ (k=1, ..., Z) [N, 3 n] from $\bar{\bar{B}}^k$, whose the generic element d_{ip}^k is:

$$d_{ip}^{k} = symb\left(\begin{cases} \max\left(\bar{B}_{iq}^{k}\right) & for\ p = 1, 4, \dots, 3n-2 \\ \text{mean}\left(\bar{B}_{iq}^{k}\right) & for\ p = 2, 5, \dots, 3n-1 \\ \min\left(\bar{B}_{iq}^{k}\right) & for\ p = 3, 6, \dots, 3n \end{cases}\right), i = 1, \dots, N \qquad (4.10)$$

where $\bar{B}_{iq}^{k}$ (q=1, …, n) are the values of the *i-th* transient in the *q-th* interval of $\bar{\bar{B}}^{k}$ and *symb( )* is a function that assigns symbols according to the discretization on the Step 4 (also shown in Figure 4.2);

Step 6: Map $\bar{\bar{B}}$ into a matrix $\bar{\bar{P}}$ [N, 3 *n Z*] as timely ordered sequence of symbols of the Z matrices $\bar{\bar{D}}^{k}$. For clarity sake, the generic *i-th* $\bar{\bar{P}}$ in which Z=3 and n=1 is:

$$\bar{P}_i = [\ d_{i1}^{1}\ d_{i1}^{2}\ d_{i1}^{3}\ d_{i2}^{1}\ d_{i2}^{2}\ d_{i2}^{3}\ d_{i3}^{1}\ d_{i3}^{2}\ d_{i3}^{3}\ ] \qquad (4.11)$$

Step 7: Calculate $\bar{\bar{M}}$ [N, N], using the distance measure *MINDIST* (Butler and Kazakov, 2015; Lin et al., 2003; Mandelli et al., 2013):

$$M_{ij} = MINDIST\left(\bar{P}_i, \bar{P}_j\right) \equiv \sqrt{\frac{L}{n}} \sqrt{\sum_{m=1}^{3\,n\,Z} \left(dist\left(p_{im}, p_{jm}\right)\right)^2} \qquad (4.12)$$

where $\bar{P}_i$ and $\bar{P}_j$ are the *i-th* and *j-th* generic rows of the matrix $\bar{\bar{P}}$, and the *dist( )* function is a lookup table (Butler and Kazakov, 2015; Lin et al., 2003) that derives from the Euclidian distance.

Step 8: Apply the FCM to $\bar{\bar{M}}$ and to classify the N transients into C clusters. Assign, the *i-th* transient is assigned to the *c-th* cluster if the corresponding membership $m_{ic} > 0.7$.

4.2.3 Comparison of the results

The goodness of the clusters identified is quantified in terms of their separation and compactness, as measured by the internal validity indexes (Al-Dahidi et al., 2018, 2015a, 2015b):

- Silhouette (Rousseeuw, 1987), that measures the similarity of the data belonging to the same cluster and the dissimilarity to those in the other clusters. The Silhouette index varies in the interval [-1,1] and should be maximized (Al-Dahidi et al., 2018);
- Davies-Bouldin (DB) (Davies and Bouldin, 1979), that is based on the ratio of within-cluster and between-cluster distances. The DB index ranges in the interval [0, ∞) and should be minimized (Al-Dahidi et al., 2018).

Large Silhouette and small DB values indicate that the obtained clusters are well separated and compacted. In what follows, the two indexes have been calculated to validate the choice on the number of the optimal number of clusters C and to compare the performance of the two methods described, i.e. spectral clustering and the ESAX algorithms. The method that

guarantees, at the same time, the larger Silhouette and the smaller DB values is selected as the best one for the purpose of post-processing abnormal transients and identifying the most critical one for the case of the superconducting magnet cooling circuit.

5 Constant current scenario

In the first case study proposed, it has been considered that inside the CSM, descripted in the Section 2.1 and 2.3, flows a constant current of 48.5 kA. This quantity is higher than the maximum value foreseen during the normal cycle of ITER but it is the operational current of the CS. In Figure 5.1 it is shown an example of the current given in input of the CSM in case in which the LOFA occurs. The first 1000 s are simulated to reach a steady state condition. In fact, this is also the time necessary to have an entire recycle of the SHe inside the cooling loop. After this time the system is in steady-state condition. Just for visual aid, in this example, it has been assumed that the LOFA is detected at 1500s. The controller C1 enters in action, closes the CVs, opens the BV and removes the current with a fast, controlled discharge. The ramp has a duration of 30s and due to the AC losses, that are proportional to the derivative of the current, the temperature of the coil increases. After the current has been completely removed from the coil, the static heat load is the only heat source for the coil; nevertheless, to reduce the computational-time and to simplify the problem, this contribution has been neglected. It is clear that if there are no more heat sources the temperature of the coil cannot increase and this means that there is no more interest to simulate the evolution of the system after the current ramp.

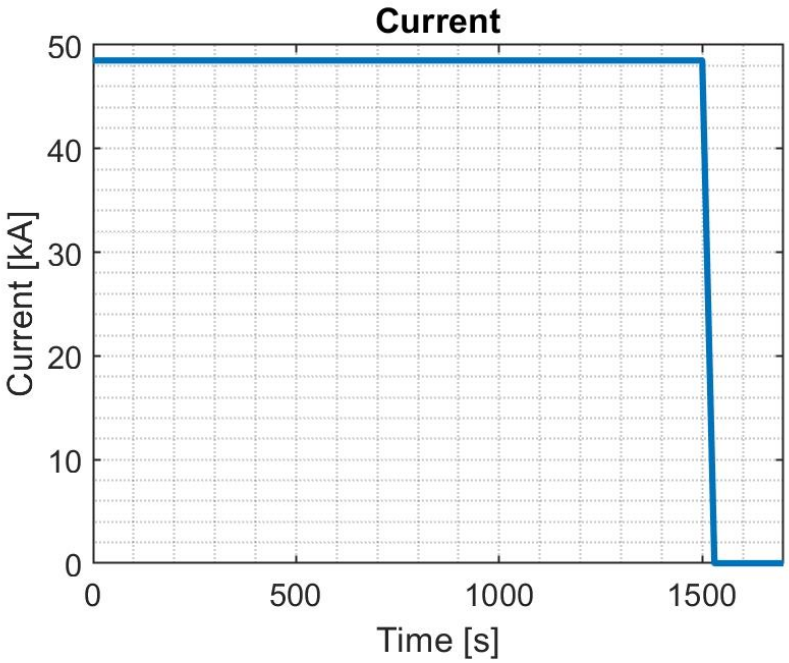

Figure 5.1 An example of the current flowing in the coil in the constant current scenario.

Since it has been assumed that the first failure of the component cannot happen before the steady-state, from now on, the time 0s is shifted to the first 1000s simulated, i.e. the time of interest starts when the steady-state condition is reached.

N=100 accidental scenarios have been generated according to the MVL. It is recalled that the failure of the components can randomly occur in the time horizon [0, T_R=600] s. It can be shown that the system reaches a steady state condition in ~100 seconds, irrespectively of the failure occurred. Therefore, we set a mission time T_M = 700 s. For clarity sake, as an example the following accidental sequence vector [4, 6, 5, 0, 0, NaN, 1, 2, 1, 2, 4, 3, 2, 5, 4, 1, 3, 2] represents a scenario where: the CP fails completely to 0% of the nominal value at a time in [501,600] s (fifth event occurring along the sequence); the CV1 correctly works throughout T_M;

the CV2 fails stuck (open) at the nominal position at a time in [101,200] s (first event occurring along the sequence); the BV fails stuck open at 50% of the nominal flow area (third event along the sequence) at a time in [301,400] s; the SV1 fails stuck open at 50% of the flow area at a time in [401, 500] s (fourth event along the sequence); finally, the SV2 fails stuck (closed) in nominal position at a time in [201,300] s (second event along the sequence).

5.1 Results

The spectral clustering algorithm described in Section 4.2.1 has been applied to classify in C clusters the N different scenarios generated. In Figure 5.2 the matrix $\overline{\overline{W}}$ is shown. Figure 5.3 shows the eigenvalues $\lambda_1, \lambda_2, \ldots, \lambda_N$ of the matrix $\overline{\overline{L}}_{sym}$ obtained by transforming $\overline{\overline{W}}$ (calculated with the ratio $-\frac{\ln(\alpha)}{\beta^2}$ equal to $1.9 \cdot 10^{-8}$). Since the first C=7 eigenvalues are very close to zero and the eighth is remarkably larger than the others, the number of clusters C is set equal to 7 (Baraldi et al., 2013).

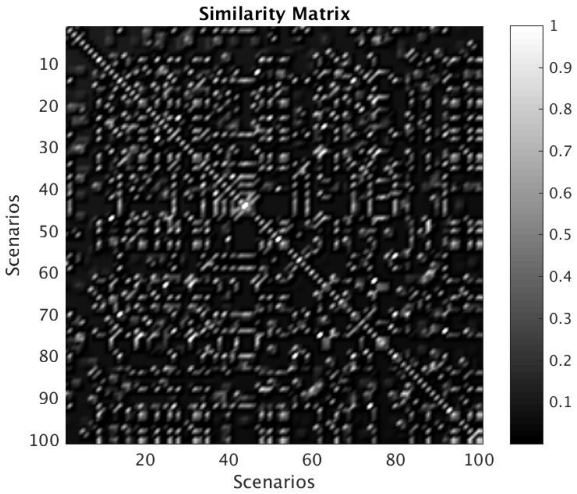

Figure 5.2 The similarity matrix $\overline{\overline{W}}$

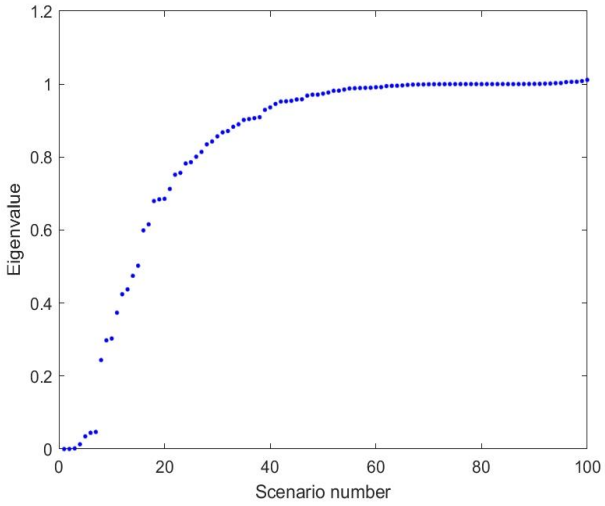

Figure 5.3 The N=100 eigenvalue of the matrix $\overline{\overline{L}}_{svm}$

Once the number of clusters has been found, the assignment of the different trajectories to the most proper cluster has been carried out. It is recall that, to avoid misclassification error and to meet the goal of identifying the prototypical abnormal behaviour of the system, the *i-th* transient is assigned to the proper *c-th* cluster if the membership $m_{ic} > 0.7$. This, conservatively, forces the different scenarios belonging to the same cluster to be very similar but, at the same time, some of them (in this case 2 transients) cannot be assigned to any of the *C* clusters.

In Figure 5.4, the similarity matrix $\bar{\bar{W}}$ is shown, properly shuffled according to the *C*=7 clusters obtained using the FCM (i.e., the most similar scenarios are grouped together).

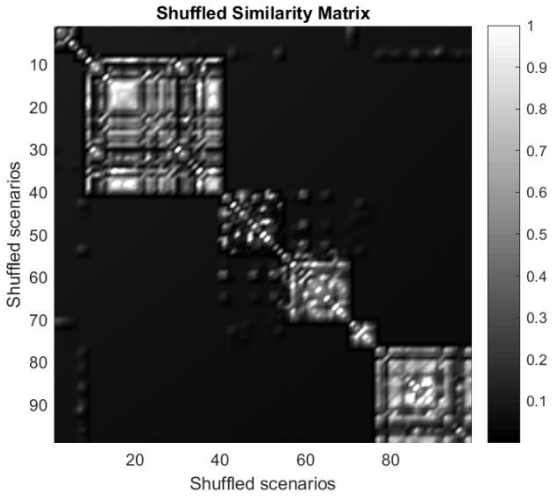

Figure 5.4 The shuffled similarity matrix $\bar{\bar{W}}$

Figure 5.5, shows the evolution of the safety features in the different clusters (on the left, *dv* and p_{cin} are plotted in time, whereas on the right T_{hs} and p_{cin} are considered). Cluster 1 is characterized by transients in which LOFA occurs at medium time, the *dv* drops to 0 following an exponentially decrease and during the current ramp the p_{cin} increases. In cluster 2, the *dv* initially increases (without relevant safety concerns) then drops to 0, whereas p_{cin} and the T_{hs} are stable along the whole transient. Clusters 3 and 6 are similar to cluster 1, except that the LOFA occurs at early and late time, respectively. An initial increase of p_{cin} and *dv* can be acknowledged for transients belonging to cluster 4, then followed by a decrease at medium time. Cluster 5 groups transients with initial increase of p_{cin} followed by a decrease with the LOFA occurrence at early time. Finally, transients of cluster 7 are those for which, despite the occurrence of components failures, the LOFA occurrence is avoided; they show an increase in *dv* and T_{hs}, whereas p_{cin} is constant to its nominal value. The characteristics of each clusters are listed in Table 5.1.

Table 5.1 Summary of the peculiar characteristics of the Z=3 safety features for each cluster.

Cluster	p_{cin}	T_{hs}	dv	LOFA (occurrence)
1	0.65 MPa	5.5 K	Reaches maximum the nominal values	Yes, at medium time
2	0.5 MPa	9 K	Increases before LOFA	Yes, at late time
3	0.65 MPa	5.5 K	Reaches maximum the nominal values	Yes, at early time
4	0.55 MPa	12 K	Increases before LOFA	Yes, at medium time
5	0.65 MPa	6 K	Reaches maximum the nominal values	Yes, at early time
6	0.6 MPa	6 K	Reaches maximum the nominal values	Yes, at late time
7	0.45 MPa	6 K	Increases (below limit)	No

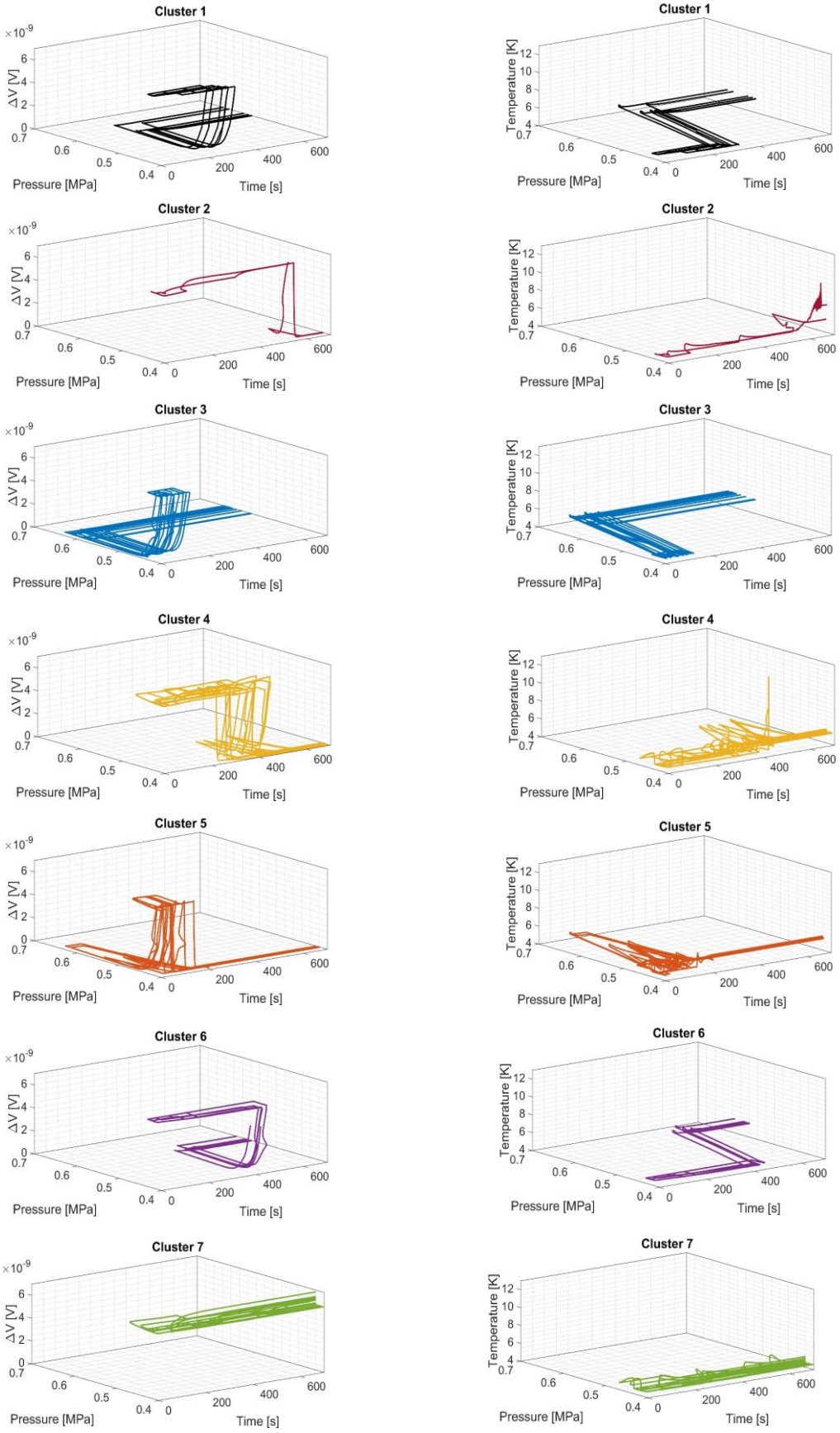

Figure 5.5 The time evolution of the three safety features in the 7 clusters using the Spectral Clustering

The phenomena described by the transients clustered in clusters 1-7 are justified by the types and timing of the components failures that are described in the MVL sequences simulated. To find the prototypical sequence of failures event that would lead to each described phenomenon (even though the pressure at the boundaries of the SC coil is kept below the safety threshold of 1.8 MPa, i.e., with a positive safety margin, out the voltage *dv* always below the threshold of 0.1 V, which means that T_{CS} is not exceeded), a bubble plot is used for retrieving the shared characteristics among the transients belonging to each cluster. Figure 5.6 shows, for each cluster, larger circles for failure with the most common failure times and magnitudes of the MVL that belong to that cluster. Table 5.2 presents a summary of the analysis.

For example, cluster 4 is the one that shows the largest values of T_{hs} (see Figure 5.5, 4th rows, left). Failure that lead the system to evolve as transients belonging to cluster 4 are CV2, that must fail stuck open at early time and as first along the sequence of events, and the BV, that must fail stuck open at 50% of nominal flow area as second along the sequence at early time. Moreover, SV1 must fail stuck open at 50% of nominal flow area at early time, whereas SV2, because all its three possible states: i) stuck closed in nominal position, ii) stuck open at 50% of the flow area, iii) stuck totally open) are equally expressed in the MVL of the cluster 4 transients, is not relevant to characterize the cluster transients. CV1 must fail stuck close at 50% of the nominal mass flow rate at early time and as second along the sequence of failure events or must fail stuck totally close as third at medium time; CP must slow down with to 25% of the nominal value (see Figure 5.6, 2nd row, right).

The prototypical accidental sequence identified is in accordance with the evolution of the safety parameter considered; in fact, the BV stuck open at 50% of the nominal mass flow rate is the most frequent failure. As consequence, a lower quantity of SHe is available to cool down the CSM and as consequence there is a hot-spot temperature increase. The LOFA cannot solely occur as a consequence of the BV stuck open at 50%. Actually, in this cluster, after the BV failure, the LOFA typically occurs because one component between the CVs or the CP fails with the higher magnitude.

For the sake of completeness, once the “critical cluster” has been identified, a more detailed analysis has been carried out to understand the physical causes of the transients presenting the higher hot-spot temperature (on the other hand, it must be clarified again that no safety issues have arisen from any of the transients of Cluster 4). The cluster is characterized by a high number of failure inside the MVL sequences. The pressure at the inlet of the coil is close to the pressure of the QT because at least one of the two SVs is open or partially open. The occurrence of this failure is, typically, at the beginning of the accidental sequence, as first or second event. The LOFA occurs as consequence of the failure of one of two CVs stuck closed or the BV that fail stack open or the CP that reduces the rotational speed until a complete stop. This failure occurs as last event in the accidental sequence. The failures happening in the middle of the accident scenario determine a reduction on the mass flow rate that cools down the CSM causing a temperature increase. These failures interest the same components that lead to the occurrence of the LOFA, but with a lower magnitude. In particular, the CVs and the BV fail stuck open at 50% of the nominal mass flow rate, instead the CP reduces the rotational speed from the nominal value to 75%, 50% or 25%.

Table 5.2 Summary of the peculiar characteristics of the Z=3 safety features for each cluster.

Cluster	Most important components	Magnitude	Time	Order
1	CV2	3	Medium	3
	BV	3	Medium	3
	SV1	1	Early	1
2	CP	1	Early/medium	-
	SV1	2/3	Early	-
	SV2	2/3	Late	-
3	CP	4	Early	1
	CV1	3	Early	1
	BV	3	Early	1
4	CV2	1	Early	1
	BV	2	Early	2
5	BV	3	Early	2
	SV1	3	Early	1
	SV2	3	Early	1
6	CP	1/3	Early	2
	CV1	1	Early	3
	CV2	3	Early	4
7	CP	3	Early	1
	CV1	1	Early	1
	SV2	1	Early	1

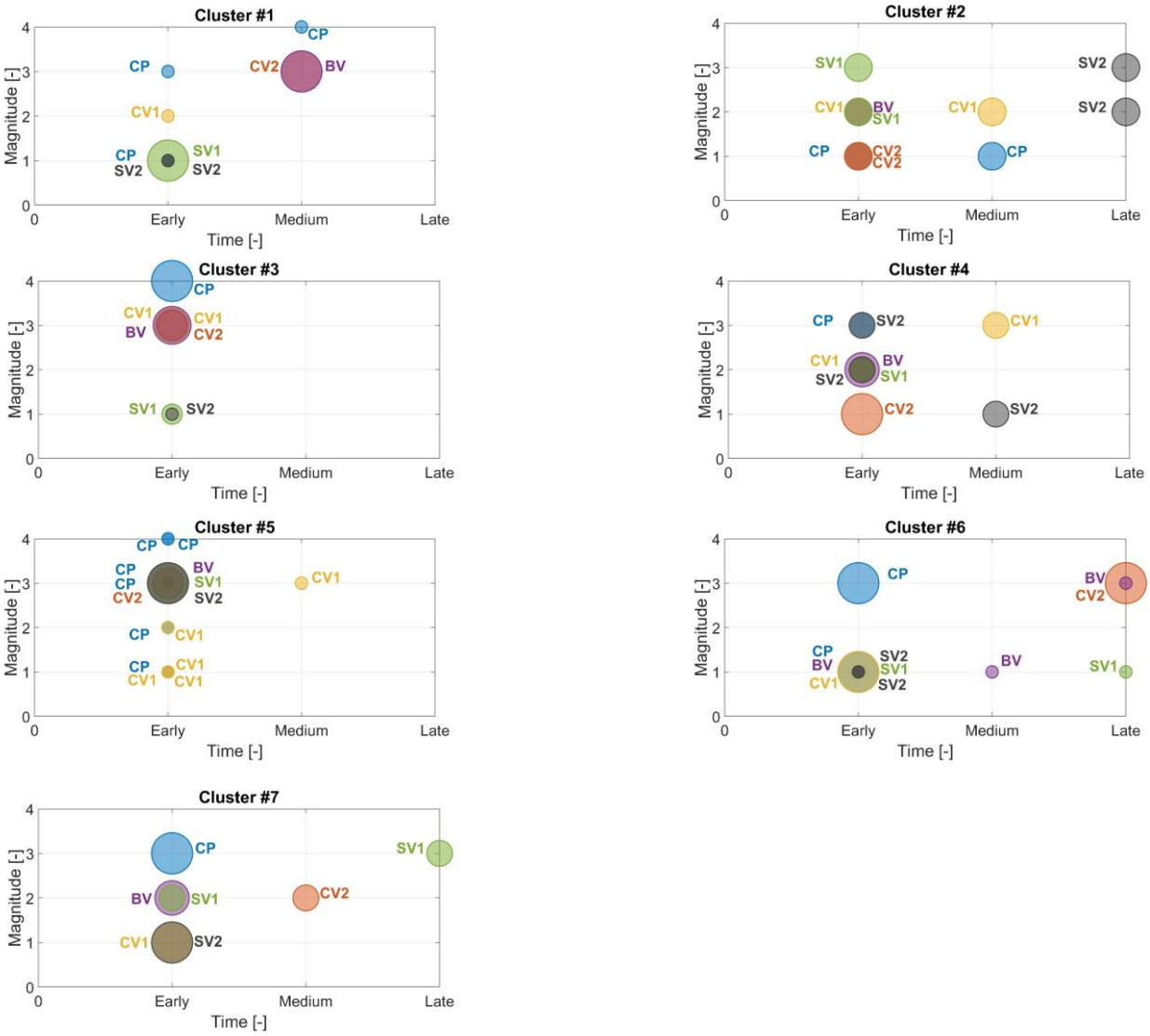

Figure 5.6 Bubble representation of the prototypical states of the components that would lead the system into the C=7 clusters

The ESAX has been used to group the N scenarios generated according to the MVL. The time has been discretized in n=4 interval and the range of the values of $\bar{\bar{X}}$ in α=19 intervals. The number of clusters C is found by calculating the Silhouette and the DB index for $C_{candidate} = [2, 10]$ number of clusters. Figure 5.7 shows the Silhouette value (circles) and the DB index (squares), that are maximized and minimized, respectively, for C=7. Also in this case, each *i-th* transient is assigned to the proper cluster if the membership m_{ic}> 0.7, excluding 13 scenarios because cannot be assigned to any of the C clusters.

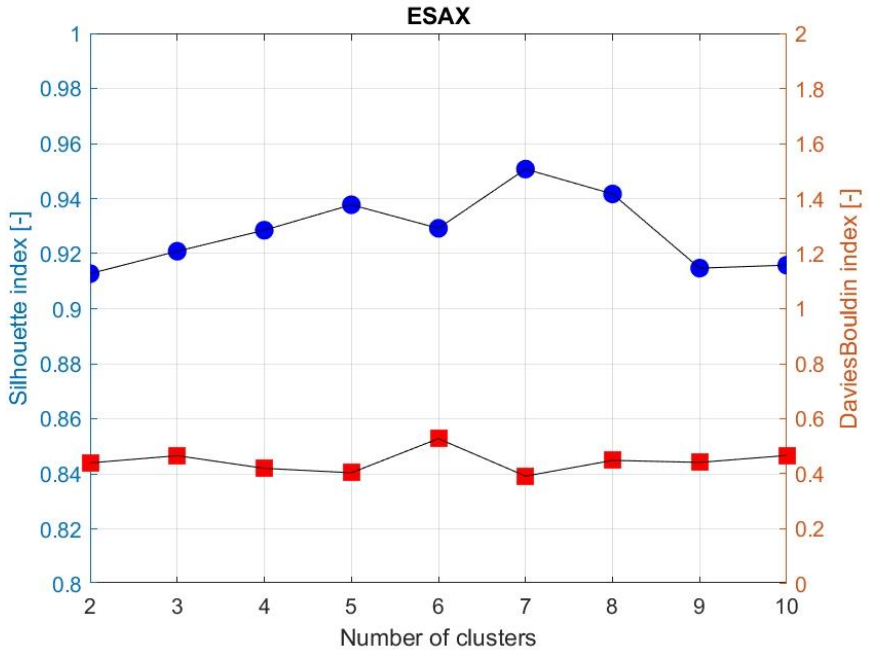

Figure 5.7 Silhouette values (circles) and the DB index (squares) for different number of clusters

The results are shown in Figure 5.8 as before. The clusters obtained are very similar to those ones shown using the spectral clustering. A notable difference can be found in cluster 2: for the ESAX, the LOFA occurs at late time with *dv* close to the nominal value before the exponential decreases, an initial increase of p_{cin} that then goes to nominal values and no significant variations are foreseen in T_{hs}, whereas for spectral clustering the *dv* initially increases (without relevant safety concerns) then drops to 0 and p_{cin} is stable along the whole transient.

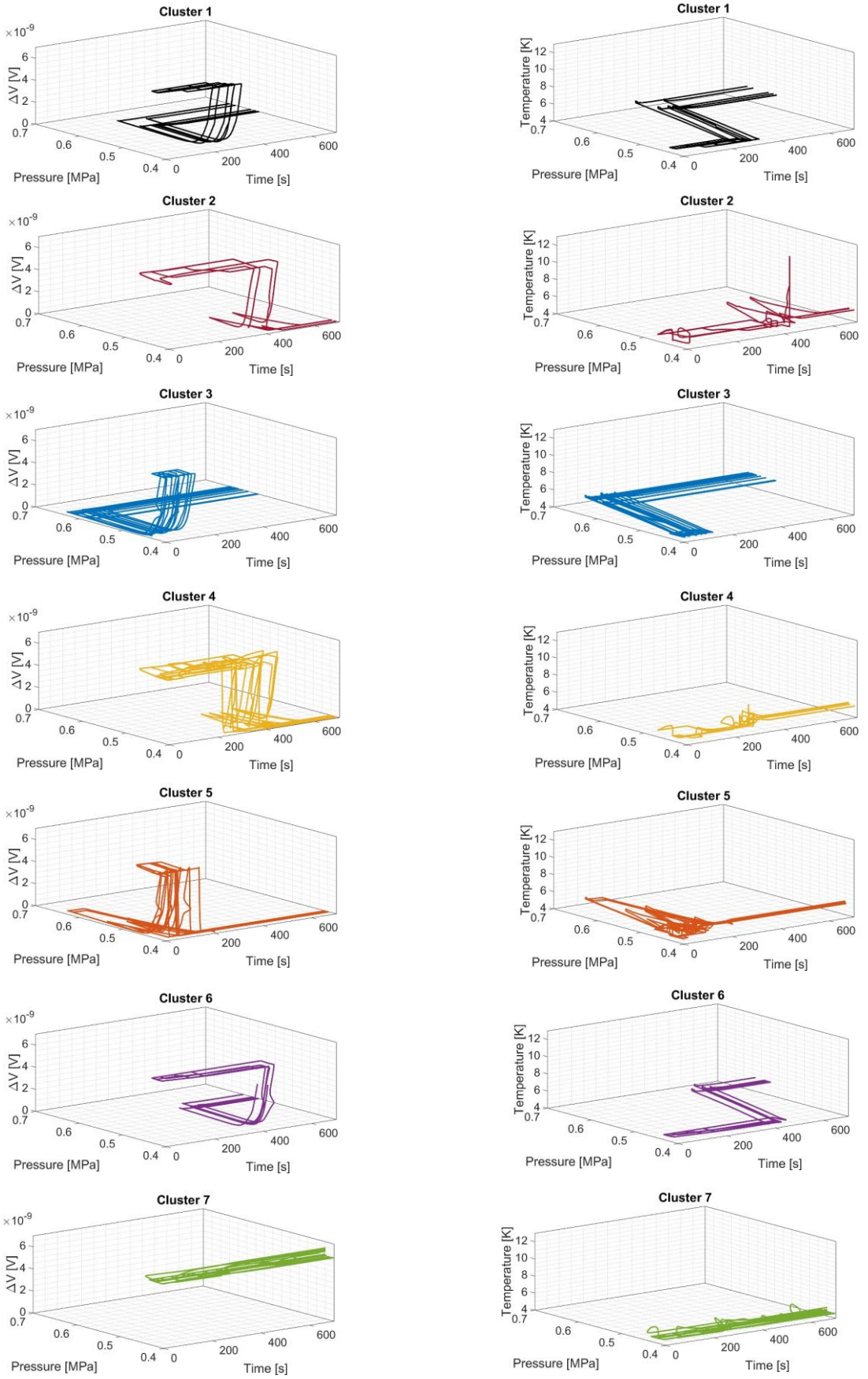

Figure 5.8 The time evolution of the three safety features in the 7 clusters using the ESAX algorithm.

However, the best clusters are obtained using the spectral clustering algorithm: Figure 5.9 shows the higher values of the Silhouette index and lower value of DB for each of the C=7 cluster for spectral clustering rather than ESAX (notably, for spectral clustering Silhouette values are almost equal to 1 for any clusters, and, correspondingly, the DB values are close to 0).

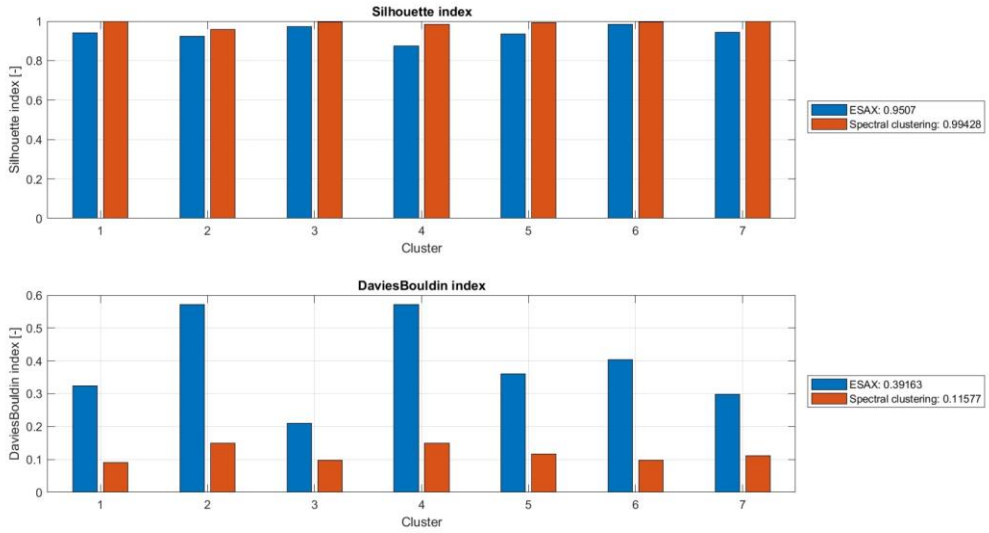

Figure 5.9 Silhouette values and the DB index for the ESAX and the Spectral Clustering algorithm

6 ITER-like current scenario

In the second case study, the current that flows in the CSM is the same one of the ITER-like normal operation scenario. The Central Solenoid in ITER will be made by six modules. The innermost central ones are called CS1U and CS1L; these act as a pair and they will carry the higher values of current. To be conservative in this analysis, it has been chosen to use as current in input to the CSM the one that it is supposed to flow in the CS1U and CS1L. In ITER the current cycle will have the duration of 1800s and the burning time of the plasma it is assumed to be 400s (Savoldi et al., 2018). In Figure 6.1 it is shown an example of the current that flows in the coil during the second part. It can be seen again the initial 1000 s of simulation at constant current. As the previous case, this initial time is needed to simulate a steady state condition. Once that the desired condition has been reached, it is simulated the first ITER cycle. It starts at 1000s and finishes at 2800, two red dots are inserted in the figure for visual aid. The cycle can be divided in five parts. The first step is the initial magnetization and it taken 130 s characterized by an initial rapid and fast ramp with a duration of 80 seconds during which the current goes from 38 kA to -38 kA. Due to the AC losses, a very high quantity of heat is deposited in the coil. The second step takes 400 s and corresponds to the burning time; the fusion reaction takes place and plasma must be confined. The end of burn coincides with the start of the ramp down: the current is removed from the CSMs and in 370s goes from -45.4 kA to 0. The AC losses continues also in this third step due the presence of these ramps characterized by lower values of the derivative. The fourth step is called dwell: for 590 seconds the current is equal to 0. The last step, with a duration of 300 seconds, is called magnetization time, in which the current is bring from 0 to the nominal value. Before to restart a new cycle, there is a plateau of 10 seconds.

In this second part has been assumed that all the component works correctly during the time necessary to reach the steady state condition and the first ITER cycle. The attention is posed on the effect of the failures of the component during the second cycle. In the example shown in Figure 6.1 the LOFA is detected at 3300 s and the current is removed with the ramp of the duration 30 seconds. Even in this case, after the dump it is no more important to investigate the state of the coil and the simulation is stopped.

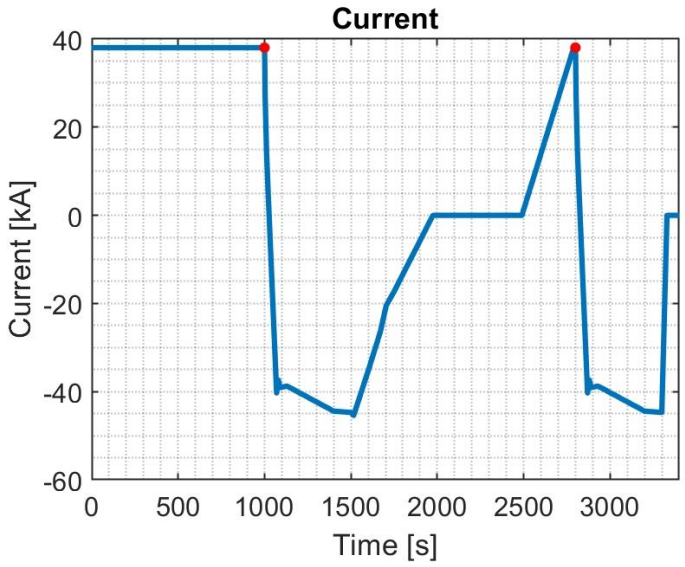

Figure 6.1 An example of the current given in input to the coil in the ITER-like current scenario.

From now on, the time 0s is shifted to the first 2800s simulated, corresponding to the second red dot in Figure 6.1, i.e. the time of interest starts when the first ITER cycle is concluded. It has been supposed that in this second part of the thesis, the failure of the components can happen in the time horizon [0, T_R=1800s]. The mission time is set equal to 3600s, i.e. two consecutive current cycle. In fact, in the case in which after T_R the LOFA has not occurred, the interest is to understand the effect of the failures on the successive cycles. It would be find out some scenario in which the new state of the systems can lead to accidental situation in the next cycles. In the test facility 10 charge and discharge will be conducted, as one can see in Table 2.1.

The choice of the ITER-like current scenario has a double interest: the first is to prove the safety operation of the facility during the test also in abnormal conditions and the second one is to predict relevant accidental transients for ITER. In fact, the hot spot temperature of the strands computed during the test of the CSM in the facility can be assumed similar to the temperature of the CSM during the same working condition of the tokamak. The hotspot temperature depends on: (i) the deposited power on the CSM, function of the current evolution (assumed the same in the facility and ITER) and the geometry of the conductor; (ii) heat capacities, functions of the operative condition (pressure, mass flow rate and initial temperature) and geometry of the conductor. The difference between the GA facility and ITER is the value of the current sharing temperature. The hot-temperature of the strands, the current that flows in the coils and the magnetic field in which the coil is immersed are the variable that influence the current sharing temperature. In the reference facility, the magnetic field felt by the CSM is the self-field generated by the superconductive module; in ITER, in each module there is sum of this contribution and magnetic field generated by the others CSMs. As consequence, in ITER the current sharing temperature is lower than in the facility. The minimum value of the ITER current sharing temperature has been assumed equal to T_{CSI} = 7.3 K; consequently, if during the simulation of an accidental transient, maximum hot-spot temperature exceeds the T_{CSI}, in the GA facility no problems arise but the occurrence of the same transient in ITER would result in the quench of the CSM.

N=100 accidental scenarios have been generated using the MVL, as in details explained in 4.1. For clarity sake, the following MVL sequence [4, 6, 5, 0, 0, NaN, 1, 2, 1, 2, 4, 3, 2, 5, 4, 1, 3, 2] represents a scenario where: the CP fails completely to 0% of the nominal value at a time in [1501, 1800] s (fifth event occurring along the sequence); the CV1 correctly works throughout T_M; the CV2 fails stuck (open) at the nominal position at a time in [301,600] s (first event occurring along the sequence); the BV fails stuck open at 50% of the nominal flow area (third event along the sequence) at a time in [901,1200] s; the SV1 fails stuck open at 50% of the flow area at a time in [1201, 1500] s (fourth event along the sequence); finally, the SV2 fails stuck (closed) in nominal position at a time in [601,900] s (second event along the sequence). It is recall that the time used in the deterministic simulation of the accidental scenario is randomly sampled from the direct Monte Carlo approach within the interval.

To post-process the results, the same methodology described in detail in Section 4.2 and applied to a reference simplified case in Section 5 has been used. In Section 6.1, Z=3 safety features have been considered: the pressure at the inlet of the coil p_{cin}, the hot-spot temperature of the strands T_{hs} and the ratio between the current I that is flowing in the CSM and the critical current I_c, for sake of simplicity I/I_c. The dv is in the order of the nanovolt resulting in unphysical value that in the real facility/plant cannot be measured because too small and for the instrumentation is equal to zero. The introduction of the I/I_c guarantees that the same information of dv is highlighting maintaining a physical relevance to the safety variable. In fact,

the *dv* is computed as the product of the electric field *E* (see. Eq. 6.1) multiplied by the length in which the *dv* is computed.

$$E = E_0 \cdot \left(\frac{I}{I_c}\right)^n \tag{6.1}$$

Where E_0 is the limit electric field equal to 10 μV/m, I is the current flowing in the conductor, I_c is the critical current and n is an index determined experimentally.

Among the N=100 accidental scenarios simulated, N_f = 17 have been not considered to identify the most relevant abnormal transients, because, during the simulation of these N_f transients, the helium at the suction of the CP is in saturation condition. This will indeed not happen in real operating conditions, as the CP will not be able to operate for a too low suction pressure. Moreover, the two-phase flow of the SHe is not implemented in 4C and the results obtained would be meaningless.

The N_s = 83 accidental scenarios have been classified using both the spectral clustering algorithm and the ESAX; the clusters obtained with the two methods are compared using the Silhouette and the DB index.

6.1 Results

It has been chosen to present first the results of the spectral clustering algorithm (Section 4.2.1). To compute the similarity between the N_s transients the similarity index μ_{ij} is computed. The results are stored in the similarity matrix $\overline{\overline{W}}$, shown in Figure 6.2. Figure 6.3 shows the eigenvalues $\lambda_1, \lambda_2, \dots, \lambda_{N_s}$ of the matrix $\overline{\overline{L}}_{sym}$ get by transforming $\overline{\overline{W}}$ (the ratio $-\frac{\ln(\alpha)}{\beta^2}$ is equal to $1.7 \cdot 10^{-9}$). According to eigengap theory, the number of cluster C is set equal to 9 since the first nine eigenvalues are close to zero and the tenth is larger than others.

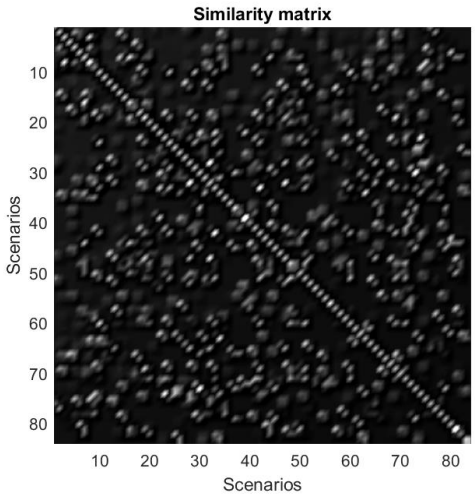

Figure 6.2 The similarity matrix $\overline{\overline{W}}$

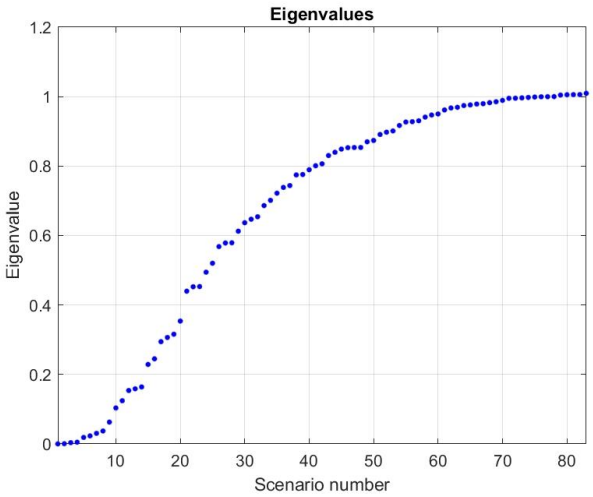

Figure 6.3 The N_s=83 eigenvalue of the matrix $\bar{\bar{L}}_{sym}$

The assignment of the different trajectories the proper cluster can be done using the FCM. Even in this case, to be more precise in the objective of identifying the prototypical abnormal behaviours of the system, the *i-th* scenario is assigned to the *c-th* clusters if the membership m_{ic} > 0.7. For this reason, 70 out 83 scenarios are assigned to one of the nine cluster, i.e. 13 transients are not assigned to any of the *C* clusters. Once the number of cluster has been found and the different transients are associated to the proper cluster, the similarity matrix is properly shuffled, shown in Figure 6.4, according to the results of the FCM. The most similar scenarios are grouped together resulting in 9 bright square; this implies that the transients inside each cluster are similar between them and dissimilar with the other scenarios correctly classified in other clusters.

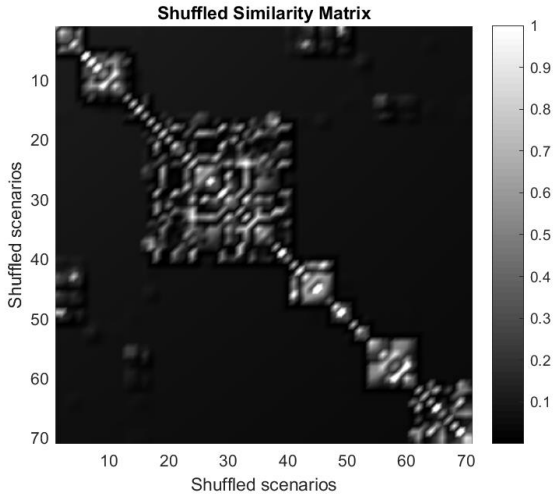

Figure 6.4 The shuffled similarity matrix $\bar{\bar{W}}$

The evolution of the safety features in the different clusters is shown in Figure 6.5 (where I/I_c and p_{cin} are plotted in time) and Figure 6.6 (in which T_{hs} and p_{cin} are considered). Cluster 1 is characterized by transients in which the LOFA occurs during the ramp down of the current from the CSM; due to the timing in which the LOFA is detected no significant increase can be seen in the three safety features. In cluster 2, the LOFA does not occurs: the I/I_c has the same

values both in the first and in the second cycle instead it can be seen an increase of the T_{hs} and a decrease of the p_{cin}. The LOFA occurs in the dwell time in cluster 3, in a moment in which no current flows in the CSM; consequently, the AC losses are not present in this case been the derivate of the current always zero. The cluster 4 is characterized by the occurrence of the LOFA in first two steps of the ITER cycle, the ones in which the higher quantity of heat is deposited in the CSM. To this cluster belongs the transients in which are computed the higher values of p_{cin} and T_{hs} that increase rapidly during the current dump. The transients belonging to the cluster 5 show an increase on the p_{cin} which corresponds to a slightly increase on the T_{hs} and the LOFA occurs at end of burn. In cluster 6, the current dump due to the LOFA occurs at late time during the last step of the ITER cycle. Due to the AC losses, it can be seen an increase both on the p_{cin} and the T_{hs}. The cluster 7 is characterized by the transients in which the LOFA does not occur. In this cluster, the combination of the failures gives as results that the p_{cin} and the T_{hs} is almost the same during both the cycle. In cluster 8, it can be simultaneously seen the lowest values of T_{hs} and p_{cin}; in this cluster the LOFA occurs during the dwell without heat deposition because the current is already null. The transients in the cluster 9 are characterized by a rapid increase on the T_{hs} when the LOFA occurs, between the end of burn and the dwell period, whereas the p_{cin} is fix at the minimum value, i.e. the value of pressure of the QT. The characteristics of each clusters are listed in Table 6.1.

Table 6.1 Summary of the peculiar characteristics of the Z=3 safety features for each cluster using the Spectral Cluster.

Cluster	p_{cin}	T_{hs}	I/I_c	LOFA (occurrence)
1	0.5 MPa	5.5 K	0.42	Yes, at medium time
2	0.35 MPa	6 K	0.42	No
3	0.35 MPa	5.2 K	0	Yes, at medium time
4	0.8 MPa	6.2 K	0.42	Yes, at early time
5	0.6 MPa	5.5 K	0	Yes, at medium time
6	0.55 MPa	5.5 K	0.2	Yes, at late time
7	0.7 MPa	6 K	0.42	No
8	0.4 MPa	4.7 K	0	Yes, at medium time
9	0.35 MPa	5.7 K	0.3	Yes, at medium time

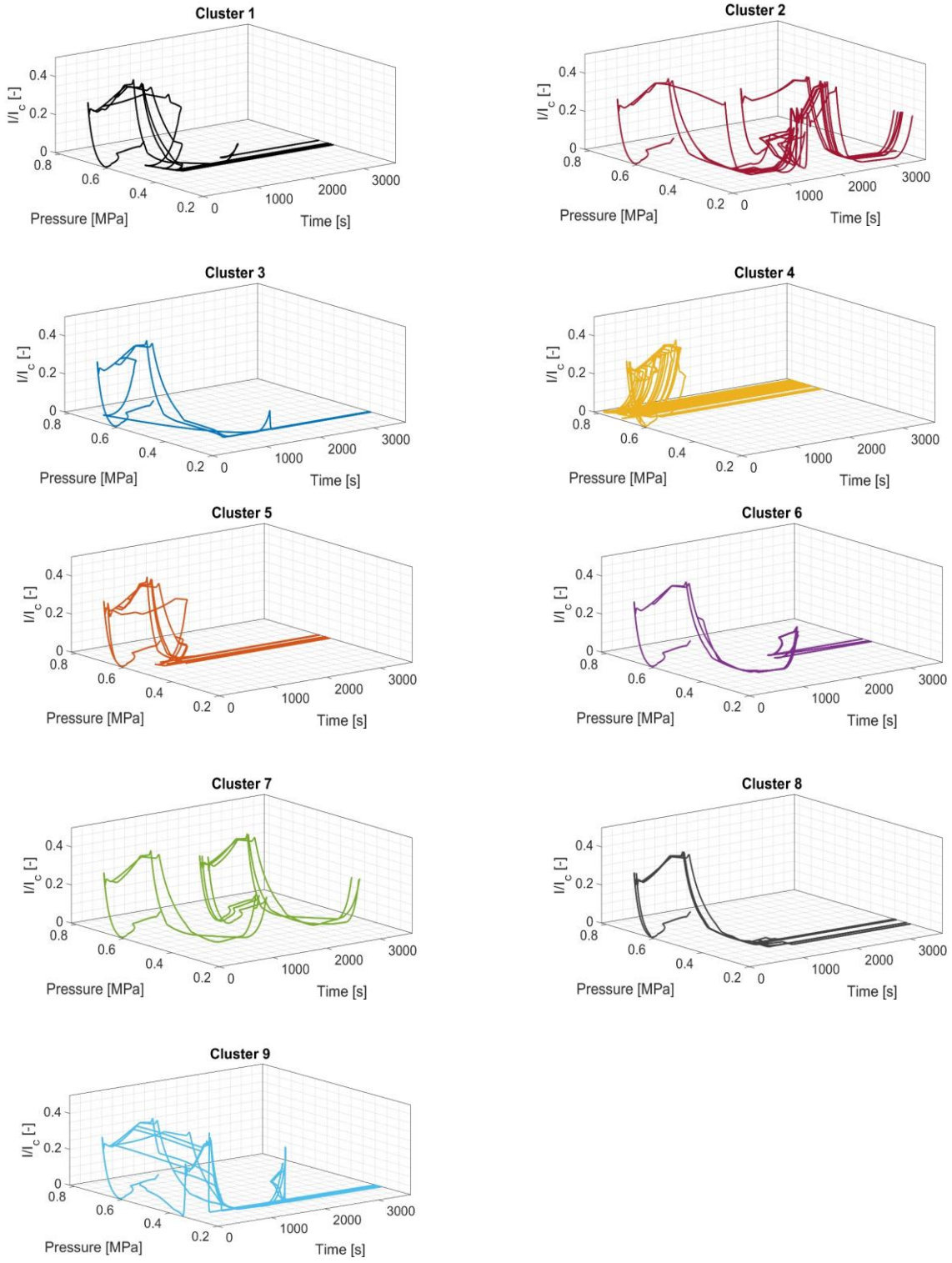

Figure 6.5 The time evolution of the I/I_c and p_{cin} in the 9 clusters using the Spectral Clustering

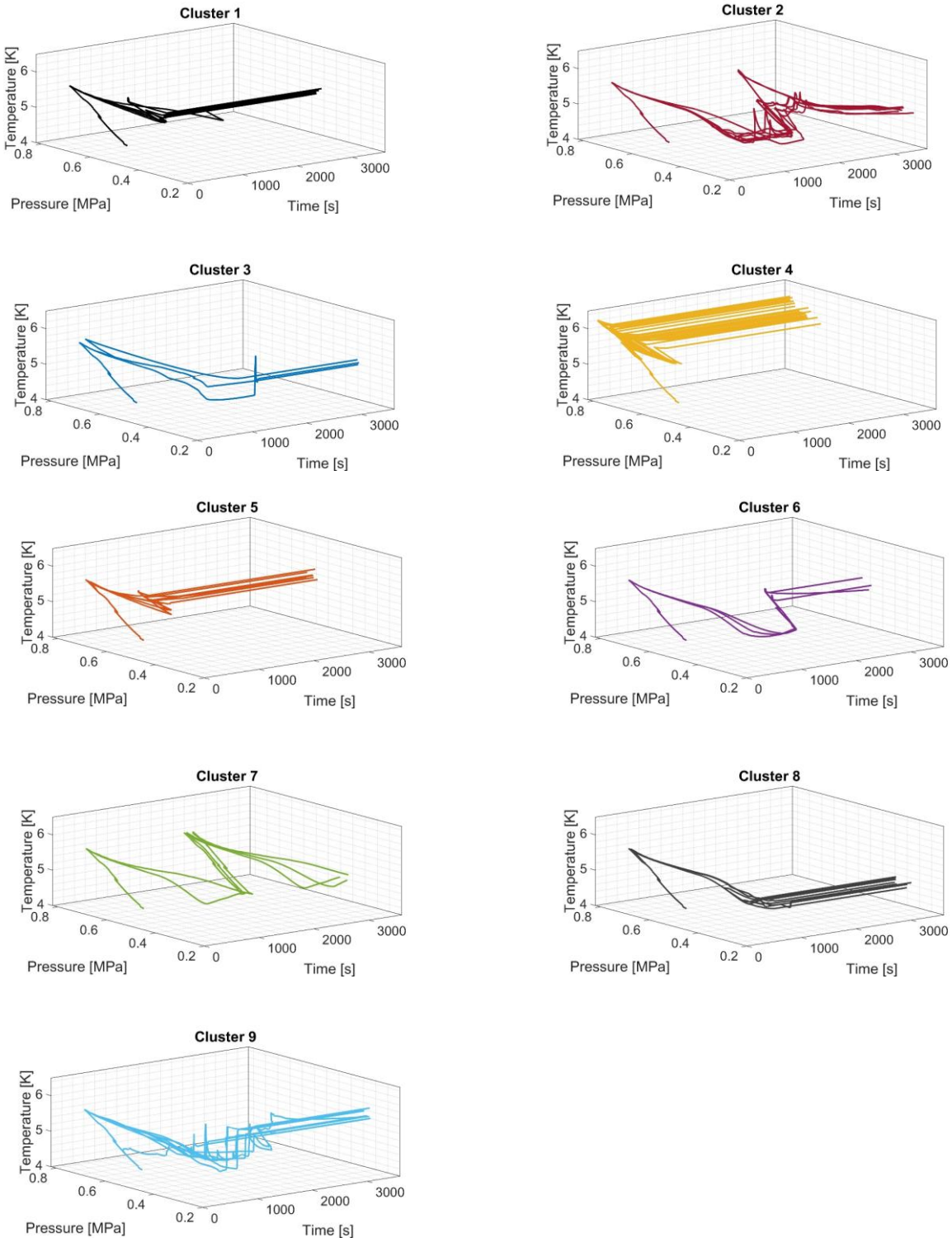

Figure 6.6 The time evolution of the T_{hs} and p_{cin} in the 9 clusters using the Spectral Clustering

The evolution of the accidental scenarios described by the transients clustered in clusters 1-9 are justified by the magnitude and timing of the components failures that are described in the MVL sequence simulated. The bubble representation, described in Section 5.1, is applied even this second case study, to find the prototypical failure that would lead the system to evolve in each described cluster. It is worth recalling that in all the N_s scenarios the pressure at the ends of the CSM is kept well below the 1.8 MPa and the hot-spot temperature T_{hs} is lower than T_{CSI},

i.e. the abnormal simulated scenarios are safe for the integrity of the CSM during both the test in the reference facility and in ITER. Figure 6.7 shows for each cluster the prototypical state of the components: larger circles are used to highlight the most common failure times and magnitude of the MVL that belong to that cluster. A summary of the analysis is reported in Table 6.2.

For clarity sake, Cluster 4 is explained in detail, being the cluster that shows the largest values of T_{hs} and p_{cin} (see Figure 6.6, 2th row, right). Even in this case T_R is discretized in 3 intervals to group the failure with same magnitude and order during the MVL sequence: the prototypical failures of the component can, thus, happen at early, medium or late time. In this case, all the failures happen in the first two steps of the ITER current cycle, as confirmed by the bubble plot (see Figure 6.7, 2th row, right), in which all the failures (small in number for this cluster) occur at early times. The timing of the failure is the reason for which the highest values of T_{hs} and p_{cin} are reached in this cluster. The failures happen when the CSM is already in the more severe operative condition and the heat deposition given by the AC losses produces a further increase in T_{hs} and p_{cin}. Nevertheless, all the transients of this cluster are not dangerous for the integrity of the CSM in the reference facility and the T_{hs} is always lower than the T_{CSI} with a positive safety margin. The most important "contributors" to the transients, i.e. the most frequent components' failures, are those with larger circles in the bubble diagram: the BV must fail stuck open as first event, the CP must reduce its rotational speed until a complete stop as second failure along the sequence, the CV2 must fail stuck closed as first or second event in the sequence and the SV2 must fail stuck closed in nominal position as first event. Moreover, other characteristic failures are the CV1 that must fail stuck closed as second event in the MVL sequence, whereas the SV1 must fail (as first or third event) stuck open at 50% of the nominal flow area, corresponding to the transients that present the lower value of pressure inside this cluster. In the present case, two prototypical failures in the same position inside the MVL sequence are equally important to the transient development (i.e., BV or CV2): this means that, in spite of the event, the evolution of the transient is the same. Considering again these two failures, they are MCS, i.e. if BV or CV2 fail with the higher magnitude the LOFA occurs. Instead, in the case in which SV2 fails stuck in nominal position as first failure in the MVL sequence, at least the failure of another component is needed to cause a LOFA.

Table 6.2 Summary of the prototypical states of the components that would lead the system into C=9 clusters.

Cluster	Most important components	Magnitude	Time	Order
1	CV1	3	Early/Medium	2/3
	BV	3	Medium	2/3
2	CV1	1	Early	1
	CV2	1	Early	1
	SV1	1	Early	1
	SV2	3	Medium/Late	2/3/5
3	SV1	3	Medium	2/3
	CV2	1	Early/Late	2/4
4	CP	4	Early	2
	BV	3	Early	1
	SV2	1	Early	1
	CV2	3	Early	1/2
5	CV1	2	Early	1
	BV	3	Medium	2
	CV2	2	Early/Medium	1/3
	CP	3	Early/Medium	2/4
6	CP	2	Medium	2
	CV2	1	Late	3/4
	BV	2	Early/Medium	1
7	CV1	1	Late	3
	CV2	1	Medium	1
	CP	1/2	Late/Early	4/2
	SV1	1	Early	1
	SV2	1	Early/Late	1/2
8	CV2	1	Early	1
	BV	2	Early	1
	CV1	3	Late	3
	CP	2/3	Medium	1/2
9	CV2	2	Medium	2
	SV1	3	Early	1
	SV2	1	Early	1

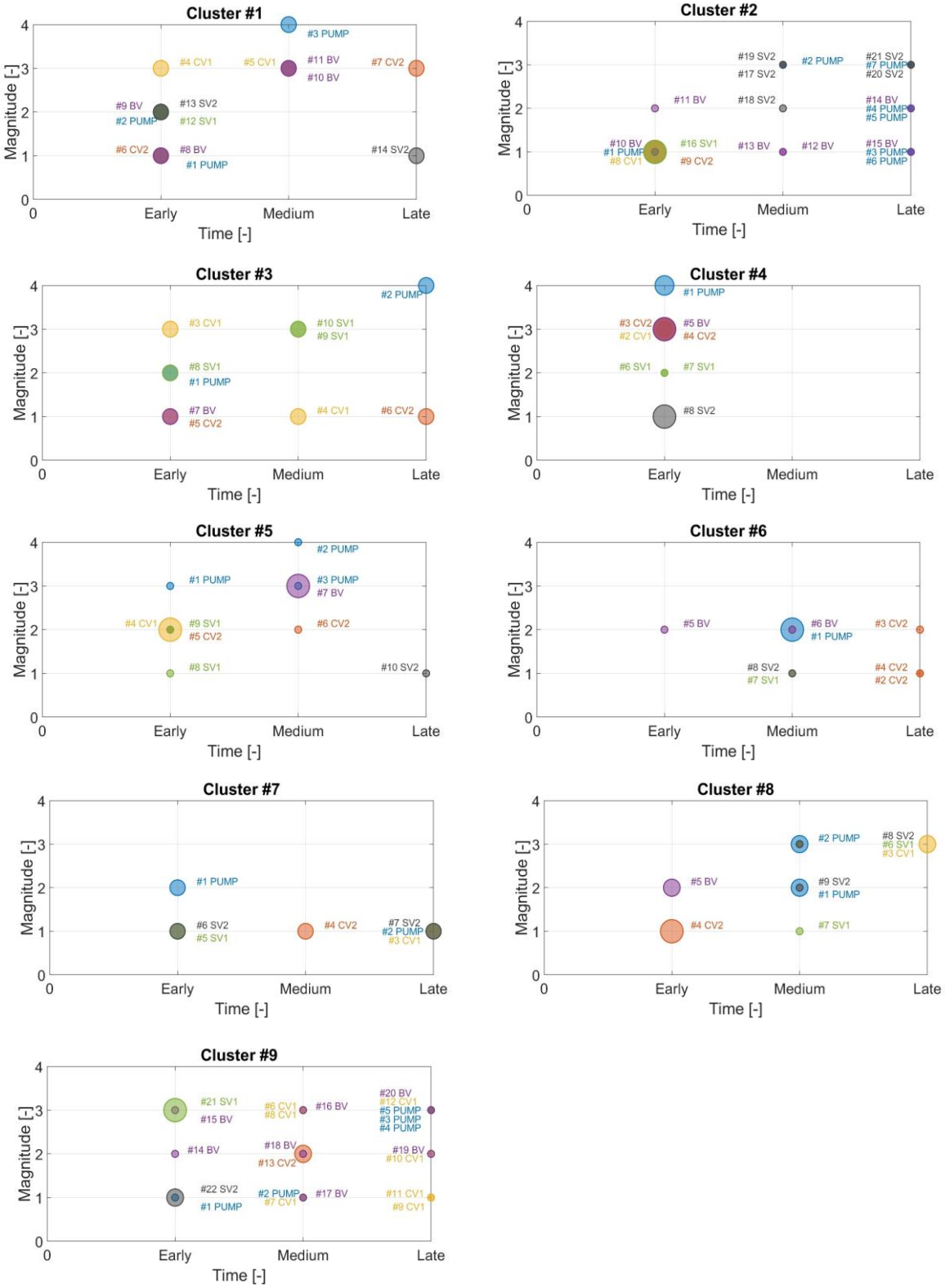

Figure 6.7 Bubble representation of the prototypical states of the components that would lead the system into C=9 clusters.

The ESAX has also been applied to cluster the N_s scenario generated. The time horizon [0, T_M] has been divided in 12 equal size intervals and the number of equi-probable intervals α has been set equal to 4. The Silhouette and DavidesBouldin indexes have been used to determine

the optimal number of cluster between a set of $C_{candidate}$ = [3,10] number of cluster. Figure 6.8 shows that for C=9 clusters the Silhouette value (circle) and DB index (square) are simultaneously maximized and minimized, respectively. To assign each *i-th* transient to the proper *c-th* cluster, the FCM has been applied with the constrain on the membership, i.e. the assignment has been occurred if m_{ic}>0.7. Some of the transients are not classified in any of the C clusters as result of the constrain; in this case, 21 transients are excluded.

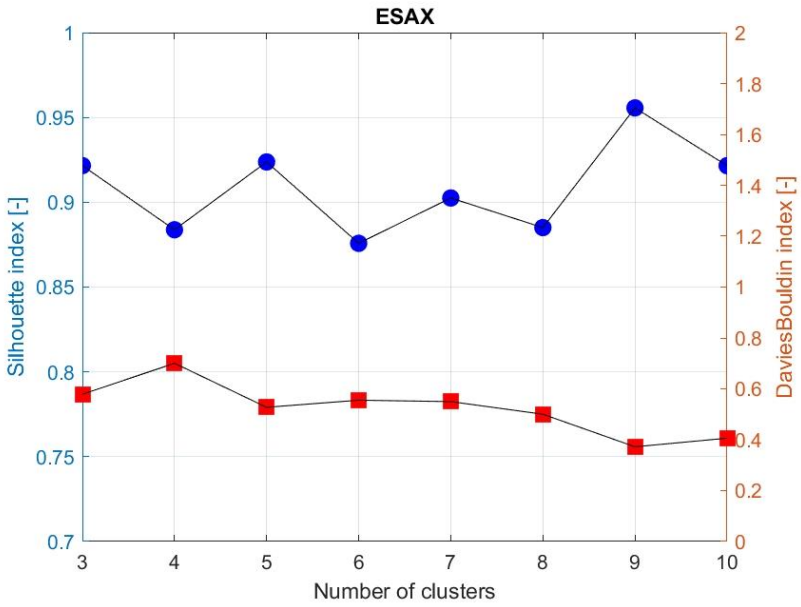

Figure 6.8 Silhouette values (circles) and the DB index (squares) for different $C_{candidate}$ = [3,10]

The results of the ESAX clustering algorithm are shown in Figure 6.9 and Figure 6.10. The clusters get are similar to the group described with the use of the spectral clustering. The cluster 3 obtain with the ESAX is different from any others shown using the spectral clustering. In this case (see Figure 6.9 and Figure 6.10, 2th row, left) the LOFA occurs during the magnetization phase of the ITER cycle, this means that an increasing ramp current is flowing in the CSM and as consequence the heat deposition in the strands due to the AC losses depends on the actual time in which the LOFA occurs. In fact, a higher current flowing in the CSM results in a higher energy accumulated in the module. Nevertheless, for the two transients classified in this cluster both T_{hs} and p_{cin} are lower than the safety threshold with a positive margin.

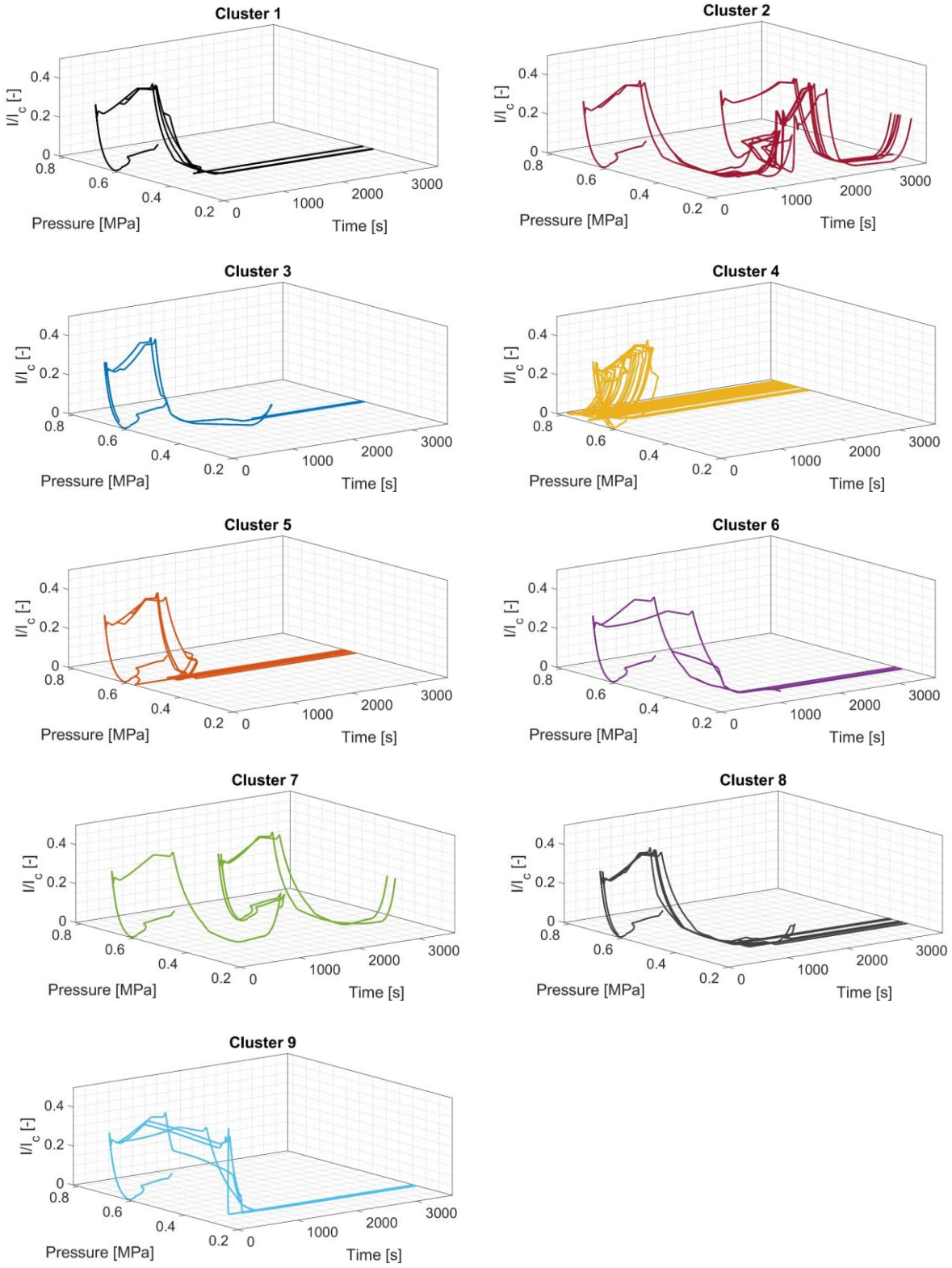

Figure 6.9 The time evolution of the I/I_c and p_{cin} in the 9 clusters using the ESAX

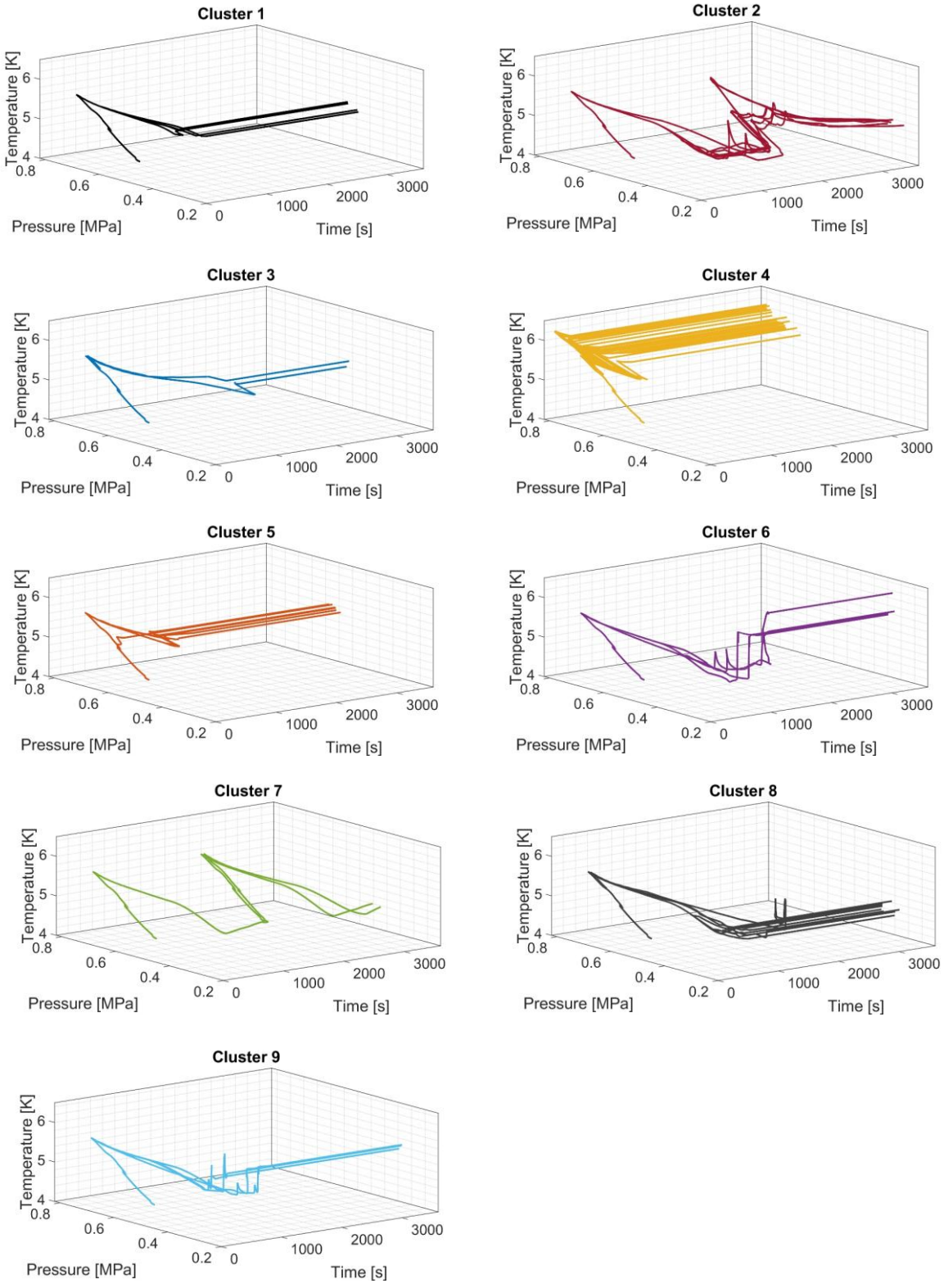

Figure 6.10 The time evolution of the T_{hs} and p_{cin} in the 9 clusters using the ESAX

To choose the best clustering algorithm, the Silhouette and the DB index have been used to compute the compactness and the separation of the cluster. Even in this approach, the spectral clustering is confirmed as the best algorithm technique to identify the most relevant abnormal

transients: Figure 6.11 shows the higher values of the Silhouette index and lower value of DB for each of the C=9 cluster for spectral clustering rather than ESAX.

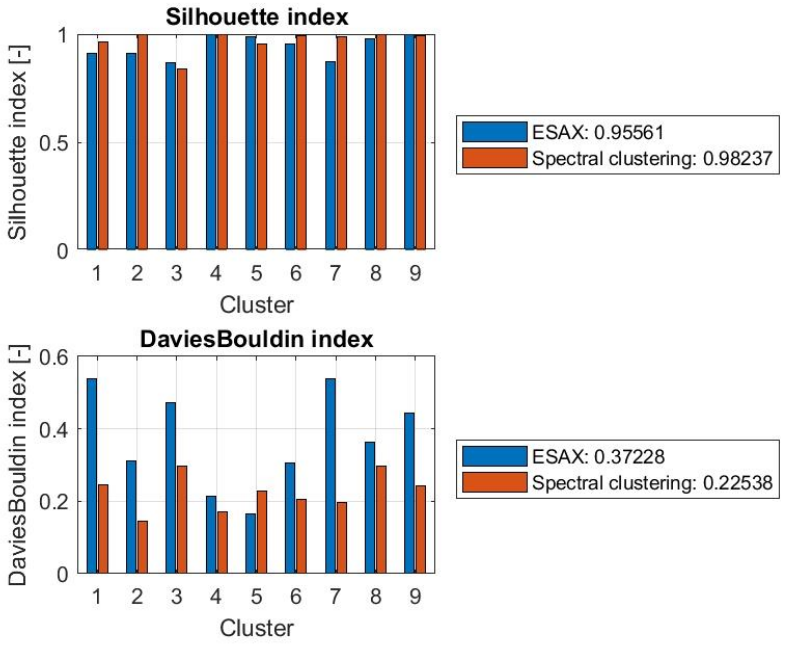

Figure 6.11 Comparison between the silhouette valued and the DB index for the ESAX and the Spectral Clustering algorithm

The bubble representation has been applied to the N_f scenarios. The results, represented in Figure 6.12, shown these transients can be considered as a further cluster due the fact that the failures that lead the system in the saturation of the helium at the suction of the pump are different from the one shown in Figure 5.6. The main contributions are the position of the SVs: the SV2 must fail stuck open at the 50 % of the nominal flow as first failure in the accidental sequence whereas the SV1 must fail stuck totally open or open at 50% of the nominal flow. Other failures are less frequent: the BV and CV2 are stack in nominal position, the CP reduces the rotational speed up to 75% of the nominal mass flow rate and the CV1 is stuck in open position at 50% of the nominal mass flow rate.

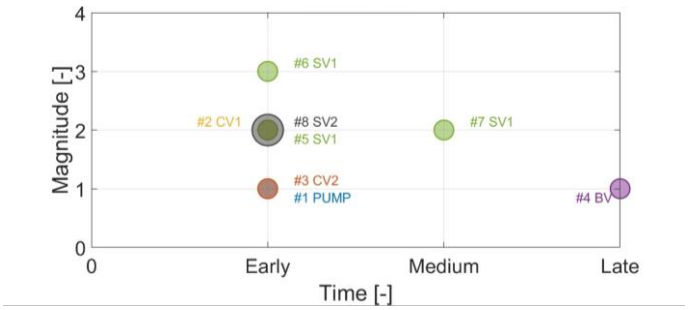

Figure 6.12 Bubble representation of the prototypical failures of the N_f transients.

7 Conclusions

The objective of this thesis was to consider the safety analysis of the simplified cooling circuit of a single module of the ITER Central Solenoid (CS) in a cold test facility, in order to classify the different possible abnormal transients and identify the (combinations of) components failures that may drive the system into a Loss-Of-Flow Accident (LOFA). The IDPSA framework has been applied (for the first time, to the best of the author's knowledge) to a fusion system and the following three steps have been undertaken to study the dynamic response of the ITER CS module (CSM): (i) random scenarios generation; (ii) scenario modelling by a deterministic code and (iii) scenarios post-processing. Two different operating conditions have been considered for the CSM: in the first, a constant current flowing in the module is assumed for the sake of simplicity (and for the sake of method demonstration); in the second, the real ITER-like current scenario is analyzed to derive some preliminary insights on the safety of the ITER reactor in the presence of abnormal transients. With respect to that, it is worth recalling that, in the case of the ITER-like current scenario, the maximum (i.e., hot-spot) temperature reached by the CSM in the test facility can be assumed to be close to the one reached by the CSM in the real ITER reactor, being the same the power deposited on the CSM and the heat capacity of the strands. In addition, the value of the current sharing temperature (T_{CS}) in the test facility (i.e., the threshold not to exceed to avoid magnet quench) is higher than that of the ITER reactor, due to the lower magnetic field felt by the CSM (the self-magnetic field generated is indeed the only contribution to the T_{CS} in the test facility).This implies that a transient, which is safe for the operation of the CSM during the tests in the reference facility, could be instead critical for the operation of the ITER reactor in abnormal conditions.

Within the IDPSA framework, the Multiple Value Logic (MVL) has been adopted for building a comprehensive set of combinations of (random) times and (discrete) magnitudes of components failures, representing the stochastic accident scenarios under analysis. The application of the MVL has generated a list of more than 10^8 possible scenarios. However, for the sake of brevity, only a "bounding analysis" of the system response has been carried out by inspecting a reduced set of $N = 100$ MVL sequences, to be used for identifying prototypical scenarios useful to characterize systems behaviours under all the possible MVL sequences (both for the constant and the ITER-like current configurations).

The 4C code (capable of reproducing the CSM behaviour and the SHe flow in the cooling circuit) has been employed to simulate the scenarios described by the MVL. In the analysis, the cooling helium pressure at the inlet and outlet of the SC coil, the hot-spot temperature of the CSM strands, and the voltage measured across the pancakes (substituted by the ratio between the current and the critical current, in the ITER-like current scenario) have been selected as "critical" safety parameters/features to monitor during each accidental transient.

To post-process the results, the spectral clustering algorithm has been adopted for grouping the scenarios according to their similarity: this has allowed the (unsupervised) identification of prototypical behaviours of abnormal transient and the corresponding (combination of) component failures, that may lead the system to a LOFA. The proposed methodology has been firstly applied to the simplified case (i.e., the constant current scenario); then, the satisfactory results obtained have been confirmed by a more realistic application (i.e., the ITER-like current scenario). The spectral clustering output is represented by a similarity matrix: each element is the degree of (fuzzy) similarity between the transients. The pressure at the inlet of the coil, the voltage measured at the extremities of the CSM and the hot-spot temperature of the strands have been used as (safety) features to compute the similarity between the transients in the first case study. The values of the computed voltages are of the order of the nV: too small to be

measured in a real plant/facility. For this reason, in the second case study, the voltage is substituted by the ratio of the actual current that flows in the coil and the critical current (and is found to be directly correlated with the voltage). To avoid misclassification error and to meet the goal of identifying the prototypical abnormal behaviour of the system, the *i-th* transient is assigned to the *c-th* clusters if the corresponding membership (i.e., confidence) m_{ic} is higher than 0.7. Nevertheless, some transients, 2 in the first case study and 13 in the second, are rejected, i.e., they are not assigns to any cluster.

A reference literature method, the ESAX, has been also applied to the classify the transients in clusters. The Silhouette and DB indexes have been used to find the optimum number of cluster for this second clustering algorithm. The ESAX confirmed the number of cluster got applying the spectral clustering algorithm, as optimal and furthermore the transient evolutions obtained with the two algorithms are similar. Even in this case, the FCM is used to assign the transient to the cluster. A lower assignment rate has been obtained with this second algorithm, i.e. 13 transients for the constant current scenario and 21 for the ITER-like scenario are not assign to any cluster.

Silhouette and DB indexes have qualified the spectral clustering as preferred post-processing approach, because the obtained clusters are more separated and compacted than those of ESAX. Thus, the spectral clustering explains better the prototypical system failure behaviour and maximize the use of the simulated transients, due to a higher assignment rate. The spectral clustering results have been used to characterize the prototypical system failures that may lead the system to evolve in the described cluster. In particular, a bubble representation has been proposed where the magnitude, time and order of the failure for each component has been represented as a bubble of variable dimension: the more frequent the state is visited by the component the bigger is the corresponding bubble. The components with the bigger bubble have been assumed as the prototypical failures of the corresponding cluster.

Results have shown that none of the MVL scenarios is critical for the CS module integrity: in particular, in all the cases considered, the pressure at the inlet of the coil is kept below the safety threshold of 1.8MPa, i.e., with a positive safety margin, voltage keeps well below the threshold of 0.1V, which implies the hot-spot temperature does not exceed the current sharing temperature T_{CS} and the magnet does not lose its SC properties. The hot-spot temperature of the CSM, in the condition simulating the ITER-like current scenario, is below the T_{CSI} implying that no relevant safety issues should be expected in ITER during the N_s accidental scenarios.

The relevance of the study can be summarized as follows. The application of the IDPSA framework has identified a set of "prototypical states" of the system (components) that may lead the CSM cooling circuit to a LOFA. Such a "mapping" is of paramount importance, because in principle it allows to characterize and classify (in a timely manner, i.e. in a real-time control) a new developing scenario as 'safe' or 'faulty'. In other words, the CSM and the cooling circuit status can be continuously classified in real-time as "normal" or as one of the C abnormal operation states pointed out as the result of this thesis. In this way, a powerful instrument is given to the facility operators that may instantaneously classify the undergoing transient as normal or abnormal. If an abnormal scenario happens in the facility, thanks to the "map" of "prototypical states" of the system components (here visualized as a bubble diagram), the time needed to locate the failures can be reduced, since the proposed tool suggests the failure of some components as the *most likely* causes of the abnormal transient. In other words, the proposed approach may help in prioritizing components' state monitoring and maintenance.

In the future, the set of the N different scenarios simulated for the two different operating conditions considered can be used to train a so-called Reduced Order Model (ROM), i.e., a surrogate (regression) model that can mimic the behaviour of the original, long-running 4C

code, but that can provide results at a much lower computational cost. This will be useful to explore more deeply the space of the possible accidental scenarios.

In addition, it is highlighted that the CSM has been analysed here in “cold mode experimental operation” (i.e., with the coil inlet temperature taken as the nominal one in the reference test facility). In future, new efforts could be also devoted to study this system in new, “more challenging” situations; for example, it should be done under more severe operating conditions, e.g., by reducing the temperature margins because of an operating temperature closer to the T_{CS}.

Finally, it is worth noting that in the second case study, the effect of a set of $N_f = 17$ simulations has not been evaluated due to the reaching of helium saturation conditions at the suction of the centrifugal pump: this should not happen in the real experiments because the pump will not be able to operate with a too low suction pressure.

Bibliography

Al-Dahidi, S., Di Maio, F., Baraldi, P., Zio, E., Seraoui, R., 2015a. A Novel Ensemble Clustering for Operational Transients Classification with Application to a Nuclear Power Plant Turbine. Int. J. Progn. Heal. Manag. 6, 1–21.

Al-Dahidi, S., Di Maio, F., Baraldi, P., Zio, E., Seraoui, R., 2015b. Unsupervised Ensemble Clustering for Transients Classification in a Nuclear Power Plant Turbine, in: The Annual European Safety and Reliability Conference ESREL2015.

Al-Dahidi, S., Maio, F. Di, Baraldi, P., Zio, E., Seraoui, R., 2018. A framework for reconciliating data clusters from a fleet of nuclear power plants turbines for fault diagnosis. Appl. Soft Comput. 69, 213–231. https://doi.org/https://doi.org/10.1016/j.asoc.2018.04.044

Alata, M., Molhim, M., Ramini, A., 2008. Optimizing of Fuzzy C-Means Clustering. World Acad. Sci. Eng. Technol. 2, 224–229.

Aldemir, T., 2013. A survey of dynamic methodologies for probabilistic safety assessment of nuclear power plants. Ann. Nucl. Energy 52, 113–124. https://doi.org/10.1016/j.anucene.2012.08.001

Alpert, C.J., Yao, S., 1995. Spectral Partitioning: The More Eigenvectors, The Better. Discret. Appl. Math 90.

Alzbutas, R., Voronov, R., 2015. Reliability and safety analysis for systems of fusion device. Fusion Eng. Des. 94, 31–41. https://doi.org/10.1016/j.fusengdes.2015.03.001

Baraldi, P., Di Maio, F., Zio, E., 2013. Unsupervised Clustering for Fault Diagnosis in Nuclear Power Plant Components. Int. J. Comput. Intell. Syst. 6, 764–777. https://doi.org/10.1080/18756891.2013.804145

Bezdek, J.C., 1981. Pattern Recognition with Fuzzy Objective Function Algorithms.

Butler, M., Kazakov, D., 2015. SAX Discretization Does Not Guarantee Equiprobable Symbols. IEEE Trans. Knowl. Data Eng. 27, 1162–1166. https://doi.org/10.1109/TKDE.2014.2382882

Carpignano, A., Pinna, T., Savoldi, L., Sobrero, G., Uggenti, A.C., Zanino, R., 2016. Safety issues related to the intermediate heat storage for the EU DEMO. Fusion Eng. Des. 109–111, 135–140. https://doi.org/10.1016/j.fusengdes.2016.01.078

Čepin, M., 2011. Event Tree Analysis, in: Assessment of Power System Reliability: Methods and Applications. Springer London, London, pp. 89–99. https://doi.org/10.1007/978-0-85729-688-7_6

D'Amico, G., Portone, A., Jong, C.T.J., 2018. An Electromagnetic and Structural Finite Element Model of the ITER Toroidal Field Coils. IEEE Trans. Appl. Supercond. 28, 1–5. https://doi.org/10.1109/TASC.2017.2769485

D'Amico, G., Reccia, L., Portone, A., Jong, C.T.J., Mitchell, N., 2016. ITER TF Magnet System Analyses in Faulted Conditions. IEEE Trans. Appl. Supercond. 26, 3–7. https://doi.org/10.1109/TASC.2016.2517449

Davies, D.L., Bouldin, D.W., 1979. A Cluster Separation Measure. IEEE Trans. Pattern Anal. Mach. Intell. PAMI-1, 224–227. https://doi.org/10.1109/TPAMI.1979.4766909

Di Maio, F., Baronchelli, S., Vagnoli, M., Zio, E., 2017. Determination of prime implicants by differential evolution for the dynamic reliability analysis of non-coherent nuclear systems. Ann. Nucl. Energy 102, 91–105. https://doi.org/10.1016/j.anucene.2016.12.018

Di Maio, F., Baronchelli, S., Zio, E., 2015. A Computational Framework for Prime Implicants Identification in Noncoherent Dynamic Systems. Risk Anal. 35, 142–156. https://doi.org/10.1111/risa.12251

Di Maio, F., Hu, J., Tse, P., Pecht, M., Tsui, K., Zio, E., 2012. Ensemble-approaches for clustering health status of oil sand pumps. Expert Syst. Appl. 39, 4847–4859. https://doi.org/10.1016/j.eswa.2011.10.008

Di Maio, F., Secchi, P., Vantini, S., Zio, E., 2011. Fuzzy C-Means Clustering of Signal Functional Principal Components for Post-Processing Dynamic Scenarios of a Nuclear Power Plant Digital Instrumentation and Control System. IEEE Trans. Reliab. 60, 415–425. https://doi.org/10.1109/TR.2011.2134230

Di Maio, F., Vagnoli, M., Zio, E., 2016. Transient identification by clustering based on Integrated Deterministic and Probabilistic Safety Analysis outcomes. Ann. Nucl. Energy 87, 217–227. https://doi.org/10.1016/j.anucene.2015.09.007

Dongiovanni, D.N., Ciattaglia, S., Porfiri, M.T., 2017. Parametric explorative study of DEMO galleries pressurization in case of ex-vessel LOCA. Fusion Eng. Des. 124, 1223–1227. https://doi.org/10.1016/j.fusengdes.2017.03.120

Dubois, D., Prade, H., Testemale, C., 1988. Weighted fuzzy pattern matching. Fuzzy Sets Syst. 28, 313–331. https://doi.org/10.1016/0165-0114(88)90038-3

European Commission. Directorate General for Research., 2004. Fusion research : an energy option for Europe's future.

European Environment Agency, 2017. Air quality in Europe — 2017 report, EEA Technical Report. https://doi.org/10.2800/22775

Everitt, D., Reiersen, W., Martovetsky, N., Hussung, R., Litherland, S., Freudenberg, K., Myatt, L., Hatfield, D., Cole, M., Irick, D.K., Reed, R., Lyraud, C., Libeyre, P., Bessette, D., Jong, C., Mitchell, N., Rodriguez-Mateos, F., Dolgetta, N., 2013. ITER Central Solenoid design, in: 2013 IEEE 25th Symposium on Fusion Engineering (SOFE). IEEE, pp. 1–8. https://doi.org/10.1109/SOFE.2013.6635515

Farmer, F.R., 1967. Siting criteria - a new approach. IAEA Symp. Contain. Sitting Nucl. Power React. Vienna 303–324.

Fisher, E.P.M., 2017. Control valve handbook, fifth edit. ed. FISHER CONTROLS CO.

Freidberg, J.P., 2007. Plasma Physics and Fusion Energy. Cambridge University Press, Cambridge. https://doi.org/10.1017/CBO9780511755705

Froio, A., Bertinetti, A., Savoldi, L., Zanino, R., Cismondi, F., Ciattaglia, S., 2017. Benchmark of the GETTHEM Vacuum Vessel Pressure Suppression System (VVPSS) model for a helium-cooled EU DEMO blanket, in: Safety and Reliability – Theory and Applications. CRC Press, CRC Press Taylor & Francis Group 6000 Broken Sound Parkway NW, Suite 300 Boca Raton, FL 33487-2742, pp. 11–11. https://doi.org/10.1201/9781315210469-9

Froio, A., Bonifetto, R., Carli, S., Quartararo, A., Savoldi, L., Zanino, R., 2016. Design and optimization of Artificial Neural Networks for the modelling of superconducting magnets operation in tokamak fusion reactors. J. Comput. Phys. 321, 476–491.

https://doi.org/10.1016/j.jcp.2016.05.028

Garribba, S., Guagnini, E., Mussio, P., 1985. Multiple-Valued Logic Trees: Meaning and Prime Implicants. IEEE Trans. Reliab. R-34, 463–472. https://doi.org/10.1109/TR.1985.5222234

Heller, R., 2009. Safety Analysis of the 70 kA ITER HTS Current Lead Demonstrator. IEEE Trans. Appl. Supercond. 19, 1504–1507. https://doi.org/10.1109/TASC.2009.2017839

Hoa, C., Bon-Mardion, M., Bonnay, P., Charvin, P., Cheynel, J.N., Lagier, B., Michel, F., Monteiro, L., Poncet, J.M., Roussel, P., Rousset, B., Vallcorba-Carbonell, R., 2012. Investigations of pulsed heat loads on a forced flow supercritical helium loop - Part A: Experimental set up. Cryogenics (Guildf). 52, 340–348. https://doi.org/10.1016/j.cryogenics.2012.02.004

Honda, T., Bartels, H.-W., Merrill, B., Inabe, T., Petti, D., Moore, R., Okazaki, T., 2000. Analyses of loss of vacuum accident (LOVA) in ITER. Fusion Eng. Des. 47, 361–375. https://doi.org/10.1016/S0920-3796(99)00067-8

Honda, T., Bartels, H.W., Uckan, N.A., Okazaki, T., Seki, Y., 1997. Analyses of passive plasma shutdown during ex-vessel loss of coolant accident in the first wall/shield blanket of fusion reactor. J. Nucl. Sci. Technol. 34, 538–543. https://doi.org/10.1080/18811248.1997.9733706

Honda, T., Maki, K., Okazaki, T., Uda, T., Seki, Y., Aoki, I., Kunugi, T., 1994a. Comprehensive Safety Analysis Code System for Nuclear Fusion Reactors II: Thermal Analyses During Plasma Disruptions for International Thermonuclear Experimental Reactor. Fusion Technol. 26, 1288–1295. https://doi.org/10.13182/FST94-A30313

Honda, T., Okazaki, T., Maki, K., Uda, T., Seki, Y., Aoki, I., Kunugi, T., 1996. Comprehensive Safety Analysis Code System for Nuclear Fusion Reactors III: Ex-Vessel LOCA Analyses Considering Passive Safety. Fusion Technol. 29, 116–125. https://doi.org/10.13182/FST96-A30661

Honda, T., Uda, T., Maki, K., Okazaki, T., Seki, Y., Aoki, I., 1994b. Comprehensive Safety Analysis Code System For Nuclear Fusion Reactors I: Model And Analyses of Overpower Events for the International Thermonuclear Experimental Reactor. Fusion Technol. 25, 451–468. https://doi.org/10.13182/FST94-A30252

Ikeda, K., 2010. ITER on the road to fusion energy. Nucl. Fusion 50. https://doi.org/10.1088/0029-5515/50/1/014002

International Atomic Energy Agency, 2006. Fundamental Safety Principles. Saf. Fundam. 2, 37.

International Energy Agency (IEA), 2018. Key Electricity Trends 2017 5.

International Energy Agency (IEA), 2017. World Energy Outlook 2017.

IPCC, 2007. Climate Change 2007 Synthesis Report, Intergovernmental Panel on Climate Change [Core Writing Team IPCC. https://doi.org/10.1256/004316502320517344

Joentgen, A., Mikenina, L., Weber, R., Zimmermann, H.-J., 1999. Dynamic fuzzy data analysis based on similarity between functions. Fuzzy Sets Syst. 105, 81–90. https://doi.org/10.1016/S0165-0114(98)00337-6

Khakzad, N., Khan, F., Amyotte, P., 2012. Dynamic risk analysis using bow-tie approach. Reliab. Eng. Syst. Saf. 104, 36–44. https://doi.org/10.1016/j.ress.2012.04.003

Kirschenbaum, J., Bucci, P., Stovsky, M., Mandelli, D., Aldemir, T., Yau, M., Guarro, S., Ekici, E., A. Arndt, S., 2009. A benchmark systems for comparing reliability modeling approaches for digital instrumentation and control systems. Nucl. Technol. 165, 53–95. https://doi.org/10.13182/NT09-A4062

Kitazawa, S., Okayama, K., Neyatani, Y., Sagot, F., van Houtte, D., 2014b. RAMI analysis of the ITER Central Safety System. Fusion Eng. Des. 89, 800–805. https://doi.org/10.1016/j.fusengdes.2014.05.014

Kitazawa, S., Okayama, K., Neyatani, Y., Sagot, F., van Houtte, D., 2014a. RAMI analysis of the ITER CIS. Fusion Eng. Des. 89, 88–93. https://doi.org/10.1016/j.fusengdes.2013.12.016

Knaster, J., Amoskov, V., Formisano, A., Gribov, Y., Lamzin, E., Martone, L., Maximenkova, N., Mitchell, N., Portone, A., Sytchevsky, S., Testoni, P., 2011. ITER non-axisymmetric error fields induced by its magnet system. Fusion Eng. Des. 86, 1053–1056. https://doi.org/10.1016/j.fusengdes.2011.02.045

Leguizamon, S., Pelgrum, H., Azzali, S., 1996. Unsupervised Fuzzy C-means classification for the determination of dynamically homogeneous areas. Rev. SELPER 12, 20–24.

Libeyre, P., Cormany, C., Dolgetta, N., Gaxiola, E., Jong, C., Lyraud, C., Reiersen, W., Everitt, D., Martovetsky, N., Rosenblad, P., Cole, M., Freudenberg, K., Liu, S., Smith, J., Wei, J., Wang, L., Yu, X., Dong, X., Xin, J., Li, C., Zheng, W., Fang, C., 2016. Status of design and manufacturing of the ITER Central Solenoid and Correction Coils. Proc. - Symp. Fusion Eng. 2016–May. https://doi.org/10.1109/SOFE.2015.7482275

Lin, J., Keogh, E., Lonardi, S., Chiu, B., 2003. A symbolic representation of time series, with implications for streaming algorithms. Proc. 8th ACM SIGMOD Work. Res. issues data Min. Knowl. Discov. - DMKD '03 2. https://doi.org/10.1145/882085.882086

Lkhagva, B., Suzuki, Y., Kawagoe, K., 2006. Extended sax: Extension of symbolic aggregate approximation for financial time series data representation. DEWS2006 4A-i8.

Madrid, A., Apostolakis, G., Conn, R.W., 1983. On the Development of Accident Sequences Involving Tokamak Impurity Control Systems. Nucl. Technol. - Fusion 4, 1135–1140. https://doi.org/10.13182/FST83-A23011

Mandelli, D., Smith, C., Yilmaz, A., Aldemir, T., 2013. Mining nuclear transient data through symbolic conversion. Int. Top. Meet. Probabilistic Saf. Assess. Anal. 2013, PSA 2013 3.

Merrill, B.J., 2000. Modeling an Unmitigated Quench Event in an ITER Toroidal Field Magnet. Fusion Technol. 37, 231–246. https://doi.org/10.13182/FST00-A137

Mitchell, N., Bessette, D., Gallix, R., Jong, C., Knaster, J., Libeyre, P., Sborchia, C., Simon, F., 2008. The ITER Magnet System. IEEE Trans. Appl. Supercond. 18, 435–440. https://doi.org/10.1109/TASC.2008.921232

Mitchell, N., Devred, A., Libeyre, P., Lim, B., Savary, F., 2012. The ITER Magnets: Design and Construction Status. IEEE Trans. Appl. Supercond. 22, 4200809–4200809. https://doi.org/10.1109/TASC.2011.2174560

Modarres, M., Kim, I.S., 2010. Deterministic and Probabilistic Safety Analysis. Handb. Nucl. Eng. 1742–1808. https://doi.org/10.1007/978-0-387-98149-9_15

Mohar, B., 1997. Some applications of Laplace eigenvalues of graphs, in: G. Hahm and G. Sabidussi (Eds.), Graph Symmetry: Algebraic Methods and Applications. pp. 225–275. https://doi.org/10.1.1.17.467

Nutt, W.T., Wallis, G.B., 2004. Evaluation of nuclear safety from the outputs of computer codes in the presence of uncertainties. Reliab. Eng. Syst. Saf. 83, 57–77. https://doi.org/10.1016/j.ress.2003.08.008

OECD, N. energy agency, 2012. The Role of Nuclear Energy in a Low-carbon Energy Future, Nuclear Development.

Perrault, D., 2016. Safety issues to be taken into account in designing future nuclear fusion facilities. Fusion Eng. Des. 109–111, 1733–1738. https://doi.org/10.1016/j.fusengdes.2015.10.012

Rausand, M., 2013. Risk Assessment: Theory, Methods, and Applications, Risk Assessment: Theory, Methods, and Applications. https://doi.org/10.1002/9781118281116

Rivas, J.C., Dies, J., Fajarnés, X., 2015. Revisiting the analysis of passive plasma shutdown during an ex-vessel loss of coolant accident in ITER blanket. Fusion Eng. Des. 98–99, 2206–2209. https://doi.org/10.1016/j.fusengdes.2015.06.143

Rousseeuw, P.J., 1987. Silhouettes: A graphical aid to the interpretation and validation of cluster analysis. J. Comput. Appl. Math. 20, 53–65. https://doi.org/10.1016/0377-0427(87)90125-7

Savoldi, L., Bonifetto, R., Pedroni, N., Zanino, R., 2018. Analysis of a Protected Loss of Flow Accident (LOFA) in the ITER TF Coil Cooling Circuit. IEEE Trans. Appl. Supercond. 28, 1–9. https://doi.org/10.1109/TASC.2017.2786688

Savoldi, L., Zanino, R., 2000a. Thermal-hydraulic analysis of Tcs measurement in conductor 1A of the ITER Central Solenoid Model Coil using the M&M code. Cryogenics (Guildf). 40, 593–604. https://doi.org/https://doi.org/10.1016/S0011-2275(01)00017-0

Savoldi, L., Zanino, R., 2000b. M & M: Multi-conductor Mithrandir code for the simulation of thermal-hydraulic transients in superconducting magnets. Cryogenics (Guildf). 40, 179–189. https://doi.org/10.1016/S0011-2275(00)00027-8

Savoldi Richard, L., Bessette, D., Bonifetto, R., Zanino, R., 2012. Parametric analysis of the ITER TF fast discharge using the 4C code. IEEE Trans. Appl. Supercond. - IEEE TRANS APPL Supercond. 22, 4704104.

Savoldi Richard, L., Bonifetto, R., Carli, S., Froio, A., Foussat, A., Zanino, R., 2014. Artificial Neural Network (ANN) modeling of the pulsed heat load during ITER CS magnet operation. Cryogenics (Guildf). 63, 231–240. https://doi.org/10.1016/j.cryogenics.2014.03.003

Savoldi Richard, L., Bonifetto, R., Zanino, R., 2017. Analysis of a Loss-of-Flow Accident (LOFA) in a tokamak superconducting toroidal field coil.

Savoldi Richard, L., Casella, F., Fiori, B., Zanino, R., 2010. The 4C code for the cryogenic circuit conductor and coil modeling in ITER. Cryogenics (Guildf). 50, 167–176. https://doi.org/10.1016/j.cryogenics.2009.07.008

Schaubel, K., Langhorn, A., Lloyd, S., Piec, Z., Salazar, E., Smith, J., 2017. The ITER Central Solenoid Module final test facility. Fusion Eng. Des. 124, 59–63. https://doi.org/10.1016/j.fusengdes.2017.05.010

Smith, J.P., Blanchard, J., Gattuso, A., Haefelfinger, R., Junge, R., Schaubel, K., Spitzer, S., Reiersen, W., 2013. ITER central solenoid module fabrication, in: 2013 IEEE 25th Symposium on Fusion Engineering (SOFE). IEEE, pp. 1–4. https://doi.org/10.1109/SOFE.2013.6635490

Spitzer, J., Stephens, A., Schaubel, K., Smith, J., Norausky, N., Khumthong, K., Gattuso, A., 2015. ITER Central Solenoid Module fabrication program, in: 2015 IEEE 26th Symposium on Fusion Engineering (SOFE). IEEE, pp. 1–6. https://doi.org/10.1109/SOFE.2015.7482276

Strang, G., Nguyen, T., 1996. Wavelets and filter banks. Wellesley, MA : Wellesley-Cambridge Press.

Taylor, N., Baker, D., Barabash, V., Ciattaglia, S., Elbez-Uzan, J., Girard, J.-P., Gordon, C., Iseli, M., Maubert, H., Reyes, S., Topilski, L., 2009. Preliminary Safety Analysis of ITER. Fusion Sci. Technol. 56, 573–580. https://doi.org/10.13182/FST56-573

Taylor, N., Ciattaglia, S., Boyer, H., Coombs, D., Jin, X.Z., Liger, K., Mora, J.C., Mazzini, G., Pinna, T., Urbonavičius, E., 2017. Resolving safety issues for a demonstration fusion power plant. Fusion Eng. Des. 124, 1177–1180. https://doi.org/10.1016/j.fusengdes.2017.02.018

Taylor, N., Cortes, P., 2014. Lessons learnt from ITER safety & licensing for DEMO and future nuclear fusion facilities. Fusion Eng. Des. 89, 1995–2000. https://doi.org/10.1016/j.fusengdes.2013.12.030

Taylor, N.P., 2016. Safety and licensing of nuclear facilities for fusion. Proc. - Symp. Fusion Eng. 2016–May. https://doi.org/10.1109/SOFE.2015.7482293

Turati, P., Cammi, A., Lorenzi, S., Pedroni, N., Zio, E., 2018. Adaptive simulation for failure identification in the Advanced Lead Fast Reactor European Demonstrator. Prog. Nucl. Energy 103, 176–190. https://doi.org/10.1016/j.pnucene.2017.11.013

Turati, P., Pedroni, N., Zio, E., 2017. Simulation-based exploration of high-dimensional system models for identifying unexpected events. Reliab. Eng. Syst. Saf. 165, 317–330. https://doi.org/10.1016/j.ress.2017.04.004

van Houtte, D., Okayama, K., Sagot, F., 2010. RAMI Approach for ITER. Fusion Eng. Des. 85, 1220–1224. https://doi.org/10.1016/j.fusengdes.2010.03.007

Von Luxburg, U., 2007. A tutorial on spectral clustering. Stat. Comput. 17, 395–416. https://doi.org/10.1007/s11222-007-9033-z

Vorobyev, Y., Kudinov, P., 2011. Development and application of a genetic algorithm based dynamic pra methodology to plant vulnerability search, in: International Topical Meeting on Probabilistic Safety Assessment and Analysis 2011, PSA 2011. pp. 559–573.

Wang, D., Wang, J., Yuan, R., Nie, M., Wang, F., 2015. RAMI Analysis of HCCB TBS for ITER. J. Fusion Energy 34, 1094–1099. https://doi.org/10.1007/s10894-015-9913-8

Wu, Y., Chen, Z., Hu, L., Jin, M., Li, Y., Jiang, J., Yu, J., Alejaldre, C., Stevens, E., Kim, K., Maisonnier, D., Kalashnikov, A., Tobita, K., Jackson, D., Perrault, D., 2016. Identification of safety gaps for fusion demonstration reactors. Nat. Energy 1, 16154.

Xu, J., Wang, D., Wang, J., Wang, J., Hu, L., 2015. Preliminary Quantitative Evaluation of Potential Risk for HCCB TBS Tritium Extraction System Based on Fault Tree Analysis. J. Fusion Energy 34, 1369–1377. https://doi.org/10.1007/s10894-015-9972-x

Zanino, R., Bessette, D., Richard, L.S., 2010. Quench analysis of an ITER TF coil. Fusion Eng. Des. 85, 752–760. https://doi.org/10.1016/j.fusengdes.2010.04.056

Zanino, R., Bonifetto, R., Casella, F., Savoldi Richard, L., 2013a. Validation of the 4C code against data from the HELIOS loop at CEA Grenoble. Cryogenics (Guildf). 53, 25–30. https://doi.org/10.1016/j.cryogenics.2012.04.010

Zanino, R., Bonifetto, R., Heller, R., Savoldi Richard, L., 2011. Validation of the 4C thermal-hydraulic code against 25 kA safety discharge in the ITER Toroidal Field Model Coil (TFMC). IEEE Trans. Appl. Supercond. 21, 1948–1952. https://doi.org/10.1109/TASC.2010.2089771

Zanino, R., Bonifetto, R., Hoa, C., Savoldi Richard, L., 2013b. 4C modeling of pulsed-load smoothing in the HELIOS facility using a controlled bypass valve. Cryogenics (Guildf). 57, 31–44. https://doi.org/10.1016/j.cryogenics.2013.04.005

Zanino, R., Bonifetto, R., Savoldi Richard, L., Casella, F., 2012. Dynamic modeling of a supercritical helium closed loop with the 4C code, in: AIP Conference Proceedings. pp. 1743–1750. https://doi.org/10.1063/1.4707109

Zanino, R., De Palo, S., Bottura, L., Savoldi, L., Zanino, R., 1995. A two-fluid code for the thermohydraulic transient analysis of CICC superconducting magnets. J. Fusion Energy 14, 25–40. https://doi.org/10.1007/BF02214031

Zio, E., 2014. Integrated deterministic and probabilistic safety assessment: Concepts, challenges, research directions. Nucl. Eng. Des. 280, 413–419. https://doi.org/10.1016/j.nucengdes.2014.09.004

Zio, E., 2013. The Monte Carlo simulation method for system reliability and risk analysis, Springer. https://doi.org/10.1007/978-1-4471-4588-2

Zio, E., Di Maio, F., 2010. A data-driven fuzzy approach for predicting the remaining useful life in dynamic failure scenarios of a nuclear system. Reliab. Eng. Syst. Saf. 95, 49–57. https://doi.org/10.1016/j.ress.2009.08.001

Zio, E., Di Maio, F., Stasi, M., 2010. A data-driven approach for predicting failure scenarios in nuclear systems. Ann. Nucl. Energy 37, 482–491. https://doi.org/10.1016/j.anucene.2010.01.017

Zio, E., Maio, F. Di, 2009. Processing dynamic scenarios from a reliability analysis of a nuclear power plant digital instrumentation and control system. Ann. Nucl. Energy 36, 1386–1399. https://doi.org/10.1016/j.anucene.2009.06.012

Zohm, H., 2015. Magnetohydrodynamic Stability of Tokamaks, Magnetohydrodynamic Stability of Tokamaks. Wiley-VCH Verlag GmbH & Co. KGaA, Weinheim, Germany. https://doi.org/10.1002/9783527677375